Fall 12-17-2022

Distribution Network Planning and Operation With Autonomous Agents

Abdulraheem Hassan Alobaidi
Southern Methodist University, aalobaidi@smu.edu

DISTRIBUTION NETWORK PLANNING AND OPERATION

WITH AUTONOMOUS AGENTS

Approved by:

Dr. Mohammad E. Khodayar
Associate Professor
Dissertation Committee Chairperson

Dr. Jianhui Wang
Professor

Dr. Khaled Abdelghany
Professor

Dr. Eli Olinick
Associate Professor

Dr. Harsha Gangammanavar
Assistant Professor

DISTRIBUTION NETWORK PLANNING AND OPERATION WITH AUTONOMOUS AGENTS

A Dissertation Presented to the Graduate Faculty of the

Bobby B. Lyle School of Engineering

Southern Methodist University

in

Partial Fulfillment of the Requirements

for the degree of

Doctor of Philosophy

with a

Major in Electrical Engineering

by

Abdulraheem Hassan Alobaidi

M.S., Electrical Engineering, University of South Florida
B.S., Electrical Engineering, King Abdulaziz University

December 17, 2022

ACKNOWLEDGMENTS

I would like to express my appreciation and gratitude to my academic adviser, Prof. Mohammad Khodayar, for his tremendous support and guidance throughout my Ph.D. studies. My research studies would not have been accomplished without his continuous help and advice. I would also like to extend my thanks and appreciation to the members of my Ph.D. supervisory committee, Prof. Jianhui Wang, Prof. Khaled Abdelghany, Prof. Eli Olinick, and Prof. Harsha Gangammanavar, for their significant support and advice during my studies. I am also grateful to the department chair, Prof. Dinesh Rajan, and the previous department coordinator Christy Ahsanullah, for their assistance in facilitating my studies at SMU.

The difficulty of graduate school is always eased and enjoyed with great friends and colleagues. I sincerely appreciate and thank all my colleagues and friends for their motivation during my studies at SMU. I greatly thank Seyed Saeed Fazlhashemi, Mohammad Ramin Feizi, Tao Wu, Anthony Villena, Khaled Alsurhani, Shengfei Yin, and Bin Huang for their friendship and enjoyable moments.

I also would like to thank King Abdulaziz University and the Saudi Arabian Cultural Mission for their financial support throughout my graduate studies. I am sincerely grateful for granting me the opportunity to study abroad and pursue my graduate studies. Lastly, I sincerely thank my beloved parents and lovely wife for their patience and heartfelt support. Their continued encouragement always helps me to go on my journey and attain my goals.

Hassan Alobaidi, Abdulraheem M.S., Electrical Engineering, University of South Florida, 2016

B.S., Electrical Engineering, King Abdulaziz University, 2011

Distribution Network Planning and Operation
With Autonomous Agents

Advisor: Dr. Mohammad E. Khodayar

Doctor of Philosophy conferred December 17, 2022

Dissertation completed November 18, 2022

With the restructured power system, different network operators and private investors are responsible for operating and maintaining the electricity networks. Moreover, with incentives for a clean environment and reducing the reliance on fossil fuel generation, future distribution networks adopt a considerable penetration of renewable energy sources. However, the variability and intermittency of renewable energy sources pose operational challenges in distribution networks. This thesis addresses the planning and operation of the distribution network with autonomous agents under uncertainty. First, a decentralized energy management system for unbalanced networked microgrids is developed. The energy management schemes in microgrids enhance the utilization of renewable energy resources and improve the reliability and resilience measures in distribution networks. While microgrids operate autonomously, the coordination among microgrid and distribution network operators contributes to the improvement in the economics and reliability of serving the demand. In the second chapter, a decentralized energy management framework for the networked microgrids is proposed in which the interactions between the microgrid and distribution network operators are captured using the Benders decomposition technique. The proposed framework limits the information shared among these autonomous operators and facilitates decentralized energy management in the distribution networks. Furthermore, the unbalanced operation of the distribution network and microgrids, as well as the uncertainty in the operating modes of the microgrids, renewable energy resources, and demand, are addressed.

The third chapter presents a stochastic expansion planning framework to determine the installation time, location, and capacity of battery energy storage systems in the distribution networks with considerable penetration of photovoltaic generation and data centers. The presented framework aims to minimize the capital cost of the battery energy storage and the operation cost of the distribution network while ensuring the security of energy supply for the data centers that serve end-users in the data network as well as the reliability requirements of the distribution network. The proposed stochastic framework captures the interactions between the distribution network and data center operators considering limited shared information among these entities. Benders decomposition is used to capture the interactions between these autonomous operators in the electricity and data networks. The uncertainties associated with the electric demand, data center workload, solar PV generation, and the availability of the distribution branches are captured using Monte Carlo simulation. The representative scenarios are selected using a dissimilarity-based sparse subset selection algorithm.

The fourth chapter proposes a coordinated expansion planning of natural gas-fired distributed generation in the power distribution and natural gas networks considering demand response. The proposed expansion planning framework captures the interactions between the distribution network operator and the natural gas supplier using the Benders decomposition. The problem is formulated as a distributionally robust optimization problem in which the uncertainties in the photovoltaic power generation, electricity load, demand bids, and natural gas demand are considered. The Wasserstein distance metric is employed to quantify the distance between the probability distribution functions. The expansion planning of the gas-fired distributed generation is determined in the master problem, and the feasibility and optimality of the decisions in the power and natural gas networks are ensured using the corresponding sub-problems.

The fifth chapter proposes a decentralized operation of the distribution network and hydrogen refueling stations equipped with hydrogen storage, electrolyzers, and fuel cells to

serve hydrogen and electric vehicles. The uncertainties in the electricity demands, PV generation, hydrogen supply, and hydrogen demands are captured, and the problem is formulated as a Wasserstein distance-based distributionally robust optimization problem. The proposed framework coordinates the dispatch of the distributed generation in the distribution network with the hydrogen storage, electrolyzer, and fuel cell dispatch considering the worst-case probability distribution of the uncertain parameters. The proposed decentralized framework would limit the information sharing among the distribution network and hydrogen refueling stations using the Benders decomposition technique.

TABLE OF CONTENTS

LIST OF FIGURES

LIST OF TABLES

Table Page

This Ph.D. dissertation is dedicated to my beloved parents and my lovely wife.

Chapter 1

Introduction

1.1 Decentralized Energy Management for Unbalanced Networked Microgrids with Uncertainty

Networked microgrids improve the economics, reliability, and resilience of distribution networks by accommodating the renewable and distributed energy resources and exchanging electricity with the distribution network in the grid-connected mode [1]. Several studies addressed the energy management for networked microgrids and distribution networks [2–21]. Distributed, decentralized, and agent-based frameworks were developed to perform this task by capturing the interactions between the microgrids and distribution networks.

Distributed energy management frameworks for multiple microgrids in the distribution network were presented in [2–10]. A stochastically distributed energy management framework for networked microgrids and distribution network is proposed in [2]. The proposed framework segregates the optimization problems solved for microgrids and the distribution network and addresses the uncertainty in demand and wind generation. An online distributed energy management scheme is proposed in [3] that leverages the Alternating Direction Method of Multipliers (ADMM) algorithm and regret minimization to coordinate energy flow in the networked microgrids considering the uncertainty in the distributed energy resources (DERs). A two-level distributed optimal control approach is proposed in [4] to carry out the energy management in multiple microgrids and a distribution network. The upper-level control strategy aims to optimize the energy flow among the microgrids and the distribution network, and the lower-level control scheme aims to obtain the optimal dispatch of the generation resources considering the grid-connected and islanding operation modes of microgrids. Ref. [5] proposed a distributed control strategy for power management that improves the power quality in ac and dc microgrids. The proposed event-triggered distributed

power routing approach balances the power among phases and enhances the voltage quality in ac microgrids. While this approach addressed the unbalanced operation of microgrids using simulation, the contingencies and the uncertainty in the operation of DERs, as well as the interactions among microgrid and distribution network operators (DNOs) were not addressed. Ref. [6] proposed a distributed nonlinear control scheme to share power among the DERs in islanded ac microgrids. The developed nonlinear mean-square cooperative control scheme features distributed event-detection to reduce the communication noise disturbances. A distributed control based on an event-driven communication mechanism was proposed in [7] to share power among current-controlled voltage source inverter-based DERs in microgrids. A risk-averse energy management framework for networked microgrids is proposed in [8] using conditional value at risk. The proposed energy management problem is formulated as a stochastic linear programming problem and the auxiliary problem principle approach is used to address the privacy constraints. A two-layer distributed cooperative control approach is used in [9] for enabling power-sharing among network microgrids using tertiary control while ensuring the frequency and voltage support using primary and secondary distributed controls. The dynamic performance of the networked microgrids is evaluated using small-signal dynamic models to ensure the effectiveness of the proposed control structure. A distributed and robust energy management framework that captures the uncertainty in renewable energy resources and demand is proposed for hybrid AC/DC microgrids in [10]. The ADMM algorithm is used to solve the problem using limited shared information among the microgrids.

Decentralized energy management solutions were developed for energy management in microgrids and distribution networks in [11–15]. A decentralized optimal control algorithm is proposed in [11] to minimize the total operation cost of the networked microgrids and to enhance the utilization of distributed storage resources. The problem is formulated as a partially observable Markov decision process, solved using dynamic programming. A two-stage robust optimization problem is formulated in [12] to address the uncertainties of demand and DERs in the operation horizon, and the ADMM method is used to coordinate the operation decisions by DNO and microgrid operators. A decentralized energy management scheme is proposed in [13] to coordinate the distribution network and microgrids operation

strategies considering the grid-connected and islanding operation modes of microgrids. The proposed energy management system considered the uncertainty in demand and generation by formulating a two-stage stochastic programming problem; however, the unbalanced operation of networked microgrids was not addressed. Leveraging the notion of transactive energy, a decentralized energy management framework is proposed in [14] to coordinate the energy management between networked microgrids. The uncertainties are captured using distributionally robust optimization models to ensure robust solutions with less conservatism compared to the robust optimization solutions. A decentralized approach for the optimal power flow considering the coordination between the microgrids and distribution network operators is presented in [15]; however, the uncertainties in demand and DERs were not considered.

A multi-agent system is introduced for energy management in [16] to control the power trades in the networked microgrids considering the demand response. The proposed framework aimed at reducing the operation cost and peak load by managing low priority demands. Multi-agent systems were used in [18] for energy management of networked microgrids to handle the non-dispatchable DERs in a competitive energy market. In the first level, each agent would balance the load and generation, and in the second level, all agents join the market as a generator or load. The energy flow is coordinated between the grid-connected microgrids and the distribution network by regulating the demand to minimize the generation cost in [17]. A multi-objective model was proposed in [19] to minimize the generation cost and peak to average ratio of demand by scheduling the energy consumption in microgrids while capturing the uncertainty in uncontrollable demands. The coordinated operation of microgrids within the distribution network is modeled as a stochastic bi-level program in [20]. Here, the upper-level problem minimizes the operation cost of the distribution network while the lower-level problem minimizes the operation cost of the microgrids. The uncertainty in renewable energy resources is addressed by formulating a stochastic two-stage optimization problem. Bi-level programming is proposed in [21] to address the market participation of the microgrids. In the upper level, the operation cost of the wholesale market is minimized while at the lower level, the payoffs of energy service providers are maximized by controlling the local generation assets and curtailable loads. The proposed algorithm ignores the uncer-

tainty in the distributed energy resources and demand.

While decentralized and distributed energy management schemes for networked microgrids were extensively studied in earlier publications, the day-ahead energy management framework that addresses the interactions between DNO and microgrid operators considering the unbalanced operation of the networked microgrids has not been addressed. Furthermore, the uncertainty in the microgrid operation modes (grid-connected and island modes) was not addressed in the previous studies.

1.2 Stochastic Expansion Planning of Battery Energy Storage for the Interconnected Distribution and Data Networks

The significant annual increase in data center energy consumption impacts the long-term security and reliability of the distribution networks. The data center energy consumption that accounted for 1.8% of the US energy consumption in 2014, is increased by 4% annually in 2014-2020 [22]. The annual growth rate of the data center market is anticipated to be 8.5% in 2020-2027 [23]. The global concerns about greenhouse gas generation are shifting the electricity generation portfolio toward variable and uncertain renewable energy resources. Coordinated with such transitions and to mitigate the carbon footprints of data centers, considerable research efforts are dedicated to serving the data center electric demand with clean and renewable energy resources. Such efforts address the challenges associated with the variability and uncertainty in data center demand and renewable generation resources. The uncertainty in renewable generation resources would lead to voltage fluctuations and violations in the distribution feeders. Moreover, the renewable power injection could alter the direction of power flow in distribution feeders and cause protection system failures. The variability and uncertainty in the data center demand stemming from serving the end users' requests and workloads in the data network, could result in excessive voltage fluctuations and voltage drops in the distribution feeders. Therefore, coordination between the uncertain distributed energy supply and variable demands could help to improve the long-term operation of the distribution networks with such resources.

Battery energy storage (BES) offers several benefits to the distribution network including reducing the peak load at the main distribution feeder, mitigating the renewable generation curtailment, and improving the reliability and power quality. Considering the sustained

growth in the data center demand, the long-term expansion planning of BES could help to achieve these objectives and postponing the potential feeder capacity expansions by balancing the generation and demand effectively. In this context, extensive research works addressed the expansion planning of BES in distribution networks [24–38].

A planning framework for BES in the distribution network was proposed in [24] that captured the uncertainty in wind generation. A probabilistic optimal power flow was performed as a part of the planning framework and Tabu search with particle swarm optimization (PSO) was utilized as the solution methodology. In [25], optimal sizing and placement of BES were determined to minimize the power loss in the distribution network; however, the uncertainties in demand and renewable generation were not addressed. Here, the problem was formulated as a mixed-integer quadratically constrained quadratic programming, solved by the D-XEMS13 procedure in MATLAB. The authors in [26] proposed an algorithm based on the Benders decomposition to determine the location and capacity of the energy storage units. Using network reconfiguration, the proposed algorithm aimed to minimize the investment cost of energy storage, the cost of electricity, network loss, feeder overloading, and bus voltage deviations. The power flow constraints were approximated by second-order cones and the uncertainties in PV generation, price of electricity and demand were considered using scenarios. A technique based on dual optimization was proposed in [27] to determine the capacity and location of distributed generation and BES units. The proposed technique sought to minimize the energy costs, greenhouse gas emissions, and real power losses and maintain the supply voltage within the acceptable limits. The proposed formulation captured the electric vehicle interconnection and Teaching Learning Based Optimization (TLBO) was adopted to solve the formulated problem. A probabilistic method for placement and sizing of energy storage units in the distribution network was proposed in [28] to improve the reliability of the energy supply. The uncertainties in demand and wind generation were considered and the optimal level of reliability was determined using load shedding in contingencies. The expansion planning of the energy storage in the distribution network was addressed in [29] to minimize the installation cost of the energy storage, the voltage deviations, network loss, and energy costs. The problem was formulated as a nonlinear programming problem and solved in two stages. The solution to the first stage problem yielded the location and size

of the energy storage while the voltage deviation, network loss, and energy cost were minimized in the second stage by solving an AC power flow problem. An expansion planning of distribution networks with energy storage systems (ESSs) was formulated as a multi-stage mixed-integer linear programming problem (MILP) in [30]. The expansion decisions included the installation of ESSs and the expansion and replacement of distribution lines, while the operation decisions were the scheduling of ESSs and the energy flow at the main substation. The formulated planning problem aimed to minimize the investment cost, the operation cost of ESS, the cost of the energy procured from the main substation, the curtailed load, and the annual outage penalties. The planning problem considered daily load scenarios to perform the economic dispatch and the extreme loading scenarios were used to check the network security and reliability of the planning decisions.

A non-parametric chance-constrained optimization was proposed in [31] for the expansion planning of ESSs in the distribution network. Here, the uncertainties in electric vehicle demands, residential loads, and renewable generation were taken into account using discrete empirical distributions. The expansion planning of ESS was formulated as a MILP problem in [32] where the uncertainties in wind and PV generations, the price of electricity at the main distribution feeder, the baseload, and the EV demand were represented by scenarios. The considered scenarios were selected using the k-means++ clustering approach. The expansion planning of distributed generation and BESs to maximize the payoff of the distribution network operator was presented in [33]. The problem was formulated as a mixed-integer nonlinear programming (MINLP) problem and solved using the PSO algorithm. A formulation for the expansion planning of BESs in the distribution network was presented in [34] to improve the utilization of wind power generation while minimizing the BES investment cost and distribution network operation cost. The uncertainties associated with the electricity demand, wind generation, and availability of micro-turbines were considered using scenarios. Chance-constrained programming was used to ensure the utilization of wind generation and a differential evolution algorithm was used to solve the proposed planning problem. The expansion planning of ESSs in a distribution network that leverages voltage sensitivity analysis and optimal power flow was presented in [35]. The location and capacity of ESSs were determined to prevent overvoltage and undervoltage incidents in the distribution network.

The worst-case realization of the generation and demand profiles were considered using the historical data sets. The authors in [36] proposed a stochastic approach for the expansion planning of BES in a distribution network with conservative voltage reduction. The uncertainties in demand and renewable generation were addressed by developing scenarios. A hierarchical framework for locating and sizing the BESs was presented in [37]. The objective was to minimize the distribution network operation cost while maintaining the nodal voltages within acceptable limits. The location of the BESs was determined using voltage sensitivity analysis and the capacity of the BES was determined by solving a MINLP problem using natural aggregation algorithm. The uncertainties in the distributed generation outputs and demands were captured using scenarios. A stochastic expansion planning of ESSs and distributed generation resources was presented in [38] that captured the demand response to maximize social welfare. Here, the expansion planning problem was formulated as a MILP problem and the uncertainties in demand, wind speed, and solar radiation were addressed using scenarios.

The coordination among the energy storage and data center was addressed in the literature [39–43]. A day ahead resource planning for data centers in grid-connected microgrid with ESSs was addressed in [39]. The problem was formulated as a MILP problem to minimize the fuel cost and carbon footprint considering the delay-sensitive and delay-tolerant workloads in the data network. An algorithm using the Lyapunov optimization technique was proposed in [40] to balance the workloads among data centers with BES and minimize the real-time energy costs associated with processing the workloads. The formulated stochastic programming problem addressed the uncertainty in the electricity prices and received workloads, to allocate the data center capacity and manage the battery energy flow. The energy management in data centers with energy storage considering carbon footprint offsets was discussed in [41]. The objective was to minimize the operation cost of the data center while satisfying the total carbon footprint requirement. A simulation-based capacity planning approach for energy storage in data centers was proposed in [42]. The power supply mix was characterized using the simulation models to quantify the capacity of energy storage. The expansion planning of the generation resources including the energy storage in the data center was presented in [43]. The proposed problem was formulated as a linear

programming (LP) problem which minimized the investment and operation costs of the data center while satisfying the emission and service availability requirements.

Distributed algorithms were used to address the energy management in data centers [44–46]. Distributed data traffic routing was proposed in [44] to improve the energy consumption in the data center while avoiding congestion in the data switches. The coordinated energy management in co-location data centers was addressed in [45] using an alternating direction method of multipliers approach. The objective was to minimize the energy consumption and workload curtailment charges to ensure the quality of service provided to the servers. The energy management of data centers in grid-connected microgrid was addressed in [46]. A distributed algorithm was proposed to minimize the operation cost including the energy trade with the main grid, local generation cost, battery utilization cost, and workload distribution charges. The formulated stochastic programming problem captured the uncertainties in workloads, renewable energy resources, and energy prices.

The expansion planning of the data center facilities considering the wind power generation in the transmission network was addressed in [47]. The proposed algorithm aimed at minimizing the capital and operation costs of data centers and data routes. The uncertainty in the transmission network assets and the received requests are captured using scenarios. The interactions between the independent system operator (ISO) and DCO are captured using Benders decomposition and sharing the electricity price. In [48], the BES expansion planning in the distribution network with data center was addressed ignoring the reliability requirements of the distribution network, the operation cost of the BES units, and the uncertainty in the outages of the distribution branches. This research extends the earlier work in [48] by addressing these shortcomings.

1.3 Distributionally Robust Generation Expansion Planning of Gas-Fired Distributed Generation with Demand Response

Natural gas generation technologies are becoming favorable options for power generation because of the low fuel prices and environmental impacts [49–52]. However, the investments in natural gas generation resources would impact the operation of the interconnected electricity and natural gas networks [49, 50]. Increasing the dispatch of the gas-fired generation units increases their demand in the natural gas network, which could eventually lead to

supply deficiency and curtailment of natural gas loads. Furthermore, the uncertainty in the interconnected electricity and natural gas networks could impact the reliability of energy supply in both networks.

Deterministic and stochastic models are used to represent the generation and demand in the expansion planning of electricity and natural gas networks. Deterministic models are used for the expansion planning of the integrated electricity and natural gas networks considering the demand and generation forecasts in [49–54]. Optimal expansion decisions for gas-fired generating units, transmission lines, and natural gas pipelines were proposed in [49] using a decentralized approach. Here, the investments were in the electricity and natural gas networks' assets, such as natural gas-fired generating units, transmission lines, and natural gas pipelines to supply the forecasted demand. The expansion planning decisions were made in the master problem, while the feasibility and optimality of these decisions were addressed in the sub-problems. In [50], a framework for the expansion planning of the energy hub is presented. The energy hub uses electricity and natural gas to serve the electric and heat demand. The proposed planning problem aimed to find the lowest expansion cost for distributed generation units, including the combined heat and power units, the transmission lines, and the natural gas furnaces to supply the forecasted electricity and heat loads. In [51], an expansion planning framework for the integrated power distribution and natural gas networks was proposed considering a high penetration of gas-fired generation resources. The problem was formulated as a mixed integer nonlinear programming (MINLP) and solved using a heuristic approach. A long-term generation and transmission expansion planning for the integrated electricity and natural gas networks was formulated as a mixed integer linear programming (MILP) problem in [52]. Here, the expansion decisions represented the investments in the natural gas supply chain and the power generation and transmission assets. A coordinated generation and transmission expansion planning framework for the integrated electricity and natural gas systems was proposed in [53] considering the investments in generation, transmission, and natural gas assets. To incorporate the nonlinear constraints of natural gas flow, the problem was formulated as an MINLP problem which is solved using the genetic algorithm. Demand-side management was considered in the expansion planning of interconnected electricity and natural gas networks in [54]. The proposed formulation aimed

to minimize the investment costs in transmission lines and gas pipelines, the operation costs, the demand participation costs, and the costs associated with carbon emissions.

In order to address the uncertainty in the planning horizon, stochastic programming (SP) is proposed in [55–58]. A two-stage SP problem was formulated for the expansion planning and operation of energy hubs in [55], where the impact of demand response on the planning and operation of energy hubs was investigated. In [56], a two-stage SP framework for the expansion planning of energy hubs was proposed that incorporated the uncertainty in the wind generation and the reliability constraints of the electricity network. In [57], an MINLP problem was formulated for the expansion planning of the integrated electricity and natural gas networks. The formulated problem aimed to maximize social welfare considering the risk of uncertainties in demand, system component outages, and market prices. A two-stage stochastic programming problem was formulated in [58] to determine the capacity of the energy hubs in the distribution networks by considering the uncertainties in electricity and heat demands, as well as the wind and PV power generation. In [59], a two-stage stochastic programming framework was proposed to jointly coordinate the expansion planning of power transmission and natural gas networks considering the uncertainties in the electricity and natural gas demands.

There are multiple challenges with the solution to the SP problem. First, the computation time to determine a solution to the SP problem grows exponentially as the number of scenarios increases. Moreover, the probability distribution functions (PDFs) of random variables are defined, which is not often a feasible assumption. Formulating the robust optimization (RO) problem lowers the computational burden of introducing the uncertainties and does not rely on prior knowledge about the probability distribution of the uncertain variables [60,61]. However, the solution to the RO problem captures the worst-case realization of the random variables, which may lead to an over-conservative solution. An adjustable RO was formulated in [60] for the expansion planning of the interconnected electricity and natural gas networks with power to gas (PtG) technology considering N-1 contingency and probabilistic reliability criteria. The problem was decomposed and solved using the column-and-constraint generation (CCG) algorithm and Benders decomposition. In [61], a collaborative planning approach for the integrated electricity and natural gas network with PtG technology was

proposed aiming to convert the excess wind power into natural gas. The proposed method considered the uncertainty in wind generation and electricity and natural gas demands in the typical scenario while ensuring that an optimal solution in the forecasted scenario was immune to the fluctuations in other scenarios.

In order to address the deficiencies with the SP and RO problems, distributionally robust optimization (DRO) problems are formulated for the operation [62–72] and planning [73–79] of the power systems. Here, the optimal solution is obtained considering the worst-case probability distribution of the random variables within an ambiguity set. The ambiguity set is constructed in a way that the true probability distribution of the uncertain variables is within this set with a certain confidence level. The moment information of the probability distribution of random variables and the probability distribution of empirical data are used to form the ambiguity set. The Wasserstein distance, L_1 norm distance, and Kullback-Leibler (KL) divergence are used as distance measures to form the ambiguity set.

In the context of expansion planning, DRO has recently been applied to address the uncertainties in the power system. In [73], a distributionally robust chance-constrained formulation was proposed for the distribution network expansion planning. The investment decisions on feeders, substations, and distributed generators were determined considering the uncertainties in renewable generation and electric demand. Such uncertainties were represented by moment-based ambiguity sets, and the problem was reformulated as a MILP problem. In [74], a two-stage data-driven stochastic programming problem was formulated for the transmission expansion planning was proposed where the L_1 norm distance metric was used to form the ambiguity set of the load. The investments in the transmission lines were determined in the first stage, while the expected operation cost under the worst probability distribution of uncertain demand profile was determined in the second stage. The problem was solved using a combined Benders decomposition and the column-and-constraint generation algorithms. Reference [75] proposed a two-stage DRO framework to determine the optimal transmission expansion decisions and the allocation of the thyristor-controlled series compensation devices. Here, the uncertainties in wind generation and electric vehicle demands were captured by forming the ambiguity sets using the L_1 norm distance measure. Similar to [74], the problem was solved using combined Benders decomposition and the

column-and-constraint generation algorithms. In [76], the Wasserstein distance-based DRO problem was formulated to capture the uncertainty in large-scale PV generation for the expansion planning of the energy storage in the distribution network. The formulated DRO problem was transformed into a mixed integer second-order cone programming (MISOCP) problem and solved using the MOSEK solver. Reference [77] proposed a two-stage DRO framework for the expansion planning of distributed generators, energy storage systems, capacitor banks, and renewable energy sources in the distribution network. The uncertainties of wind and solar PV outputs were captured using the moment-based ambiguity sets. The problem was reformulated as a MISOCP problem and solved using the column-and-constraint generation algorithm.

A few research efforts are focused on formulating the generation expansion planning of the integrated electricity and natural gas networks as a DRO problem. In [78], a two-stage data-driven robust capacity planning of energy hubs in the distribution network was proposed. The empirical data on electric and heat demands, as well as the wind generation, are used to form an ambiguity set, and the KL divergence measure is used to quantify the distance between the empirical and the true PDFs. A generation capacity planning scheme for the integrated electricity and natural systems was proposed in [79] by incorporating the demand response for the electrical and thermal loads. Here, the problem was formulated as a DRO problem using the moments of uncertain wind generation. The risk associated with the power balance violation due to the wind generation uncertainty was considered in the proposed planning framework, and the problem was reformulated as a second-order cone programming (SOCP) problem.

In the distribution networks, the gas-fired distributed generation (GFDG) units, operated by the distribution system operator (DSO), are served by the natural gas network. Since DSO and the natural gas supplier are autonomous entities with distinct objectives and system constraints, the GFDG expansion planning framework should address the coordination among these entities [80]. Most of the above research works considered one decision-maker, i.e., the system operator, to carry out the expansion planning in the electricity and natural gas networks. In [49, 61], decentralized frameworks using Benders decomposition and game theory were introduced for the expansion planning of gas-fired power generation technologies

in the electricity and natural gas networks. A deterministic formulation is proposed in [49] while the uncertainty in renewable energy resources and electricity and natural gas demands are captured by forming the uncertainty sets in [61]. Therefore, the fourth chapter proposes a distributionally robust expansion planning of GFDG in the interconnected power distribution and natural gas networks considering the demand response. The expansion planning decisions are determined considering the worst-case probability distribution of the uncertain variables. Benders decomposition is used to decompose the long-term expansion planning and short-term operation problems and captures the coordination among the DSO and the natural gas supplier.

1.4 Distributionally Robust Decentralized Operation of Distribution networks with Hydrogen Refueling Stations

The transportation sector is responsible for 34% of the greenhouse gas generation in the U.S. [81]. Emerging vehicular technology, including hydrogen fuel cell vehicles (HFCVs) and battery electric vehicles (BEVs), are promising solutions to mitigate the carbon footprint of the transportation sector. The HFCVs provide a longer range, and fast refueling compared to the BEVs [82–84]. The hydrogen required to serve HFCVs is produced by the reforming process using fossil fuels, including natural gas and coal [85], or by the electrolysis process using water. The majority of the hydrogen is produced using the reforming process; however, the emission of this process contributes to the overall carbon footprint of the HFCV technology. In the electrolysis process, the water molecule is split into hydrogen and oxygen molecule. While this process does not produce carbon dioxide, it requires a considerable amount of energy that is usually supplied by the power network. Serving this process with renewable resources would reduce the cost of the procured hydrogen [86, 87].

Hydrogen is mainly used in petroleum refinery, fertilizer production, and food processing industries [88]. However, the growing need for hydrogen fuel in the transportation sector would increase the number of hydrogen refueling stations. To serve the HFCVs in the U.S., 74 hydrogen refueling stations were built by the end of 2019 [89]. This number is expected to increase to 220 and 2500 stations by 2030 and 2040, respectively [90]. Using water electrolyzers in the refueling stations would increase the electricity demand for hydrogen generation and affects the operation of the distribution network serving these stations. Furthermore,

the generated and stored hydrogen could be used to produce electricity using fuel cells. The generated electricity could be used to charge the BEVs connected to the hydrogen fueling stations or serve the demand in the distribution network. The considerable power exchanged by the hydrogen refueling stations requires an effective integrated operation framework that captures the impacts of these stations on the distribution network operation. The coordinated operation of the electricity and hydrogen systems was addressed in [82–84, 87, 91–97]. The coordination among the distributed hydrogen refueling stations equipped with local hydrogen production was addressed in [84] to serve the transportation demands and to participate in demand response programs in the distribution network. The electrolyzers in the hydrogen refueling station were represented as controllable loads that provided demand response services considering the hydrogen demand of the transportation network, the available hydrogen in the hydrogen storage, and the price of electricity. In [91], the distributed hydrogen refueling stations were centrally managed to serve the hydrogen demands and provide operating reserve in the electricity market. The stations participate in the electricity market using fuel cells in the off-peak demands in the transportation network. The hydrogen generation units, including an electrolyzer, PV unit, and battery storage system, were coordinated in [97] to serve the load in an industrial hydrogen facility. The proposed energy management system coordinated the energy supply from the electricity grid and the local generation units to serve the hydrogen and electricity demands of the hydrogen facility and minimize the total operation costs. The coordinated operation frameworks in [84, 91, 97] were deterministic models, and the system uncertainties in the distribution and hydrogen refueling stations were not considered.

To account for the uncertainties, stochastic programming [82, 83, 96] and robust optimization [92, 93] formulations were proposed in the literature. The coordination between the power network and hydrogen transportation system with hydrogen-based vehicle refueling stations was proposed in [82]. The objective was to minimize the total operation costs, including electricity generation, hydrogen production, and transportation costs. The uncertainties in hydrogen demands and wind generation were considered using scenarios. The alternating direction method of multipliers (ADMM) algorithm was used to coordinate the operational decisions using the information shared among the electricity network and hy-

drogen transportation operators. A bi-level formulation is proposed in [83] to coordinate hydrogen production and transportation in the hydrogen energy systems, considering the influence of hydrogen energy services on the market prices. The upper-level problem aimed to coordinate the operation of hydrogen production, transportation, and storage and bid for the electricity used in hydrogen production, to minimize the total hydrogen operation costs. The lower-level problem determined the market clearing price for the electricity considering the impact of hydrogen energy services. The uncertainty of renewable generation was quantified using the conditional-value-at-risk (CVaR). A decentralized framework for the operation of electricity and natural gas systems was proposed in [96], where the power-to-hydrogen, hydrogen-to-gas, and gas-fired power units coupled the two systems. The uncertainty in wind generation was considered using scenarios, and the ADMM algorithm is used to ensure the privacy of the independent operators. The coordinated operation of the power distribution and district heating networks was addressed in [92] considering the power to hydrogen and heat technology to serve the electricity, hydrogen, and heat demands. Here, the heat generated in the electrolysis process was recovered and used in the district heating network. The problem was formulated as an RO problem to capture the worst-case realization of PV and wind generations. The coordination among networked microgrids with power-to-hydrogen and power-to-heat technologies, electric vehicle charging stations, and hydrogen refueling stations was addressed in [93]. The problem was formulated as an RO problem to determine the worst-case realization of electricity prices. A decentralized framework using the ADMM algorithm was proposed to solve the operation problem in multi-microgrids with limited information shared among microgrid operators.

Distributionally robust optimization (DRO) problems for the operation of the integrated power, hydrogen, and natural gas systems coupled with the power-to-hydrogen and hydrogen-to-gas technologies were proposed in [87, 94, 95]. Reference [94] addressed the coordinated operation of electricity and natural gas distribution networks with power-to-hydrogen and hydrogen-to-gas technologies. The problem was formulated as a DRO problem to capture the worst-case probability distribution of wind generation. The Kullback-Leibler (KL) divergence metric was used to construct the ambiguity set. In [95], the volt-var optimization for the interconnected distribution and natural gas networks with the power-to-hydrogen

and hydrogen-to-gas facilities and the gas-fired distributed generators was proposed. The problem was formulated as a moment-based DRO problem aiming to minimize the voltage deviations in the distribution network, considering the worst-case probability distribution of PV generation given the moments of the empirical distributions. The impact of hydrogen supply on the reliability and economics of integrated hydrogen, power, heat, and natural gas system was investigated in [87]. The power network operation problem was formulated as the Wasserstein distance-based DRO problem considering the worst-case probability distribution of wind generation.

Although earlier research addressed the coordination between the electricity and hydrogen systems, hydrogen production was managed in a centralized manner. The works in [87, 92, 94, 95, 97] assumed one centralized operator managing the integrated energy systems. However, the electricity and hydrogen providers may be owned and operated by independent operators [82–84, 91, 93]. In [82, 83], hydrogen production, storage, and transportation are operated by an entity that resides away from the load centers. Although centralized hydrogen production facilities would have a lower investment cost compared to distributed hydrogen production, the transportation costs for hydrogen delivery to hydrogen refueling stations could be considerable [91]. Furthermore, the scheduling of hydrogen transportation would impact the hydrogen availability in the onsite service providers. Moreover, with the advent of market deregulation, private stakeholders such as hydrogen refueling stations are participating in critical infrastructures to provide energy services [84].

In the fifth chapter, distributed hydrogen production, and storage facilities are located near the load centers and managed by independent operators. These operators coordinate with the distribution system operator (DSO) to use electricity to produce hydrogen and serve the hydrogen demand. Unlike the centralized hydrogen production scheme, the distributed hydrogen production facilities will reduce the dependence on the hydrogen transportation network by generating hydrogen locally using electrolyzers. The electrolyzers and fuel cells installed in these facilities provide a bi-directional power flow to the distribution network. In [84,91], hydrogen is produced locally in each hydrogen refueling station using electrolyzers. Here, a central entity manages the hydrogen production in all stations, where the electrolyzers are controllable demands in the distribution network. However, the hydrogen production

facilities may be owned and operated by autonomous entities with limited data sharing [93].

Chapter 2

Decentralized Energy Management for Unbalanced Networked Microgrids with Uncertainty

This chapter proposes a decentralized energy management system for unbalanced networked microgrids, which considers the uncertainty in demand and PV power generation and the probabilistic operation modes of microgrids using Monte Carlo simulation and backward scenario reduction. Benders decomposition algorithm is used as the solution methodology to ensure the autonomous operation of the distribution network and microgrids. The modified IEEE 34-bus and IEEE 123-bus distribution networks are used to validate the effectiveness of the proposed algorithm.

The interaction between the distribution network operator and microgrid controllers is captured using the Benders decomposition technique. The physical and control layouts of the energy network in the distribution network are shown in Fig. 2.1. As shown in this figure, each microgrid operator communicates with the DNO in the control layer to manage the consumption and generation. The DNO would schedule the generation resources while considering the probabilistic islanding of microgrids in the distribution network. As microgrids are operated autonomously, the proposed framework ensures that limited information is exchanged between the DNO and the microgrid operators. The contributions of this chapter are as follows:

- The interactions among microgrids and the distribution network operator are captured using the Benders decomposition technique.

- The unbalanced operation of microgrids and distribution network was addressed by determining the power flow on each phase in the coupling lines between the microgrids and the distribution network.

- Probabilistic operation modes of microgrids and the uncertainty in DERs and demand were considered using scenarios. Furthermore, the impacts of islanding and outages in microgrids on the operation cost of the distribution network and microgrids are assessed.

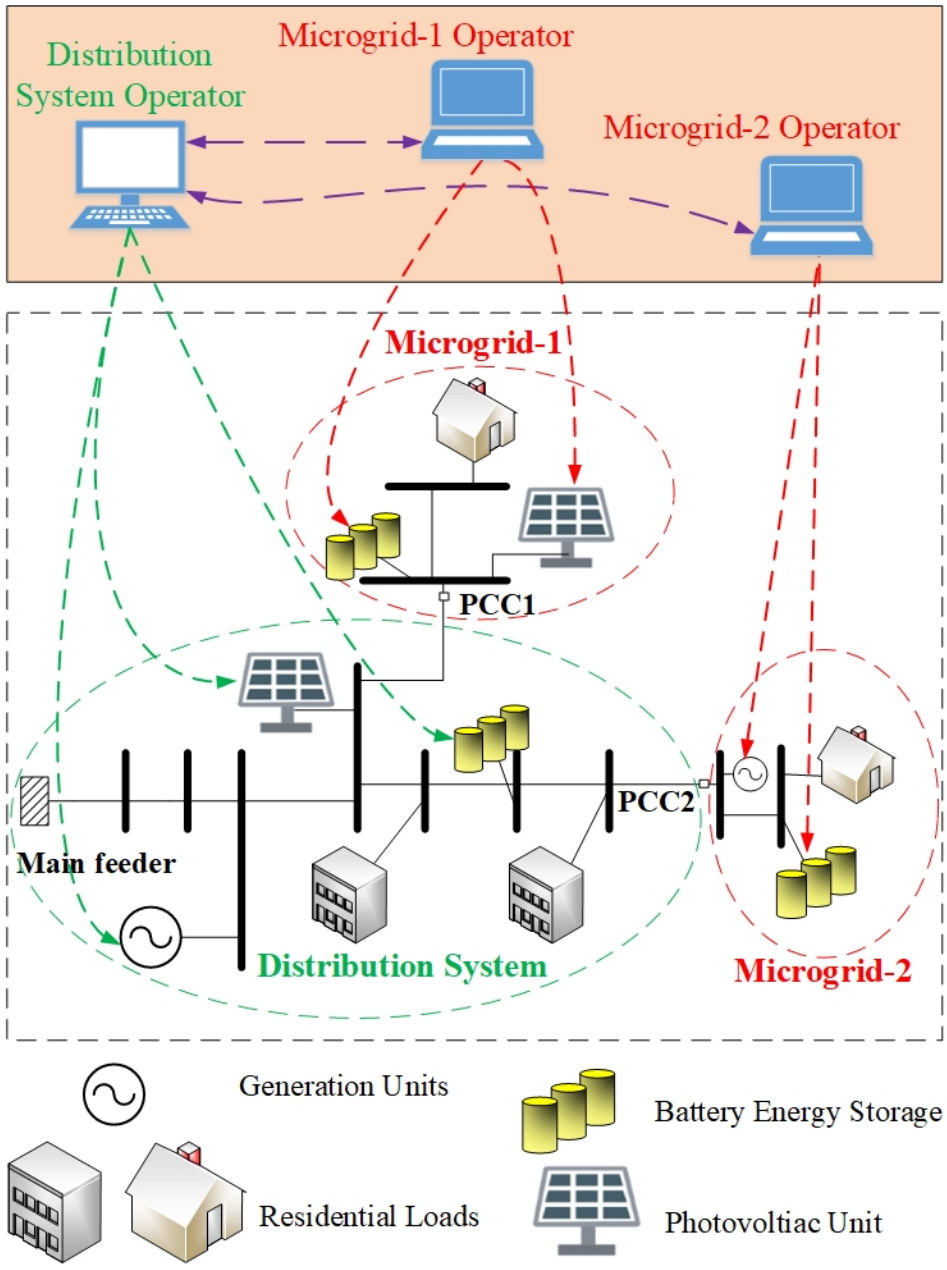

Figure 2.1: Physical and control layouts of networked microgrids in the distribution network.

It is worth noting that the proposed framework addresses the hourly energy management for networked microgrids in a 24-hour horizon. Therefore, communication delays compared to the simulation time step are ignored. The rest of the chapter is organized as follows: a list of symbols is presented in section 2.1. The problem formulation and solution methodology are presented in section 2.2 and section 2.3 respectively. Numerical analysis is shown in section 2.4, and the solution time and scalability of the proposed algorithm are presented in section 2.5. Finally, the conclusion is presented in section 2.6.

2.1 List of Symbols

Indices and Sets:

d	Index of demand
f	Index of distribution feeder
g	Index of distributed generation unit
s	Index of scenario
t	Index of time
ϕ	Index of phase
e	Index of energy storage unit
i, j	Index of bus
m	Index of microgrid
v	Index of photovoltaic generation unit
τ	Index of iteration
$\mathcal{K}_m$	Set of buses in microgrid m
$\mathcal{B}$	Set of buses in the distribution network
$\mathcal{B}_i$	Set of buses connected to bus i
$\mathcal{B}_f$	Set of buses connected to the distribution feeder f
r	Index of voltage regulator
$\mathcal{B}_r$	Set of buses connected to the secondary of voltage regulator r
$\mathcal{D}$	Set of demands in distribution network
$\mathcal{D}_m$	Set of demands in microgrid m
$\mathcal{H}$	Set of DERs in the distribution network

$\mathcal{H}_m$	Set of DERs in microgrid m
$\mathcal{E}$	Set of energy storage units in the distribution network
$\mathcal{E}_m$	Set of energy storage units in microgrid m
$\mathcal{V}$	Set of photovoltaic generation units in the distribution network
$\mathcal{V}_m$	Set of photovoltaic generation units in microgrid m

Variables:

$\alpha_{t,s}$	Auxiliary variable
$F_g(.)$	Production cost of DER g
$P^{\phi}_{(.),t,s}$	Real power dispatch on phase ϕ at time t in scenario s
$Q^{\phi}_{(.),t,s}$	Reactive power dispatch on phase ϕ at time t in scenario s
$PL^{\phi}_{ij,t,s}$	Real power flow of line ij on phase ϕ at time t in scenario s
$QL^{\phi}_{ij,t,s}$	Reactive power flow of line i-j on phase ϕ at time t in scenario s
$Q^{D,\phi}_{t,s}$	Reactive power demand on phase ϕ at time t in scenario s
$P^{dc,\phi}_{e,t,s}$	Real power of energy storage e in discharging mode on phase ϕ at time t in scenario s
$P^{ch,\phi}_{e,t,s}$	Real power of energy storage e in charging mode on phase ϕ at time t in scenario s
$P^{d,\phi}_{t,s}$	Served real power demand on phase ϕ at time t in scenario s
$U^{\phi}_{j,t,s}$	Squared voltage at bus j on phase ϕ at time t in scenario s
$\lambda^{m,\phi}_{(.),t,s}$	Dual variable
$\gamma^{m,\phi}_{(.),t,s}$	Dual variable
$E^{\phi}_{e,t,s}$	Available energy in battery energy storage e connected to phase ϕ at time t in scenario s
$y_{ij,s}$	The binary variable representing the microgrid operation mode connected to bus i in the distribution network
$Z^{m}_{(.),t,s}$	Slack variable

Parameters:

pr_s	Probability of scenario s
T	The total number of hours
ρ^{t}_{f}	Hourly price of electricity for feeder f

ρ_e	Operation cost of battery storage e
$VOLL$	Value of lost load
$P_{t,s}^{D,\phi}$	Real power demand on phase ϕ at time t in scenario s
$A_i^{(.)}$	Element of unit-bus incidence matrix in the distribution network
$N_i^{m,(.)}$	Elements of unit-bus incidence matrix in microgrid m
p_{ij}^{ϕ}	Availability of phase ϕ on line i-j
r_{ij},x_{ij}	Resistance and reactance of line i-j
E_e^{min}	Minimum available energy in battery storage e
E_e^{max}	Maximum available energy in battery storage e
l_{ij}	Availability of line i-j
$P_{(.)}^{\phi,min}$	Minimum real power dispatch of a unit on phase ϕ
$P_{(.)}^{\phi,max}$	Maximum real power dispatch of a unit on phase ϕ
$Q_{(.)}^{\phi,min}$	Minimum reactive power dispatch of a unit on phase ϕ
$Q_{(.)}^{\phi,max}$	Maximum reactive power dispatch of a unit on phase ϕ
$\mathcal{R}_{t,s}$	Solar irradiation at time t and scenario s
S_f^{max}	The maximum apparent power of the distribution feeder f
SL_{ij}^{max}	The maximum apparent power of line i-j
ΔO_e	The allowable variation in the state of charge of battery storage e
V_j^{min}	Minimum allowable voltage at bus j
V_j^{max}	Maximum allowable voltage at bus j
ψ_v^{ϕ}	Availability of phase ϕ on PV panel v
η_v	The efficiency of solar panel v
S_v	The total area of solar PV panel v
η_e^{dc}	Charging efficiency for energy storage e
η_e^{ch}	Discharging efficiency for energy storage e
μ_m	Islanding probability for microgrid m
Z_{upper}	The upper bound of the solution
Z_{lower}	The lower bound of the solution
ϵ	Convergence tolerance

2.2 Problem Formulation

2.2.1 Decentralized energy management using Benders decomposition

The general form of the energy management problem is formulated as a mixed-integer linear programming problem (MILP) shown in (2.1)-(2.5) where $\boldsymbol{x}_c$ and $\boldsymbol{x}_b$ are the vectors of continuous and binary variables respectively. These variables represent the operational decisions in the distribution network, and $\boldsymbol{y}_m$ is a vector of continuous variables representing the operational decisions in the microgrid m. The first and second terms in (2.1) are the operation costs of the distribution network and networked microgrids respectively. The problem is subjected to (2.2)-(2.5) where (2.2) and (2.3) represent the nodal power balance in the distribution network and microgrid m respectively. Here, $\boldsymbol{k}_m$ is a vector of complicating continuous variables representing the exchanged power flow between the distribution network and microgrid m. The constraint (2.4) represents all the inequality constraints for the distribution network operation problem. The set of inequality constraints for microgrid m is shown in (2.5).

$$min\ f\left(\boldsymbol{x}_c\right) + \sum_m g(\boldsymbol{y}_m) \tag{2.1}$$

s.t.

$$\boldsymbol{A}_c \cdot \boldsymbol{x}_c + \sum_m \boldsymbol{B}_m.\ \boldsymbol{k}_m = \boldsymbol{d} \qquad \boldsymbol{k}_m \in \boldsymbol{y}_m \tag{2.2}$$

$$\boldsymbol{A}_m.\boldsymbol{y}_m + \boldsymbol{B}'_m \cdot \boldsymbol{k}_m = \boldsymbol{d}_m \qquad \boldsymbol{k}_m \in \boldsymbol{y}_m \tag{2.3}$$

$$\boldsymbol{G}_c \cdot \boldsymbol{x}_c + \boldsymbol{G}_b \cdot \boldsymbol{x}_b \leq \boldsymbol{h} \tag{2.4}$$

$$\boldsymbol{F}_m \cdot \boldsymbol{y}_m \leq \boldsymbol{r}_m \tag{2.5}$$

Using Benders decomposition, the problem is decomposed into a master problem (MP) shown in (2.6)-(2.9) and m-subproblems (SPs) presented in (2.10)-(2.14). The master MILP problem represents the distribution network operation problem. An auxiliary positive variable α shown in (2.7), is introduced in (2.6) to represent the operation cost of the networked microgrids plus the absolute mismatch in nodal real and reactive power [98]. The solution to the MP problem (Z_{lower}) represents the lower bound of the problem solution. The solution

($\hat{\boldsymbol{k}}_m$) is passed to the microgrid operation subproblems (2.10)-(2.14), which are formulated as linear programming (LP) problems.

$$min\ Z_{lower} = f\left(\boldsymbol{x}_c\right) + \alpha \tag{2.6}$$

s.t.

$$\alpha \geq 0 \tag{2.7}$$

$$\boldsymbol{A}_c \cdot \boldsymbol{x}_c + \sum_m \boldsymbol{B}_m \cdot \boldsymbol{k}_m = \boldsymbol{d} \tag{2.8}$$

$$\boldsymbol{G}_c \cdot \boldsymbol{x}_c + \boldsymbol{G}_b \cdot \boldsymbol{x}_b \leq \boldsymbol{h} \tag{2.9}$$

The first term of the objective function of SP in (2.10) is the operation cost of the microgrid m. The vectors of slack variables are introduced in the second term in (2.10). The mismatch in the nodal power balance is minimized using the penalty vector $\boldsymbol{M}$. The slack variables are introduced in the nodal power balance (2.11). The set of inequality constraints in the microgrid operation's sub-problem is shown in (2.12). Constraint (2.13) fixes the complicating variables to the values obtained from the MP. The slack variables are non-negative as shown in (2.14). Once SPs (2.10)-(2.14) are solved, the upper bound of the solution is calculated in (2.15) using the solutions of the distribution network operation problem (MP) and microgrids' operation problems (SPs). If the mismatch between the lower and upper bounds of the solution is greater than a specified tolerance, Benders cut (2.16) is formed and added to the distribution network operation problem. Adding a new hyperplane (Benders cut) to the feasible region of the master problem improves the solution at each iteration. This process will continue until the gap between the lower and upper bounds of the solution is smaller than a certain tolerance.

$$min\ w_m = g\left(\boldsymbol{y}_m\right) + \boldsymbol{M} \cdot \left(\boldsymbol{u}_m + \boldsymbol{v}_m\right) \tag{2.10}$$

s.t.

$$\boldsymbol{A}_m \cdot \boldsymbol{y}_m + \boldsymbol{B}'_m \cdot \boldsymbol{k}_m + \boldsymbol{u}_m - \boldsymbol{v}_m = \boldsymbol{d}_m \tag{2.11}$$

$$\boldsymbol{F}_m \cdot \boldsymbol{y}_m \leq \boldsymbol{r}_m \tag{2.12}$$

$$\boldsymbol{k}_m = \hat{\boldsymbol{k}}_m \qquad : \boldsymbol{\lambda}_m \tag{2.13}$$

$$\boldsymbol{u}_m, \boldsymbol{v}_m \geq 0 \tag{2.14}$$

It is worth noting that this framework will be used by both microgrid operators and DNO as it captures the interactions between these entities. The master problem is solved by the DNO while the sub-problems are solved by the microgrid operators. The Benders cuts generated by the subproblems represent the microgrids' responses to the decisions made by the DNO. The DNO updates its decisions by updating the power flows between the distribution network and microgrids and sends this decision to the microgrids.

$$Z_{upper} = f(\hat{\boldsymbol{x}}_c) + \sum_m (\hat{w}_m) \tag{2.15}$$

$$\alpha \geq \sum_m \left(\hat{w}_m + \hat{\boldsymbol{\lambda}}_m^{\top} . \left(\boldsymbol{k}_m - \hat{\boldsymbol{k}}_m \right) \right) \tag{2.16}$$

2.2.2 Distribution network operation problem-Master Problem

The distribution network operation problem is formulated as a MILP problem (2.17)-(2.53). The objective is to minimize the expected operation cost of the distribution network with microgrids. The objective function (2.17) includes the expected cost of providing electricity from the main distribution feeder, the expected operation cost of DERs, the expected operation cost of the energy storage [99], and the expected demand curtailment penalties. The fifth term in (2.17) represents the expected operation cost of microgrids and the mismatch in the nodal real and reactive power balance for given values of the exchanged real and reactive power flow. At each iteration, the value of this scalar is updated by adding Bender cuts from the microgrid subproblems. The scalar is always positive as enforced by (2.18).

The network constraints are shown in (2.19)-(2.53). The constraints representing the nodal real and reactive power balance are shown in (2.19)-(2.20) respectively. The first terms in (2.19) and (2.20) are the exchanged real and reactive power flows on the branches between the distribution network and microgrids respectively. Here, the positive power flow direction is assumed to be from the distribution network to the microgrids. The second

terms in (2.19) and (2.20) are the real and reactive power flows in the other branches of the distribution network respectively. The real and reactive power demands served are limited by (2.21) and (2.22) respectively. Here, it is assumed that the power factor of the demand remains the same in case of curtailment; therefore, the served reactive demand is proportional to the served real demand as enforced by (2.22). The constraints (2.23)-(2.26) are the linearized approximation of the unbalanced power flow formulated in [100]. The real and reactive power flows on each phase of the distribution branches are presented in (2.23)-(2.24) except for the branches that are connected to the microgrids. For these branches, the real and reactive power flows are formulated as (2.25) and (2.26). Here,$\{\phi_1, \phi_2, \phi_3\}$ represents the positive sequence of phases on the branch i-j. i.e. $\{a, b, c\}$, $\{b, c, a\}$, and $\{c, a, b\}$. Constraints (2.23)-(2.26) used Big-M reformulation to incorporate the availability of the distribution branch phases. The power factor at the distribution feeder is within the desirable limits by enforcing (2.27). The capacity of the distribution feeder is constrained by a circular constraint, which it is further linearized in (2.28)-(2.30) by hexagon approximation introduced in [101]. The power dispatch of DER is limited by (2.31)-(2.32). Considering the availability of phases on a branch, the real and reactive power flows in a distribution branch are limited by (2.33)-(2.34), respectively. The exchanged real and reactive power flows in branches between the distribution network and microgrids are limited by (2.35)-(2.36) respectively. Similar to (2.28)-(2.30), hexagon approximation is used in (2.37)-(2.39) to linearize the circular constraints that limit the apparent power flow in a branch. The real and reactive power output limits of a PV unit are shown in (2.40)-(2.42). The solar generation output is limited by the capacity of the PV generation unit as enforced by (2.40). The reactive power output of a PV generation unit is limited by the capacity of its inverter as enforced by (2.41). The real power output of a PV generation unit is limited by the available solar irradiance as shown in (2.42).

The constraints representing the energy storage units are shown in (2.43)-(2.49) [99], [102]. The charging and discharging real power are limited by (2.43)-(2.44). The reactive power output is limited by (2.45). The hourly available energy is limited by (2.46). The available energy is limited by minimum and maximum limits as shown in (2.47). The available energy at the initial time ($t = 0$) is equal to the available energy at the final time ($t = NT$) as

shown in (2.48). The available energy at the final time step is set to a certain value E_e^{ini} in (2.48). The depth of charge/discharge is limited by (2.49).

The squared bus voltage is limited by upper and lower limits as shown in (2.50). This constraint does not capture the slack bus and the buses connected to the secondary of the voltage regulator. The voltage of the slack bus (main distribution feeder) is fixed. Three-phase voltage regulators are represented by three single-phase ideal transformers in series with branches that represent the leakage impedances. Constraints (2.51)-(2.52) represent the relationship between the voltage magnitudes on both sides of the voltage regulator where i is the primary side, j is the secondary side. Here, $a_{T,r}^{\phi,max}$ and $a_{T,r}^{\phi,min}$ are the maximum and minimum transformer ratios on phase ϕ, respectively [100] The probabilistic islanding of microgrids is enforced by (2.53). The probability of a grid-connected operating mode of microgrid m cannot exceed (1-μ_m) and the minimum probability of islanding is μ_m.

$$min \sum_s pr_s \cdot \Bigg(\sum_{t\in T} \Big(\rho_f^t \cdot (\sum_\phi P_{f,t,s}^\phi) + \sum_{g\in\mathcal{H}} F_g(\sum_\phi P_{g,t,s}^\phi) + \sum_{e\in\mathcal{E}} \rho_e \cdot (\sum_\phi P_{e,t,s}^{ch,\phi} + P_{e,t,s}^{dc,\phi}) + VOLL \cdot \sum_{d\in\mathcal{D}} \sum_\phi (P_{t,s}^{D,\phi} - P_{t,s}^{d,\phi}) \Big) \Bigg) + \sum_s \sum_{t\in T} \alpha_{t,s} \quad (2.17)$$

$$\alpha_{t,s} \geq 0 \quad (2.18)$$

$$- \sum_{j\in\mathcal{B}_i\cap\mathcal{K}_m} PL_{ij,t,s}^\phi + \sum_{j\in\mathcal{B}_i} PL_{ij,t,s}^\phi + \sum_f A_i^f.P_{f,t,s}^\phi + \sum_{g\in\mathcal{H}} A_i^g.P_{g,t,s}^\phi + \sum_{v\in\mathcal{V}} A_i^v.P_{v,t,s}^\phi + \sum_{e\in\mathcal{E}} A_i^e.P_{e,t,s}^{dc,\phi} - \sum_{e\in\mathcal{E}} A_i^e.P_{e,t,s}^{ch,\phi} = \sum_{d\in\mathcal{D}} A_i^d.P_{t,s}^{d,\phi} \quad ;\forall i \in \mathcal{B} \quad (2.19)$$

$$- \sum_{j\in\mathcal{B}_i\cap\mathcal{K}_m} QL_{ij,t,s}^\phi + \sum_{j\in\mathcal{B}_i} QL_{ij,t,s}^\phi + \sum_f A_i^f.Q_{f,t,s}^\phi + \sum_{g\in\mathcal{H}} A_i^g.Q_{g,t,s}^\phi + \sum_{v\in\mathcal{V}} A_i^v.Q_{v,t,s}^\phi + \sum_{e\in\mathcal{E}} A_i^e.Q_{e,t,s}^\phi = \sum_{d\in\mathcal{D}} A_i^d.Q_{t,s}^{d,\phi} \quad ;\forall i \in \mathcal{B} \quad (2.20)$$

$$P_{t,s}^{d,\phi} \leq P_{t,s}^{D,\phi} \quad ;\forall d \in \mathcal{D} \tag{2.21}$$

$$Q_{t,s}^{d,\phi} = \tan(\cos^{-1} PF_d) \cdot P_{t,s}^{d,\phi} \tag{2.22}$$

$$\begin{aligned} U_{i,t,s}^{\phi_1} - U_{j,t,s}^{\phi_1} \leq\ & 2r_{ij}^{\phi_1\phi_1} \cdot PL_{ij,t,s}^{\phi_1} + 2x_{ij}^{\phi_1\phi_1} QL_{ij,t,s}^{\phi_1} - r_{ij}^{\phi_1\phi_2} PL_{ij,t,s}^{\phi_2} + \sqrt{3} \cdot x_{ij}^{\phi_1\phi_2} PL_{ij,t,s}^{\phi_2} \\ & - x_{ij}^{\phi_1\phi_2} \cdot QL_{ij,t,s}^{\phi_2} - \sqrt{3} \cdot r_{ij}^{\phi_1\phi_2} QL_{ij,t,s}^{\phi_2} - r_{ij}^{\phi_1\phi_3} \cdot PL_{ij,t,s}^{\phi_3} - \sqrt{3} \cdot x_{ij}^{\phi_1\phi_3} PL_{ij,t,s}^{\phi_3} \\ & - x_{ij}^{\phi_1\phi_3} \cdot QL_{ij,t,s}^{\phi_3} + \sqrt{3} \cdot r_{ij}^{\phi_1\phi_3} \cdot QL_{ij,t,s}^{\phi_3} + M \cdot (1 - p_{ij}^{\phi_1}) \quad ;\forall i,j \in \mathcal{B} \end{aligned} \tag{2.23}$$

$$\begin{aligned} U_{i,t,s}^{\phi_1} - U_{j,t,s}^{\phi_1} \geq\ & 2r_{ij}^{\phi_1\phi_1} \cdot PL_{ij,t,s}^{\phi_1} + 2x_{ij}^{\phi_1\phi_1} QL_{ij,t,s}^{\phi_1} - r_{ij}^{\phi_1\phi_2} PL_{ij,t,s}^{\phi_2} + \sqrt{3} \cdot x_{ij}^{\phi_1\phi_2} PL_{ij,t,s}^{\phi_2} \\ & - x_{ij}^{\phi_1\phi_2} \cdot QL_{ij,t,s}^{\phi_2} - \sqrt{3} \cdot r_{ij}^{\phi_1\phi_2} QL_{ij,t,s}^{\phi_2} - r_{ij}^{\phi_1\phi_3} \cdot PL_{ij,t,s}^{\phi_3} - \sqrt{3} \cdot x_{ij}^{\phi_1\phi_3} PL_{ij,t,s}^{\phi_3} \\ & - x_{ij}^{\phi_1\phi_3} \cdot QL_{ij,t,s}^{\phi_3} + \sqrt{3} \cdot r_{ij}^{\phi_1\phi_3} \cdot QL_{ij,t,s}^{\phi_3} - M \cdot (1 - p_{ij}^{\phi_1}) \quad ;\forall i,j \in \mathcal{B} \end{aligned} \tag{2.24}$$

$$\begin{aligned} U_{i,t,s}^{\phi_1} - U_{j,t,s}^{\phi_1} \leq\ & 2r_{ij}^{\phi_1\phi_1} \cdot PL_{ij,t,s}^{\phi_1} + 2x_{ij}^{\phi_1\phi_1} QL_{ij,t,s}^{\phi_1} - r_{ij}^{\phi_1\phi_2} PL_{ij,t,s}^{\phi_2} + \sqrt{3} \cdot x_{ij}^{\phi_1\phi_2} PL_{ij,t,s}^{\phi_2} \\ & - x_{ij}^{\phi_1\phi_2} \cdot QL_{ij,t,s}^{\phi_2} - \sqrt{3} \cdot r_{ij}^{\phi_1\phi_2} QL_{ij,t,s}^{\phi_2} - r_{ij}^{\phi_1\phi_3} \cdot PL_{ij,t,s}^{\phi_3} - \sqrt{3} \cdot x_{ij}^{\phi_1\phi_3} PL_{ij,t,s}^{\phi_3} \\ & - x_{ij}^{\phi_1\phi_3} \cdot QL_{ij,t,s}^{\phi_3} + \sqrt{3} \cdot r_{ij}^{\phi_1\phi_3} \cdot QL_{ij,t,s}^{\phi_3} + M \cdot (1 - y_{ij,s} \cdot p_{ij}^{\phi_1}) \quad ;\forall i \in \mathcal{B}_j \cap \mathcal{B}, \forall j \in \mathcal{B}_i \cap \mathcal{K}_m \end{aligned} \tag{2.25}$$

$$\begin{aligned} U_{i,t,s}^{\phi_1} - U_{j,t,s}^{\phi_1} \geq\ & 2r_{ij}^{\phi_1\phi_1} \cdot PL_{ij,t,s}^{\phi_1} + 2x_{ij}^{\phi_1\phi_1} QL_{ij,t,s}^{\phi_1} - r_{ij}^{\phi_1\phi_2} PL_{ij,t,s}^{\phi_2} + \sqrt{3} \cdot x_{ij}^{\phi_1\phi_2} PL_{ij,t,s}^{\phi_2} \\ & - x_{ij}^{\phi_1\phi_2} \cdot QL_{ij,t,s}^{\phi_2} - \sqrt{3} \cdot r_{ij}^{\phi_1\phi_2} QL_{ij,t,s}^{\phi_2} - r_{ij}^{\phi_1\phi_3} \cdot PL_{ij,t,s}^{\phi_3} - \sqrt{3} \cdot x_{ij}^{\phi_1\phi_3} PL_{ij,t,s}^{\phi_3} \\ & - x_{ij}^{\phi_1\phi_3} \cdot QL_{ij,t,s}^{\phi_3} + \sqrt{3} \cdot r_{ij}^{\phi_1\phi_3} \cdot QL_{ij,t,s}^{\phi_3} - M \cdot (1 - y_{ij,s} \cdot p_{ij}^{\phi_1}) \quad ;\forall i \in \mathcal{B}_j \cap \mathcal{B}, \forall j \in \mathcal{B}_i \cap \mathcal{K}_m \end{aligned} \tag{2.26}$$

$$-\tan(\cos^{-1} PF_f) \cdot P_{f,t,s} \leq Q_{f,t,s} \leq \tan(\cos^{-1} PF_f) \cdot P_{f,t,s} \tag{2.27}$$

$$-\sqrt{3} \cdot (P_{f,t,s}^{\phi} + S_f^{max}) \leq Q_{f,t,s} \leq -\sqrt{3} \cdot (P_{f,t,s}^{\phi} - S_f^{max}) \tag{2.28}$$

$$-\frac{\sqrt{3}}{2} \cdot S_f^{max} \leq Q_{f,t,s}^{\phi} \leq \frac{\sqrt{3}}{2} \cdot S_f^{max} \tag{2.29}$$

$$\sqrt{3} \cdot (P_{f,t,s}^{\phi} - S_f^{max}) \leq Q_{f,t,s} \leq \sqrt{3} \cdot (P_{f,t,s}^{\phi} + S_f^{max}) \tag{2.30}$$

$$P_g^{min} \leq P_{g,t,s}^{\phi} \leq P_g^{max} \quad ; \forall g \in \mathcal{H} \tag{2.31}$$

$$-Q_g^{max} \leq Q_{g,t,s}^{\phi} \leq Q_g^{max} \quad ; \forall g \in \mathcal{H} \tag{2.32}$$

$$-M \cdot p_{ij}^{\phi} \leq PL_{ij,t,s}^{\phi} \leq M \cdot p_{ij}^{\phi} \quad ; \forall i,j \in \mathcal{B} \tag{2.33}$$

$$-M \cdot p_{ij}^{\phi} \leq QL_{ij,t,s}^{\phi} \leq M \cdot p_{ij}^{\phi} \quad ; \forall i,j \in \mathcal{B} \tag{2.34}$$

$$-M \cdot y_{ij,s} \cdot p_{ij}^{\phi} \leq PL_{ij,t,s}^{\phi} \leq M \cdot y_{ij,s} \cdot p_{ij}^{\phi} \quad ; \forall i \in \mathcal{B}_j \cap \mathcal{B}, \forall j \in \mathcal{B}_i \cap \mathcal{K}_m \tag{2.35}$$

$$-M \cdot y_{ij,s} \cdot p_{ij}^{\phi} \leq QL_{ij,t,s}^{\phi} \leq M \cdot y_{ij,s} \cdot p_{ij}^{\phi} \quad ; \forall i \in \mathcal{B}_j \cap \mathcal{B}, \forall j \in \mathcal{B}_i \cap \mathcal{K}_m \tag{2.36}$$

$$-\sqrt{3} \cdot (PL_{ij,t,s}^{\phi} + SL_{ij}^{max}) \leq QL_{ij,t,s}^{\phi} \leq -\sqrt{3} \cdot (PL_{ij,t,s}^{\phi} - SL_{ij}^{max}) \tag{2.37}$$

$$-\frac{\sqrt{3}}{2} \cdot SL_{ij}^{max} \leq QL_{ij,t,s}^{\phi} \leq \frac{\sqrt{3}}{2} \cdot SL_{ij}^{max} \tag{2.38}$$

$$\sqrt{3}(PL_{ij,t,s}^{\phi} - SL_{ij}^{max}) \leq QL_{ij,t,s}^{\phi} \leq \sqrt{3}(PL_{ij,t,s}^{\phi} + SL_{ij}^{max}) \tag{2.39}$$

$$0 \leq P_{v,t,s}^{\phi} \leq P_v^{max} \cdot \psi_v^{\phi} \quad ; \forall v \in \mathcal{V} \tag{2.40}$$

$$-Q_v^{max} \psi_v^{\phi} \leq Q_{v,t,s}^{\phi} \leq Q_v^{max} \psi_v^{\phi} \quad ; \forall v \in \mathcal{V} \tag{2.41}$$

$$P_{v,t,s}^{\phi} \leq \eta_v \cdot \mathcal{R}_{t,s} \cdot S_v \cdot \psi_v^{\phi} \quad ; \forall v \in \mathcal{V} \tag{2.42}$$

$$0 \leq P_{e,t,s}^{\phi,dc} \leq P_e^{dc,max} \quad ; \forall e \in \mathcal{E} \tag{2.43}$$

$$0 \leq P_{e,t,s}^{\phi,ch} \leq P_e^{ch,max} \quad ; \forall e \in \mathcal{E} \tag{2.44}$$

$$-Q_e^{max} \leq Q_{e,t,s}^{\phi} \leq Q_e^{max} \quad ;\forall e \in \mathcal{E} \tag{2.45}$$

$$E_{e,t,s}^{\phi} = E_{e,t-1,s}^{\phi} + (P_{e,t,s}^{\phi,ch} \cdot \eta_e^{ch} - P_{e,t,s}^{\phi,dc}/\eta_e^{dc}) \quad ;\forall e \in \mathcal{E} \tag{2.46}$$

$$E_e^{min} \leq E_{e,t,s}^{\phi} \leq E_e^{max} \quad ;\forall t \in T \quad ;\forall e \in \mathcal{E} \tag{2.47}$$

$$E_{e,0,s}^{\phi} = E_{e,NT,s}^{\phi} = E_e^{ini} \quad ;\forall e \in \mathcal{E} \tag{2.48}$$

$$\left| E_{e,t,s}^{\phi} - E_{e,t-1,s}^{\phi} \right| \leq \Delta O_e \quad ;\forall e \in \mathcal{E} \tag{2.49}$$

$$(V_i^{min})^2 \leq U_{i,t,s}^{\phi} \leq (V_i^{max})^2 \quad ;\forall i \in \mathcal{B}\ , i \notin \mathcal{B}_f \cup \mathcal{B}_r \tag{2.50}$$

$$-M \cdot (1 - p_{ij}^{\phi}) \leq (a_{T,r}^{\phi,max})^2 . U_{j,t,s}^{\phi} - U_{i,t,s}^{\phi}; \forall i \in \mathcal{B}_j, \forall j \in \mathcal{B}_r \tag{2.51}$$

$$(a_{T,r}^{\phi,min})^2 . U_{j,t,s}^{\phi} - U_{i,t,s}^{\phi} \leq M \cdot (1 - p_{ij}^{\phi}) \quad ;\forall i \in \mathcal{B}_j, \forall j \in \mathcal{B}_r \tag{2.52}$$

$$\sum_s pr_s . y_{ij,s} \leq 1 - \mu_m \quad ;\forall i \in \mathcal{B}_j \cap \mathcal{B}, \forall j \in \mathcal{B}_i \cap \mathcal{K}_m \tag{2.53}$$

2.2.3 Microgrid Operation Subproblem

At this stage, each microgrid operator solves the SP to check the feasibility of the solution obtained from the distribution network operation problem (MP) and to ensure its optimal operation. The microgrid subproblem is formulated as a LP problem in which, the objective function is shown in (2.54). The first, second, and third terms of the objective function are the expected operation cost of DERs, the expected operation cost of energy storage, and the penalty associated with the expected loss of load, respectively. The last term is the summation of the absolute value of slack variables that represents the nodal real and reactive power mismatches. As the procured solution from the distribution network operation

problem may lead to an infeasible solution in the microgrid operation SP, these slack variables are introduced.

The network constraints for microgrids are similar to those in the distribution networks shown in (2.21)-(2.22),(2.31)-(2.32), and (2.37)-(2.50) for $d \in \mathcal{D}_m$, $e \in \mathcal{E}_m$, and $v \in \mathcal{V}_m$. Here, (2.19) and (2.20) are replaced by (2.55) and (2.56) which include the slack variables to capture the mismatch in the nodal generation and demand balance; (2.23) and (2.24) are replaced by (2.57) and (2.58) to address the outages in microgrid's branches; and (2.25) and (2.26) are replaced by (2.59) and (2.60) given the states of the coupling branches between microgrid and distribution network. These states are procured by solving the distribution network problem (MP). Similarly, (2.33) and (2.34) are replaced by (2.61) and (2.62), and (2.35) and (2.36) are replaced by (2.63) and (2.64) respectively. The real and reactive power exchanges between microgrid and distribution network are equal to the solutions of the master problem as enforced by (2.65)-(2.66). The slack variables are non-negative as shown (2.67).

$$min \sum_{s} pr_s \cdot \Bigg(\sum_{t \in T} \Big(\sum_{g \in \mathcal{H}_m} F_g(\sum_{\phi} P^{\phi}_{g,t,s}) + \sum_{e \in \mathcal{E}_m} \rho_e \cdot (\sum_{\phi} P^{ch,\phi}_{e,t,s} + P^{dc,\phi}_{e,t,s}) + VOLL \cdot \sum_{d \in \mathcal{D}_m} \sum_{\phi} (P^{D,\phi}_{t,s} - P^{d,\phi}_{t,s}) + M \cdot (\sum_{\phi} \sum_{i \in \mathcal{K}_m} Z^{i,m,\phi}_{1,t,s} + Z^{i,m,\phi}_{2,t,s} + Z^{i,m,\phi}_{3,t,s} + Z^{i,m,\phi}_{4,t,s}) \Big) \Bigg) \tag{2.54}$$

$$\sum_{j \in \mathcal{B}_i \cap \mathcal{K}_m} PL^{\phi}_{ij,t,s} + \sum_{j \in \mathcal{K}^i_m} PL^{\phi}_{ij,t,s} + \sum_{g \in \mathcal{H}_m} N^{m,g}_i . P^{\phi}_{g,t,s} + \sum_{v \in \mathcal{V}_m} N^{m,v}_i . P^{\phi}_{v,t,s} + \sum_{e \in \mathcal{E}_m} N^{m,e}_i . P^{dc,\phi}_{e,t,s} - \sum_{e \in \mathcal{E}_m} N^{m,e}_i . P^{ch,\phi}_{e,t,s} + Z^{i,m,\phi}_{1,t,s} - Z^{i,m,\phi}_{2,t,s} = \sum_{d \in \mathcal{D}_m} N^{m,d}_i . P^{d,\phi}_{t,s} \quad ; \forall i \in \mathcal{K}_m \tag{2.55}$$

$$\sum_{j \in \mathcal{B}_i \cap \mathcal{K}_m} QL^{\phi}_{ij,t,s} + \sum_{j \in \mathcal{K}^i_m} QL^{\phi}_{ij,t,s} + \sum_{g \in \mathcal{H}_m} N^{m,g}_i . Q^{\phi}_{g,t,s} + \sum_{v \in \mathcal{V}_m} N^{m,v}_i . Q^{\phi}_{v,t,s} + \sum_{e \in \mathcal{E}_m} N^{m,e}_i . Q^{\phi}_{e,t,s} + Z^{i,m,\phi}_{3,t,s} - Z^{i,m,\phi}_{4,t,s} = \sum_{d \in \mathcal{D}_m} N^{m,d}_i . Q^{d,\phi}_{t,s} \quad ; \forall i \in \mathcal{K}_m \tag{2.56}$$

$$U_{i,t,s}^{\phi_1} - U_{j,t,s}^{\phi_1} \leq 2r_{ij}^{\phi_1\phi_1} \cdot PL_{ij,t,s}^{\phi_1} + 2x_{ij}^{\phi_1\phi_1} \cdot QL_{ij,t,s}^{\phi_1} - r_{ij}^{\phi_1\phi_2} \cdot PL_{ij,t,s}^{\phi_2} + \sqrt{3} \cdot x_{ij}^{\phi_1\phi_2} \cdot PL_{ij,t,s}^{\phi_2}$$
$$- x_{ij}^{\phi_1\phi_2} \cdot QL_{ij,t,s}^{\phi_2} - \sqrt{3} \cdot r_{ij}^{\phi_1\phi_2} \cdot QL_{ij,t,s}^{\phi_2} - r_{ij}^{\phi_1\phi_3} \cdot PL_{ij,t,s}^{\phi_3} - \sqrt{3} \cdot x_{ij}^{\phi_1\phi_3} \cdot PL_{ij,t,s}^{\phi_3}$$
$$- x_{ij}^{\phi_1\phi_3} \cdot QL_{ij,t,s}^{\phi_3} + \sqrt{3} \cdot r_{ij}^{\phi_1\phi_3} \cdot QL_{ij,t,s}^{\phi_3} + M \cdot (1 - p_{ij}^{\phi_1} \cdot l_{ij}) \quad ; \forall i, j \in \mathcal{K}_m \quad (2.57)$$

$$U_{i,t,s}^{\phi_1} - U_{j,t,s}^{\phi_1} \geq 2r_{ij}^{\phi_1\phi_1} \cdot PL_{ij,t,s}^{\phi_1} + 2x_{ij}^{\phi_1\phi_1} \cdot QL_{ij,t,s}^{\phi_1} - r_{ij}^{\phi_1\phi_2} \cdot PL_{ij,t,s}^{\phi_2} + \sqrt{3} \cdot x_{ij}^{\phi_1\phi_2} \cdot PL_{ij,t,s}^{\phi_2}$$
$$- x_{ij}^{\phi_1\phi_2} \cdot QL_{ij,t,s}^{\phi_2} - \sqrt{3} \cdot r_{ij}^{\phi_1\phi_2} \cdot QL_{ij,t,s}^{\phi_2} - r_{ij}^{\phi_1\phi_3} \cdot PL_{ij,t,s}^{\phi_3} - \sqrt{3} \cdot x_{ij}^{\phi_1\phi_3} \cdot PL_{ij,t,s}^{\phi_3}$$
$$- x_{ij}^{\phi_1\phi_3} \cdot QL_{ij,t,s}^{\phi_3} + \sqrt{3} \cdot r_{ij}^{\phi_1\phi_3} \cdot QL_{ij,t,s}^{\phi_3} - M \cdot (1 - p_{ij}^{\phi_1} \cdot l_{ij}) \quad ; \forall i, j \in \mathcal{K}_m \quad (2.58)$$

$$U_{i,t,s}^{\phi_1} - U_{j,t,s}^{\phi_1} \leq 2r_{ij}^{\phi_1\phi_1} \cdot PL_{ij,t,s}^{\phi_1} + 2x_{ij}^{\phi_1\phi_1} \cdot QL_{ij,t,s}^{\phi_1} - r_{ij}^{\phi_1\phi_2} \cdot PL_{ij,t,s}^{\phi_2} + \sqrt{3} \cdot x_{ij}^{\phi_1\phi_2} \cdot PL_{ij,t,s}^{\phi_2}$$
$$- x_{ij}^{\phi_1\phi_2} \cdot QL_{ij,t,s}^{\phi_2} - \sqrt{3} \cdot r_{ij}^{\phi_1\phi_2} \cdot QL_{ij,t,s}^{\phi_2} - r_{ij}^{\phi_1\phi_3} \cdot PL_{ij,t,s}^{\phi_3} - \sqrt{3} \cdot x_{ij}^{\phi_1\phi_3} \cdot PL_{ij,t,s}^{\phi_3} - x_{ij}^{\phi_1\phi_3} \cdot QL_{ij,t,s}^{\phi_3}$$
$$+ \sqrt{3} \cdot r_{ij}^{\phi_1\phi_3} \cdot QL_{ij,t,s}^{\phi_3} + M \cdot (1 - \hat{y}_{ij,s}^{(\tau)} \cdot p_{ij}^{\phi_1}) \quad ; \forall i \in \mathcal{B}_j \cap \mathcal{B}, \forall j \in \mathcal{B}_i \cap \mathcal{K}_m \quad (2.59)$$

$$U_{i,t,s}^{\phi_1} - U_{j,t,s}^{\phi_1} \geq 2r_{ij}^{\phi_1\phi_1} \cdot PL_{ij,t,s}^{\phi_1} + 2x_{ij}^{\phi_1\phi_1} \cdot QL_{ij,t,s}^{\phi_1} - r_{ij}^{\phi_1\phi_2} \cdot PL_{ij,t,s}^{\phi_2} + \sqrt{3} \cdot x_{ij}^{\phi_1\phi_2} \cdot PL_{ij,t,s}^{\phi_2}$$
$$- x_{ij}^{\phi_1\phi_2} \cdot QL_{ij,t,s}^{\phi_2} - \sqrt{3} \cdot r_{ij}^{\phi_1\phi_2} \cdot QL_{ij,t,s}^{\phi_2} - r_{ij}^{\phi_1\phi_3} \cdot PL_{ij,t,s}^{\phi_3} - \sqrt{3} \cdot x_{ij}^{\phi_1\phi_3} \cdot PL_{ij,t,s}^{\phi_3} - x_{ij}^{\phi_1\phi_3} \cdot QL_{ij,t,s}^{\phi_3}$$
$$+ \sqrt{3} \cdot r_{ij}^{\phi_1\phi_3} \cdot QL_{ij,t,s}^{\phi_3} - M \cdot (1 - \hat{y}_{ij,s}^{(\tau)} \cdot p_{ij}^{\phi_1}) \quad ; \forall i \in \mathcal{B}_j \cap \mathcal{B}, \forall j \in \mathcal{B}_i \cap \mathcal{K}_m \quad (2.60)$$

$$-M \cdot p_{ij}^{\phi} \cdot l_{ij} \leq PL_{ij,t,s}^{\phi} \leq M \cdot p_{ij}^{\phi} \cdot l_{ij} \quad ; \forall i, j \in \mathcal{K}_m \quad (2.61)$$

$$-M \cdot p_{ij}^{\phi} \cdot l_{ij} \leq QL_{ij,t,s}^{\phi} \leq M \cdot p_{ij}^{\phi} \cdot l_{ij} \quad ; \forall i, j \in \mathcal{K}_m \quad (2.62)$$

$$-M.\hat{y}_{ij,s}^{(\tau)} \cdot p_{ij}^{\phi} \leq PL_{ij,t,s}^{\phi} \leq M \cdot \hat{y}_{ij,s}^{(\tau)} \cdot p_{ij}^{\phi} \quad ; \forall i \in \mathcal{B}_j \cap \mathcal{B}, \forall j \in \mathcal{B}_i \cap \mathcal{K}_m \quad (2.63)$$

$$-M.\hat{y}_{ij,s}^{(\tau)} \cdot p_{ij}^{\phi} \leq QL_{ij,t,s}^{\phi} \leq M \cdot \hat{y}_{ij,s}^{(\tau)} \cdot p_{ij}^{\phi} \quad ; \forall i \in \mathcal{B}_j \cap \mathcal{B}, \forall j \in \mathcal{B}_i \cap \mathcal{K}_m \quad (2.64)$$

$$PL_{ij,t,s}^{\phi} = \widehat{PL}_{ij,t,s}^{\phi,(\tau)} : \lambda_{t,s}^{m,\phi}; \forall i \in \mathcal{B}_j \cap \mathcal{B}, \forall j \in \mathcal{B}_i \cap \mathcal{K}_m \quad (2.65)$$

$$QL^{\phi}_{ij,t,s} = \widehat{QL}^{\phi,(\tau)}_{ij,t,s} : \gamma^{m,\phi}_{t,s}; \forall i \in \mathcal{B}_j \cap \mathcal{B}, \forall j \in \mathcal{B}_i \cap \mathcal{K}_m \tag{2.66}$$

$$Z^{i,m,\phi}_{1,t,s}, Z^{i,m,\phi}_{2,t,s}, Z^{i,m,\phi}_{3,t,s}, Z^{i,m,\phi}_{4,t,s} \geq 0 \quad ; \forall i, j \in \mathcal{K}_m \tag{2.67}$$

2.3 Solution Methodology

The flowchart of the proposed decentralized energy management is shown in Fig. 2.2 and summarized as follows:

Step (a): The distribution network operation problem (MP) is solved to obtain $\widehat{PL}^{\phi,(\tau)}_{ij,t,s}$, $\widehat{QL}^{\phi,(\tau)}_{ij,t,s}$ and $\hat{y}^{(\tau)}_{ij,s}$ considering any additional constraints from step d. The lower bound of the solution ($\hat{Z}^{(\tau)}_{lower}$) is calculated using (2.68).

$$\hat{Z}^{(\tau)}_{lower} = \sum_s pr_s \cdot \Bigg(\sum_{t\in T} \Big(\rho^t_f \cdot \big(\sum_{\phi} \hat{P}^{\phi,(\tau)}_{f,t,s} \big) + \sum_{g\in\mathcal{H}} F_g \big(\sum_{\phi} \hat{P}^{\phi,(\tau)}_{g,t,s} \big) + \sum_{e\in\mathcal{E}} \rho_e \cdot \big(\sum_{\phi} \hat{P}^{ch,\phi,(\tau)}_{e,t,s} + \hat{P}^{dc,\phi,(\tau)}_{e,t,s} \big) + VOLL \cdot \sum_{d\in\mathcal{D}} \sum_{\phi} \big(P^{D,\phi}_{t,s} - \hat{P}^{d,\phi,(\tau)}_{t,s} \big) \Big) \Bigg) + \sum_s \big(\sum_{t\in T} \hat{\alpha}^{(\tau)}_{t,s} \big) \tag{2.68}$$

Step (b): Microgrid operation problems (SPs) are solved. The upper bound of the solution ($Z^{(\tau)}_{upper}$) is calculated using (2.69).

$$\begin{aligned} \hat{Z}^{(\tau)}_{upper} = & \sum_s pr_s \cdot \Bigg(\sum_{t\in T} \Big(\rho^t_f \cdot \big(\sum_{\phi} \hat{P}^{\phi,(\tau)}_{f,t,s} \big) + \sum_{g\in\mathcal{H}} F_g \big(\sum_{\phi} \hat{P}^{\phi,(\tau)}_{g,t,s} \big) \\ & + \sum_{e\in\mathcal{E}} \rho_e \cdot \big(\sum_{\phi} \hat{P}^{ch,\phi,(\tau)}_{e,t,s} + \hat{P}^{dc,\phi,(\tau)}_{e,t,s} \big) + VOLL \cdot \sum_{d\in\mathcal{D}} \sum_{\phi} \big(P^{D,\phi}_{t,s} - \hat{P}^{d,\phi,(\tau)}_{t,s} \big) \Big) \Bigg) \\ & + \sum_m \Bigg(\sum_s pr_s \cdot \Bigg(\sum_{t\in T} \Bigg(\sum_{g\in\mathcal{H}_m} F_g \big(\sum_{\phi} \hat{P}^{\phi,(\tau)}_{g,t,s} \big) + \sum_{e\in\mathcal{E}_m} \rho_e \cdot \big(\sum_{\phi} \hat{P}^{ch,\phi,(\tau)}_{e,t,s} + \hat{P}^{dc,\phi,(\tau)}_{e,t,s} \big) \\ & + VOLL \cdot \sum_{d\in\mathcal{D}_m} \sum_{\phi} \big(P^{D,\phi}_{t,s} - \hat{P}^{d,\phi,(\tau)}_{t,s} \big) \Bigg) \Bigg) \Bigg) \end{aligned} \tag{2.69}$$

Step (c): If $\left| \frac{\hat{Z}^{(\tau)}_{upper} - \hat{Z}^{(\tau)}_{lower}}{\hat{Z}^{(\tau)}_{upper} + \hat{Z}^{(\tau)}_{lower}} \right| \leq \epsilon$, then terminate the algorithm. Otherwise, go to step d.

Step (d): Microgrid operators form the aggregated Benders cut (2.70) and add it to the

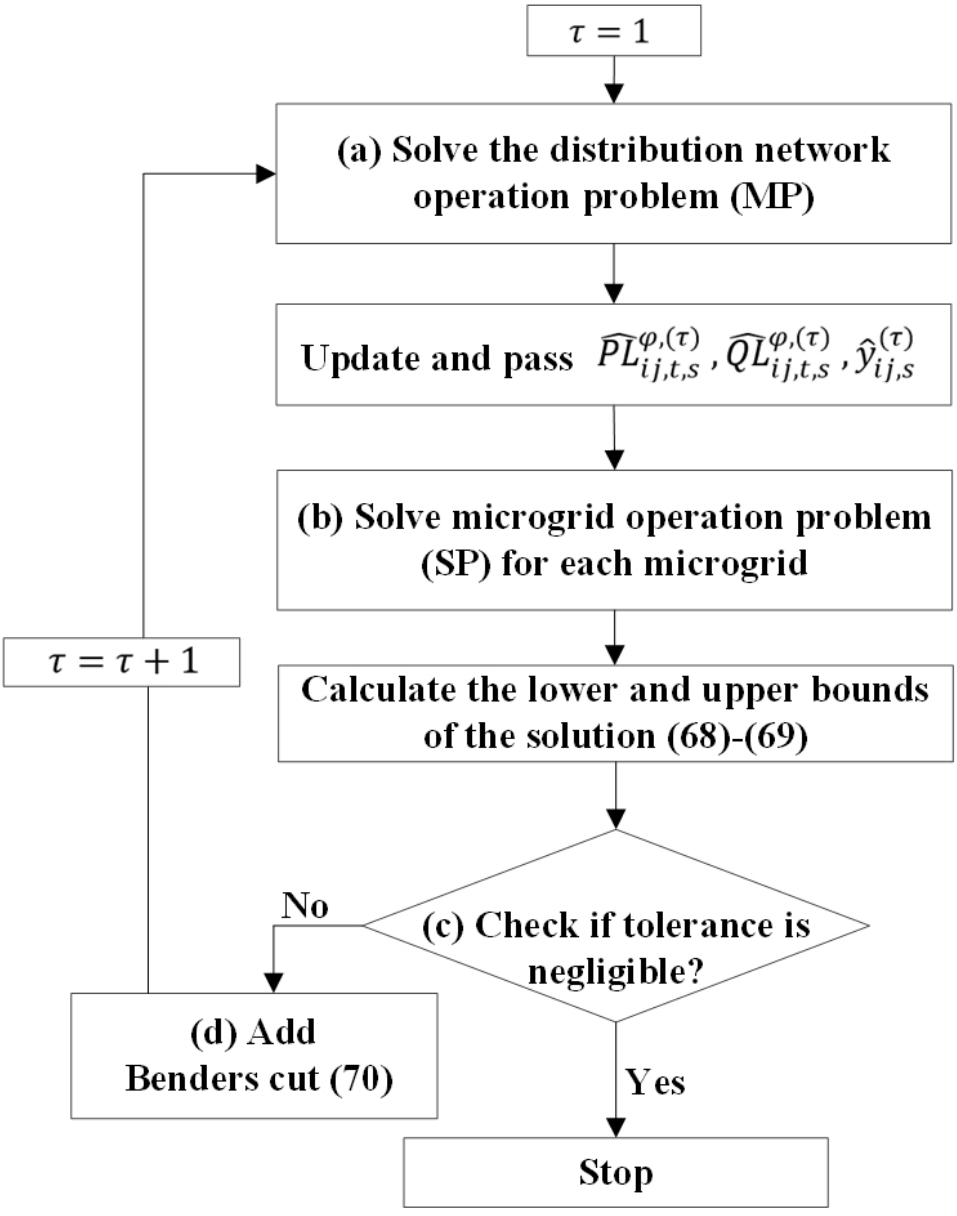

Figure 2.2: Flow chart of the proposed algorithm.

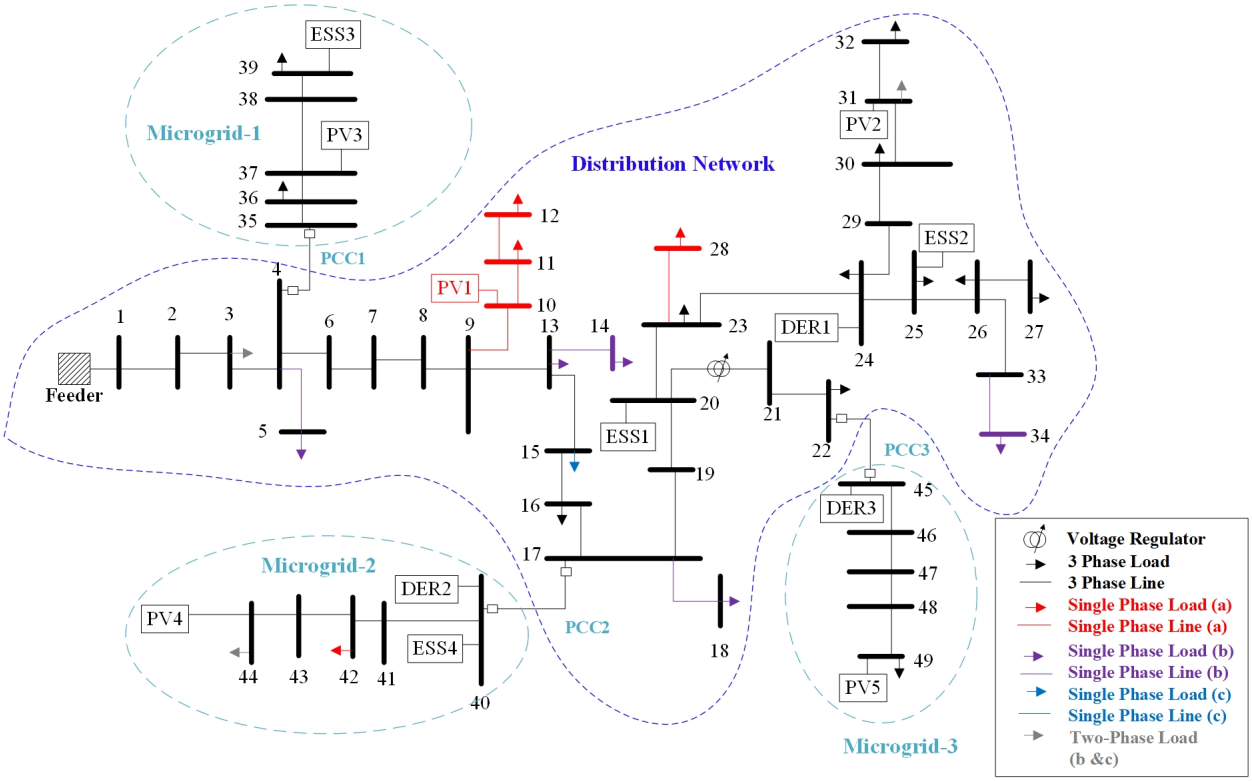

Figure 2.3: The modified IEEE-34 bus distribution network with networked microgrids.

distribution network operation problem (MP), where $\hat{W}_{t,s}^{m,(\tau)}$ is given in (2.71), then go to step a.

$$\alpha_{t,s} \geq \sum_{m} \Big(\hat{W}_{t,s}^{m,(\tau)} + \sum_{\phi} \hat{\lambda}_{t,s}^{m,\phi,(\tau)} \cdot (PL_{ij,t,s}^{\phi} - \widehat{PL}_{ij,t,s}^{\phi,(\tau)}) + \sum_{\phi} \hat{\gamma}_{t,s}^{m,\phi,(\tau)} \cdot (QL_{ij,t,s}^{\phi} - \widehat{QL}_{ij,t,s}^{\phi,(\tau)}) \Big)$$
$$; \forall i \in \mathcal{B}_j \cap \mathcal{B}, \forall j \in \mathcal{B}_i \cap \mathcal{K}_m \quad (2.70)$$

$$\hat{W}_{t,s}^{m,(\tau)} = pr_s \cdot \Big(\sum_{g \in \mathcal{H}_m} F_i(\sum_{\phi} \hat{P}_{g,t,s}^{\phi,(\tau)}) + \sum_{e \in \mathcal{E}_m} \rho_e \cdot (\sum_{\phi} \hat{P}_{e,t,s}^{ch,\phi,(\tau)} + \hat{P}_{e,t,s}^{dc,\phi,(\tau)})$$
$$+VOLL \cdot (\sum_{d \in \mathcal{D}_m} \sum_{\phi} P_{t,s}^{D,\phi} - \hat{P}_{t,s}^{d,\phi,(\tau)}) + M \cdot (\sum_{\phi} \sum_{i \in \mathcal{K}_m} \hat{Z}_{1,t,s}^{i,m,\phi,(\tau)} + \hat{Z}_{2,t,s}^{i,m,\phi,(\tau)} + \hat{Z}_{3,t,s}^{i,m,\phi,(\tau)} + \hat{Z}_{4,t,s}^{i,m,\phi,(\tau)}) \Big)$$
(2.71)

2.4 Numerical Results

The modified IEEE-34 bus distribution network is used with three unbalanced microgrids to show the effectiveness of the proposed framework. Later, the IEEE-123 bus distribution network with three microgrids is used to evaluate the scalability of the proposed framework. The IEEE-34 bus distribution network with three microgrids is shown in Fig. 2.3. The microgrids are connected to the three-phase distribution network through the points of common coupling (PCC). The objective is to minimize the expected operation cost of the distribution network and microgrids. The upper and lower limits for the bus voltage magnitudes are 1.05 and 0.95 of their nominal values respectively. The voltage on slack bus is set to 1.05 of the nominal value. The maximum and minimum transformer ratios for the voltage regulator is 1.1 and 0.9 respectively. The main distribution feeder capacity is 1.8 MVA with a minimum power factor of 0.9. Lithium-ion battery is used as the energy storage system (ESS) with the capital cost of 450 \$/kWh [103]. The operation cost of the energy storage is 0.25 \$/kWh using the model presented in [104] The charging and discharging efficiency for the energy storage unit is 90%. The value of lost load (VOLL) is \$40/kWh and the convergence tolerance ϵ is 0.01%. The hourly energy prices and total hourly demand in the distribution network and microgrids are shown in Fig. 2.4 The characteristics of DERs, ESS, and PVs are shown in Tables 2.2, 2.3, and 2.4 respectively. The quadratic cost of DERs are piecewise linearized using four segments, each covering 1/4 of maximum power capacity of the unit. The marginal costs of DERs at each segment are shown in Table 2.5. The simulation is performed on a server with dual 14 Core Intel Xeon 2.6 GHz, 380 GB of memory, with Cplex 12.8. The following cases are considered:

Case 1 – Deterministic solution under normal operating condition.

Case 2 – Deterministic solution considering the islanding of microgrid-2.

Case 3 – Stochastic solution considering the branch outage in microgrid-1.

Case 4 – Stochastic solution considering the islanding of microgrid-2.

Case 5 – Stochastic solution considering the probabilistic islanding of microgrids.

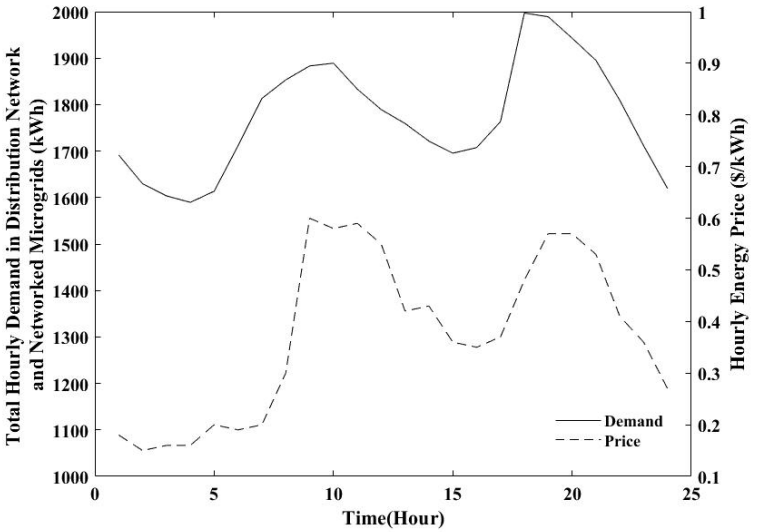

Figure 2.4: Total hourly demand in the distribution network and networked microgrids and the hourly energy prices.

Table 2.2: Dispatchable generation resources

Unit	Bus	P_{min} (kW)	P_{max} (kW)	Q_{min} (kVAR)	Q_{max} (kVAR)
Distribution Feeder	1	0	1800	-850	850
DER1	24	0	100	-50	50
DER2	40	0	80	-40	40
DER3	45	0	90	-45	45

Table 2.3: ESS Characteristics

Unit	Bus	P_{max} (kW)	Q_{max} (kVAR)	E_{min} (kWh)	E_{max} (kWh)
ESS1	20	50	25	10	100
ESS2	25	60	30	10	120
ESS3	39	40	20	5	60
ESS4	40	30	15	5	50

Table 2.4: Generation limits of PV units

Unit	Bus	P_{min} (kW)	P_{max} (kW)	Q_{min} (kVAR)	Q_{max} (kVAR)
PV1	10	0	100	-80	80
PV2	30	0	100	-90	90
PV3	37	0	50	-40	40
PV4	44	0	65	-55	55
PV5	49	0	75	-60	60

Table 2.5: The marginal costs of DERs

Units	Marginal Costs ($/kWh)			
	Segment 1	Segment 2	Segment 3	Segment 4
DER1	0.06	0.16	0.21	0.36
DER2	0.05	0.15	0.20	0.35
DER3	0.04	0.13	0.22	0.30

2.4.1 Case 1 - Deterministic solution under normal operating condition

In this case, the deterministic solution under normal operation is procured. The upper and lower bounds for the solution i.e. $\hat{Z}^{(\tau)}_{lower}$ and $\hat{Z}^{(\tau)}_{upper}$ are shown in Fig. 2.5 and the algorithm converges after 698 iterations. The exchanged real and reactive power flows between the distribution network and microgrid-1 on phase "a" are shown in Fig. 2.6 and Fig. 2.7 respectively. The exchanged real power on each phase between the distribution network and microgrids at hour 18 (hour of peak demand) is shown in Table 2.6. Here, a positive value refers to the power flow from the distribution network to a microgrid. The operation costs and load curtailments are shown in Table 2.7. As shown in this table, the operation cost of microgrid-1 is $22.05. In microgrid-1, the operation cost is limited to its energy storage operation cost as there is no DER or load curtailment in this microgrid. At hour 18, the real power flows from the distribution network to microgrid-1 as shown in Table 2.6. The oper-

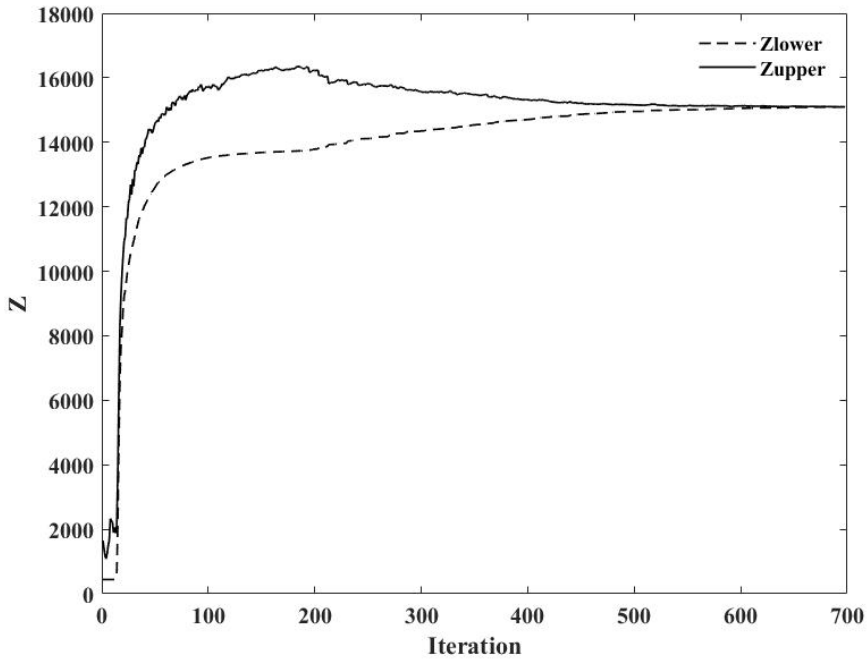

Figure 2.5: The upper and lower bounds of the solution in Case 1.

ation costs associated with DERs for microgrid-2 and microgrid-3 are \$151.96 and \$146.33 respectively. Microgrid-2 provides energy to the distribution network on phase "b" during the peak hour. Meanwhile, microgrid-3 supports the distribution network on phases "a" and "c" with cheaper DER. The distribution network operation cost is \$14,773.99 which includes the cost of serving microgrids. The total operating cost in this case is \$15,094.33.

Here, the procured solution is compared with the solution procured by solving the energy management problem for distribution network with microgrids as a single mixed integer linear programming (MILP) problem using branch and cut search algorithm, and as a distributed optimization problem using the ADMM technique. Table 2.8 presents the operation costs of the distribution network and microgrids procured by solving a MILP problem using branch and cut algorithm. As shown in this table, because $\epsilon = 10^{-4}$, the solution procured using the proposed algorithm is \$4.23 higher than the solution to the MILP problem using branch and cut search method. Selecting lower value for ϵ will reduce the difference between the procured solution and the solution to MILP problem. It is worth noting that solving

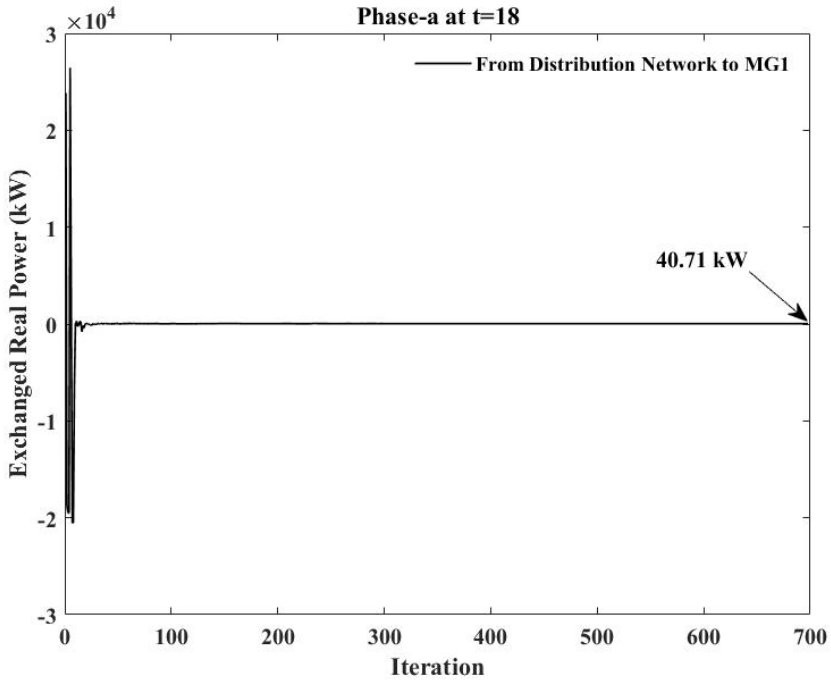

Figure 2.6: Exchanged real power flow between the distribution network and microgrid-1 on phase "a" in Case 1.

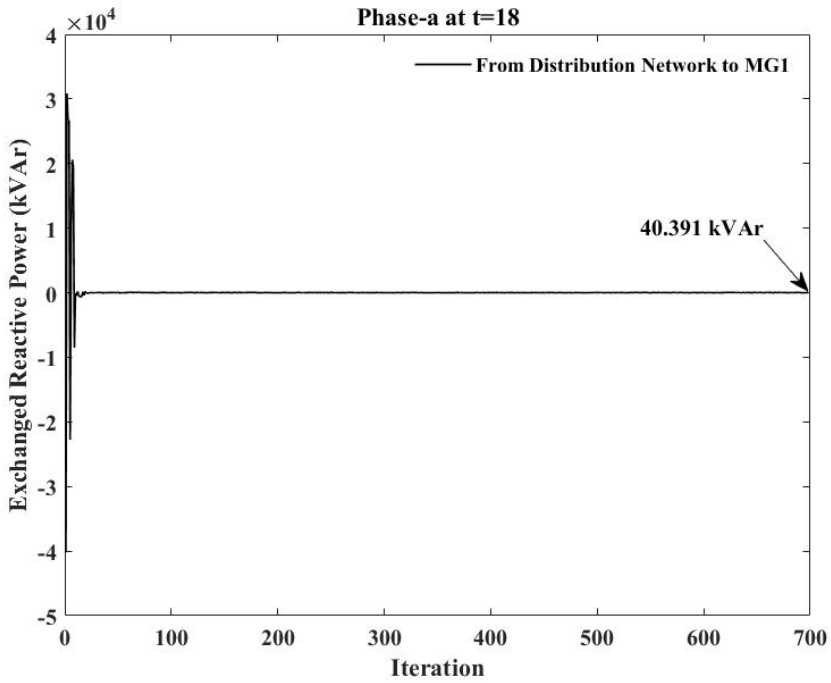

Figure 2.7: Exchanged reactive power flow between the distribution network and microgrid-1 in on phase "a" in Case 1.

Table 2.6: Exchanged real power flow between the distribution network and microgrids at hour 18 in Case 1

Line	Power Flow on phases (kW)		
	a	b	c
DN-Microgrid-1	40.71	33.487	33.171
DN-Microgrid-2	11.416	-9.91	9.152
DN-Microgrid-3	-11.744	14.97	-14.989

Table 2.7: Operation cost and demand curtailment in Case 1

Operator	Operation Cost	Total Curtailment (kWh)
DNO	\$14,773.99	0
Microgrid-1	\$22.05	0
Microgrid-2	\$151.96	0
Microgrid-3	\$146.33	0
Total	\$15,094.33	0

the MILP problem requires access to the distribution network's and networked microgrids' data, which may not be a practical assumption. The proposed algorithm to solve the energy management problem requires limited information sharing among the DNO and microgrids' operators.

Here, the solution procured by the proposed algorithm is compared with the solution procured using the ADMM method. The simulation outcomes for Case 1 using the ADMM method are shown in Table 2.9. Considering the convergence tolerance $\epsilon = 10^{-4}$ in both algorithms, the total operation cost of the distribution network and microgrids using the ADMM algorithm is \$86.05 higher than that procured using the proposed algorithm. Moreover, the proposed algorithm converges faster than the ADMM algorithm. The solution time using the proposed algorithm is 47 min and 4 sec, while the solution time using the ADMM algorithm is 58 min and 36 sec. To solve this problem using the ADMM algorithm, the real and

Table 2.8: The operation cost using the proposed algorithm and MILP formulation in Case1

Operator	Operation cost ($) using the proposed algorithm	Operation cost ($) using MILP formulation
DNO	$14,773.99	$14,768.70
Microgrid-1	$22.05	$19.27
Microgrid-2	$151.96	$158.42
Microgrid-3	$146.33	$143.71
Total	$15,094.33	$15,090.10

Table 2.9: The operation cost using the proposed algorithm and the ADMM approach in Case 1

Operator	Operation cost using the proposed algorithm ($)	Operation cost using ADMM approach ($)
DNO	$14,773.99	$14,896.92
Microgrid-1	$22.05	$0.36
Microgrid-2	$151.96	$138.95
Microgrid-3	$146.33	$144.15
Total	$15,094.33	$15,180.38

reactive power in the coupling lines between the distribution network and microgrids, and the bus voltages at the PCCs are shared among the microgrids' and distribution network's operators. It is worth noting that ADMM method suffers from divergence when applied to solve non-convex optimization problems [105].

2.4.2 Case 2 – Deterministic solution considering the islanding of microgrid-2

In this case, all microgrids are operating in grid-connected mode, except microgrid-2 which is islanded from the distribution network. Table 2.10 shows the exchanged real power between the distribution network and microgrids at hour 18. The operation costs and load curtailments for the distribution network and microgrids are shown in Table 2.11. Compared to Case 1, at hour 18, the power flows on phases "a" and "c" from distribution network

Table 2.10: Exchanged real power flow between the distribution network and microgrids at hour 18 in Case 2

Line	Power Flow on phases (kW)		
	a	b	c
DN-Microgrid-1	34.771	40.001	29.095
DN-Microgrid-2	0	0	0
DN-Microgrid-3	-1.139	-1.789	12.428

Table 2.11: Operation cost and demand curtailment in Case 2

Operator	Operation Cost	Total Curtailment (kWh)
DNO	$14,689.95	0
Microgrid-1	$32.55	0
Microgrid-2	$409.99	0
Microgrid-3	$80.96	0
Total	$15,213.45	0

to microgrid-1 are reduced because of ESS operation in microgrid-1. Here, the operation cost of ESS in microgrid-1 is increased to $32.55 and the total operation cost is increased to $15,213.45 because of the increase in the operation costs of microgrid-1 and microgrid-2. The operation cost of microgrid-2 is increased to $409.99 as it is operated in the island mode. Compared to Case 1, as distribution network and microgrid-3 do not support microgrid-2, their operation costs are reduced to $14,689.95 and $80.96 respectively. The algorithm converged after 276 iterations.

2.4.3 Case 3 – Stochastic solution considering the branch outage in microgrid-1

In this case, the stochastic solutions considering the uncertainty in demand and renewable energy resources are presented. Here, 3000 scenarios are generated using Monte Carlo simulation to capture the uncertainty in the PV generation and demand. The forecast errors in solar irradiation and demand are represented by Gaussian distribution function with the

Table 2.12: Probability of scenarios

Scenario	1	2	3	4	5
Probability	0.1093	0.09	0.1077	0.1163	0.111
Scenario	6	7	8	9	10
Probability	0.0823	0.0931	0.1023	0.1207	0.0673

Table 2.13: Stochastic solution under normal operating condition

Operator	Expected operation cost	Total expected Load curtailment (kWh)
DNO	$14,785.19	0
Microgrid-1	$21.67	0
Microgrid-2	$179.70	0
Microgrid-3	$142.28	0
Total	$15,128.84	0

mean value equal to the forecasted values in Case 1, and the standard deviation equal to 3% of the mean values. The backward scenario reduction technique is used to reduce the number of scenarios to 10. The probability of each scenario is shown in Table 2.12. In this case all microgrids are operating in grid-connected mode. The expected operation cost and the expected load curtailments in the microgrids and distribution network under normal operating condition are shown in Table 2.13. Compared to Case 1, the total expected operation cost is increased to $15,128.84 as the expected demand is increased by 22.544 kWh.

The outage on the branch between buses 37 and 38 in microgrid-1 for 24 hours, results in demand curtailment and consequently decreases the expected real power flow between the distribution network and microgrid-1. The expected operation costs and expected load curtailments in microgrids and distribution network are shown in Table 2.14. Compared to normal operating condition, the total expected operation cost is increased to $51,433.51 because of the penalty associated with the demand curtailment in microgrid-1. The total expected demand curtailments in microgrid-1 on phases “a”, “b”, and “c” are 303.270 kWh,

Table 2.14: Expected operation cost and demand curtailment in Case 3

Operator	Expected operation cost	Total expected load curtailment (kWh)
DNO	\$14,452.74	0
Microgrid-1	\$36,718.22	917.956
Microgrid-2	\$141.94	0
Microgrid-3	\$120.61	0
Total	\$51,433.51	917.956

366.738 kWh, and 247.948 kWh respectively. The expected operation cost of the distribution network is reduced to \$14,452.74 because of the reduction in the served demand of microgrid-1. Similarly, the expected operation costs of microgrid-2 and microgrid-3 are reduced to \$141.94 and \$120.61 respectively. The algorithm converged after 307 iterations.

2.4.4 Case 4 – Stochastic solution considering the islanding of microgrid-2.

In this case, microgrid-2 is islanded from the distribution network for 24 hours. The expected exchanged real power on three phases between the distribution network and microgrids at hour 18 are presented in Table 2.15. The expected operation costs and the expected demand curtailments are presented in Table 2.16. Compared to Case 2, the expected real power flow between the distribution network and microgrid-1 is increased because of the increase in the total expected demand in this microgrid. Here, the total expected demand of microgrid-1 is increased by 1.366 kWh compared to Case 2. Furthermore, the total expected operation cost is increased by \$23.68 as the expected power outputs of the DERs are increased to address the uncertainty in demand and PV generation.

Compared to the stochastic solution under normal condition, the total expected operation cost is increased to \$15,237.13 because of the increase in the expected operation cost of microgrid-1 and the higher expected operation cost of microgrid-2 with more expensive DER. Here, microgrid-2 has enough generation capacity to supply its load, and the expected operation cost is increased to \$409.36 as more expensive local generation assets are used to serve the load in the island mode. The expected operation cost of the distribution network is

Table 2.15: Expected exchanged real power flow between the distribution network and microgrids at hour 18 in Case 4

Line	Power Flow on phases (kW)		
	a	b	c
DN-Microgrid-1	40.227	42.124	37.985
DN-Microgrid-2	0	0	0
DN-Microgrid-3	-17.37	4.849	8.604

Table 2.16: Expected operation cost and demand curtailment in Case 4

Operator	Expected operation cost	Total expected load curtailment (kWh)
DNO	$14,672.52	0
Microgrid-1	$22.37	0
Microgrid-2	$409.36	0
Microgrid-3	$132.88	0
Total	$15,237.13	0

reduced to $14,672.52 as the demand is reduced by islanding microgrid-2. Similarly, the expected operation cost of microgrid-3 is reduced from $142.28 in normal condition to $132.88 in this case, as this microgrid will not supply microgrid-2. The algorithm converged after 224 iterations.

2.4.5 Case 5 – Stochastic solution considering the probabilistic islanding of microgrids

In this case, the lower bound for the probability of islanding in each microgrid is 13%. The expected exchanged real powers between the microgrids and distribution network at hour 18 are shown in Table 2.17. Compared to the stochastic solution under normal operation, the expected power flow between the distribution network and microgrid-1 is reduced as the demand is curtailed in the islanded operation of microgrid-1 in some scenarios. Here, microgrid-1 is in island mode in scenarios 6 and 10 with the total probability of 14.96%. Microgrid-2 is in island mode in scenarios 2 and 4 with the total probability of 20.63% and

Table 2.17: Expected exchanged real power flow between the distribution network and microgrids at hour 18 in Case 5

Line	Power flow on phases (kW)		
	a	b	c
DN-Microgrid-1	33.554	35.769	35.794
DN-Microgrid-2	0.055	2.651	11.475
DN-Microgrid-3	-7.832	1.372	-2.564

Table 2.18: Expected operation cost and demand curtailment in Case 5

Operator	Expected operation cost	Expected load curtailment (kWh)
DNO	$14,659.33	0
Microgrid-1	$13,538.49	337.998
Microgrid-2	$242.31	0
Microgrid-3	$147.52	0
Total	$28,587.65	337.998

microgrid-3 is in island mode in scenarios 1 and 2 with the total probability of 19.93%. The expected operation costs and the expected demand curtailments are presented in Table 2.18. Compared to the stochastic solution under normal condition, the expected operation cost of the distribution network is reduced to $14,659.33 as the microgrid demands are not served by the distribution network in some scenarios. The expected operation cost of microgrid-1 is increased to $13,538.49 because of the penalty associated with the loss of demand in some scenarios. In microgrid-2, as the power dispatch of the expensive DER is increased, the expected operation cost is increased to $242.31. Similarly, the expected operation cost of microgrid-3 is increased to $147.52. There is no demand curtailment in microgrid-2 and microgrid-3 and the algorithm converged after 517 iterations.

Table 2.19 summarizes the operation cost of the microgrids and distribution network in Cases 1-5. Furthermore, the sensitivity of the total expected operation cost to the probability

Table 2.19: Expected operation cost ($) in Cases 1-5

	Case 1	Case 2	Case 3	Case 4	Case 5
DNO	14,773	14,689	14,452	14,672	14,659
Microgrid-1	22.05	32.55	36,718	22.37	13,538
Microgrid-2	151.96	409.99	141.94	409.36	242.31
Microgrid-3	146.33	80.96	120.61	132.88	147.52
Total	15,094	15,213	51,433	15,237	28,587

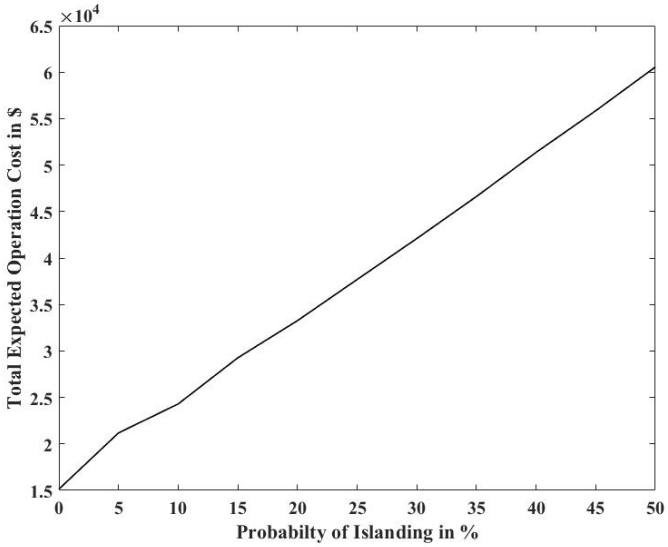

Figure 2.8: Sensitivity of the total expected operation cost to the probability of islanding in microgrids.

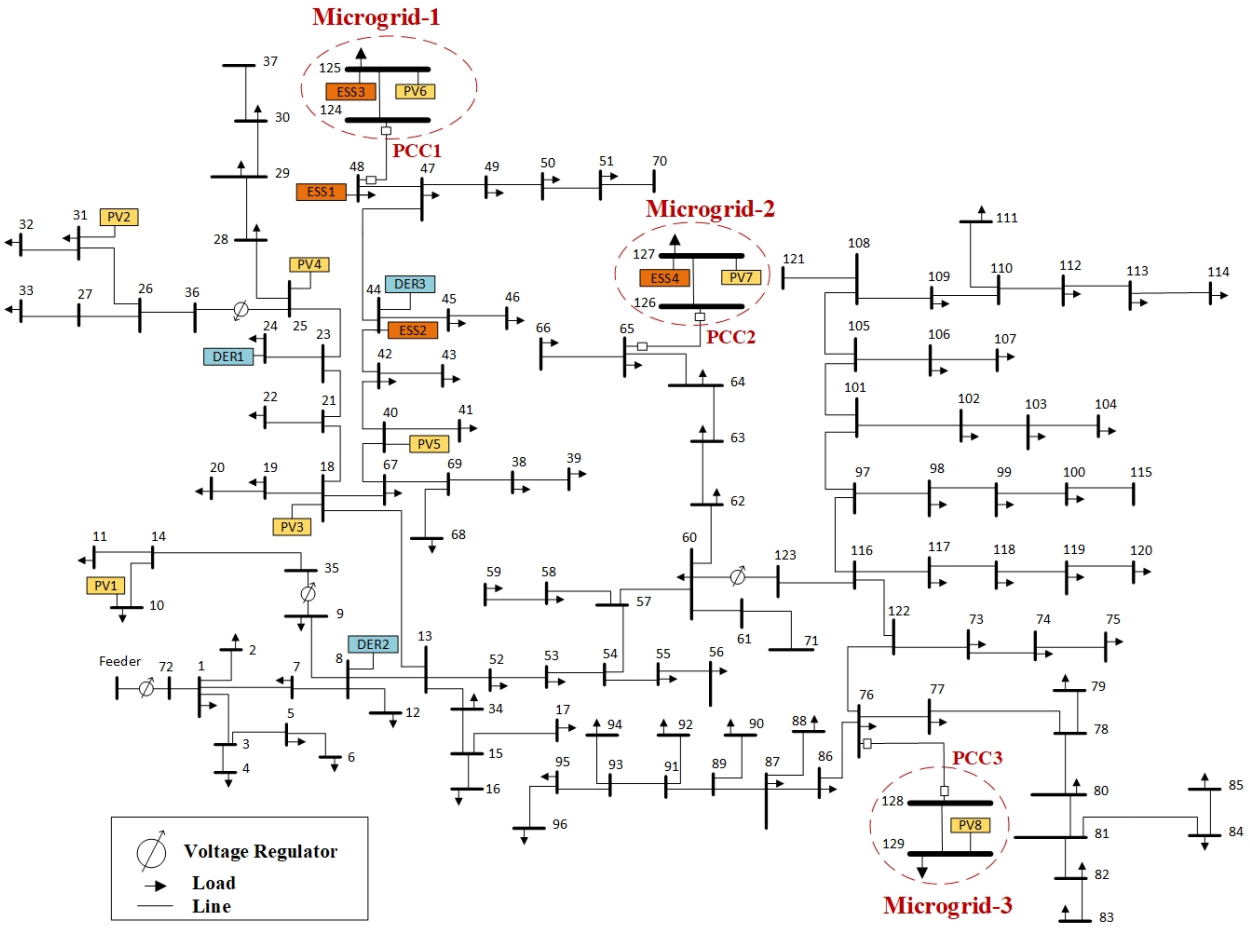

Figure 2.9: The modified IEEE-123 bus distribution network with networked microgrids.

of islanding in the microgrids is evaluated. Here, the probability of islanding in each microgrid is changing from 0% to 50%. As shown in Fig. 2.8, the total expected operation cost is increased as the probability of islanding increases.

2.5 Scalability and Computation Efficiency

In this section, the computation efficiency of the proposed approach is discussed. Table 2.20 shows the solution time of the proposed algorithm for five cases applied to the IEEE-34 bus with the relative optimality gap $\epsilon = 10^{-4}$. To validate the scalability of the proposed algorithm, the modified IEEE-123 bus distribution network with three unbalanced microgrids shown in Fig. 2.9, is used. Five scenarios with the probabilities shown in Table 2.21 are

Table 2.20: Solution time of the proposed algorithm for Cases 1-5

Case	Tolerance	Solution Time
IEEE-34 bus system - Case 1	0.01%	47 min 04 sec
IEEE-34 bus system - Case 2	0.01%	17 min 55 sec
IEEE-34 bus system - Case 3	0.01%	2 hr 41 min 42 sec
IEEE-34 bus system - Case 4	0.01%	2 hr 12 min 14 sec
IEEE-34 bus system - Case 5	0.01%	6 hr 46 min 55 sec
IEEE-123 bus system - Case 5	1%	12 hr 58 min 4 sec
IEEE-123 bus system - Case 5	2%	9 hr 38 min 19 sec
IEEE-123 bus system - Case 5	5%	5 hr 39 min 45 sec

Table 2.21: Probability of scenarios for the modified IEEE-123 bus system

Scenario	1	2	3	4	5
Probability	0.1707	0.1593	0.2217	0.1610	0.2873

considered. The characteristics of DER, ESS, and PV units are shown in Tables 2.22, 2.23, and 2.24 respectively. The marginal costs of DERs are similar to those in Table 2.5. Four voltage regulators are considered as shown in Fig. 2.9. The relative optimality gap for this case is 0.01. If the probability of islanding of each microgrid is 5%, the total expected operation cost of the distribution network and microgrids is $30,422.83. The solution time for the day-ahead operation, in this case, is 12 hr, 58 min, and 4 sec. The solution time reduces as the optimality gap increases as shown in Table 2.20 and therefore, there is a trade-off between accuracy and solution time [98]. The solution time could be further decreased by solving the microgrid operation problems (SPs) in parallel [106] and using network reduction techniques to reduce the size of the problem [107]

2.6 Conclusion

In this chapter, a decentralized operation framework for the distribution network and microgrids is proposed that leverages Bender's decomposition technique. The algorithm

Table 2.22: Dispatchable resources' characteristics in the modified IEEE-123 bus system

Unit	Bus	P_{min} (kW)	P_{max} (kW)	Q_{min} (kVAR)	Q_{max} (kVAR)
Distribution Feeder	1	0	3500	-2500	2500
DER1	24	0	100	-50	50
DER2	8	0	80	-70	70
DER3	44	0	90	-70	70

Table 2.23: ESS characteristics in the modified IEEE-123 bus system

Unit	Bus	P_{max} (kW)	Q_{max} (kVAR)	E_{min} (kWh)	E_{max} (kWh)
ESS1	48	50	25	10	100
ESS2	44	60	30	10	120
ESS3	125	40	20	5	60
ESS4	127	30	15	5	50

Table 2.24: PV units' characteristics in the modified IEEE-123 bus system

Unit	Bus	P_{min} (kW)	P_{max} (kW)	Q_{min} (kVAR)	Q_{max} (kVAR)
PV1	10	0	100	-80	80
PV2	31	0	100	-90	90
PV3	18	0	100	-50	50
PV4	25	0	200	-100	100
PV5	40	0	100	-50	50
PV6	125	0	50	-40	40
PV7	127	0	65	-55	55
PV8	129	0	75	-60	60

aims to coordinate the operation decisions between the distribution network and the microgrids considering the unbalanced demand and PV generation in the distribution network. The uncertainties in PV generation and demand in microgrids and distribution network are captured using Monte Carlo simulation and the risk associated with the islanded operation of microgrids was addressed. The interaction between the distribution and microgrids' operators aims to reduce the total operation cost under multiple operating conditions. The proposed algorithm is applied to the IEEE 34-bus distribution network with three connected microgrids. The modified IEEE-123 bus distribution network with three unbalanced microgrids is also used to validate the performance of the proposed algorithm. The impact of the outages in microgrids, as well as the islanding of microgrids, were evaluated on the operation of the distribution network with networked microgrids. It is shown that the islanding in microgrids with expensive generation resources will increase the operation cost of the microgrid while reducing the operation cost of the distribution network. Furthermore, the expected total operation cost will increase as the probability of the grid-connected operation mode of the microgrids decreases.

Chapter 3

Stochastic Expansion Planning of Battery Energy Storage for the Interconnected Distribution and Data Networks

This chapter presents a stochastic expansion planning approach to determine the installation time, location, and capacity of battery energy storage systems in distribution networks with data centers. Benders decomposition is used to capture the interactions between these autonomous operators in the electricity and data networks. The uncertainties associated with the electric demand, data center workload, solar PV generation, and the availability of the distribution branches are captured using Monte Carlo simulation. The representative scenarios are selected using a dissimilarity-based sparse subset selection algorithm. To evaluate the effectiveness of the proposed framework, numerical results are presented for a modified IEEE-34 bus distribution network with data centers and PV generation units.

The physical layout of the distribution network supplying energy to data centers is shown in Fig.3.1. As shown in this figure, the distribution network and data centers are operated by two independent entities [43], [45], [47]. The data center operator (DCO) distributes the workloads received from the end-users among the data centers. The data centers process the workloads by using the electricity supplied by the distribution network. The distribution network is operated and managed by the distribution network operator (DNO). The decisions made by the DCO on allocating the workloads to the data centers will impact their electricity demands. The variations in data center demands modify the spatiotemporal demand profile in the distribution network and impact the economics and security of the distribution network. Similarly, the decisions made by the DNO impact the long-term security and reliability of energy supply to the data centers. Such decisions could further affect the efficiency and reliability of the services offered by the data centers to the end-users in data networks. As the information shared between DNO and DCO is limited, lacking coordination among these entities could lead to deficiency in energy supply to data centers

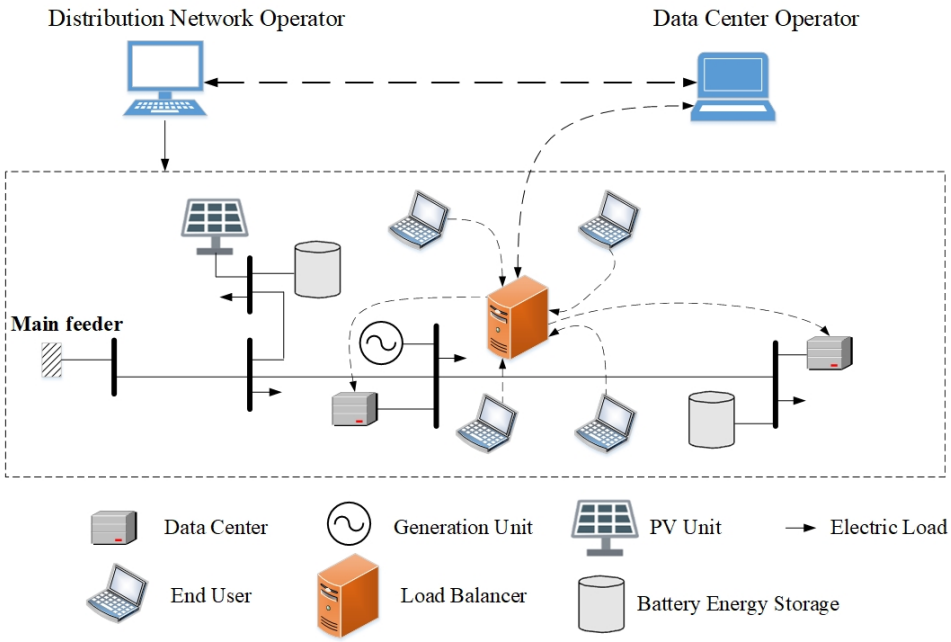

Figure 3.1: Physical and control layouts of the distribution network with data centers.

and therefore shortage in the workload processing capacity, or increase in the electricity demand in the distribution network and eventually violation of the network constraints which could lead to demand curtailments. Therefore, effective coordination among DCO and DNO benefits the end-users in the data network by improving the quality of service provided by the data centers and improves the economics and security of the distribution network in the long-term operation.

In this chapter, a stochastic framework for the expansion planning of BES in a distribution network that serves data centers is presented. The presented framework captures the interaction between DNO and DCO. As the information sharing among DNO and DCO is limited, the presented framework leverages Benders decomposition to formulate the expansion planning problem for the DNO and the long-term operation problem for the DCO. The uncertainties in demand, data center workload, the power output of PV generation, and the availability of the distribution branches are considered using scenarios. The proposed framework determines the expansion plans for BES units while ensuring energy security for the data centers and the reliability of the distribution network. The contributions of this

work are summarized as follows:

– An expansion planning framework for BES units is proposed to determine the location, capacity, and installation time of the BES units in the distribution network with PV generation and data centers.

– The interactions among DNO and DCO are captured using the Bender decomposition technique to address the limited information shared among data center and distribution network operators.

– The uncertainties in electric demand, data center workload, the power output of PV generation units, and the outages of the distribution lines are considered in the long-term planning horizon. A dissimilarity-based sparse subset selection (DS3) algorithm is used to cluster the hourly data, select the most effective representative data, and determine the representative scenarios.

The chapter is organized as follows, a list of symbols used in this chapter is presented in Section 3.1. The problem formulation and solution methodology are presented in Sections 3.2 and 3.3, respectively. DS3 algorithm is presented in Section 3.4. A case study using the modified IEEE-34 bus distribution network is presented in Section 3.5. Finally, the conclusions are drawn in Section 3.6.

3.1 List of Symbols

Indices and Sets:

t	Index of hour
d	Index of representative day
y	Index of year
s	Index of scenario
i,j	Index of bus
l	Index of load in the distribution network
f	Index of distribution feeder
g	Index of distributed generation
b	Index of distribution network branch
e	Index of battery energy storage (BES) unit

c	Index of data center
v	Index of solar photovoltaic unit
ch	Index of battery charging mode
dc	Index of battery discharging mode
Ω_i	Set of candidate buses to install BES unit

Variables:

$Y_e^{i,y}$	Binary variable representing the installation decision for BES unit e on bus i
$\mu_e^{i,y}$	Binary variable for existence of BES unit e at bus i
$E_{e,s}^{t,d,y}$	Stored energy in the battery storage e
$p_{f,s}^{t,d,y}$	Purchased real power from the main feeder f
$q_{f,s}^{t,d,y}$	Reactive power from the main feeder f
$p_{g,s}^{t,d,y}$	Real power dispatch of distributed generation unit g
$q_{g,s}^{t,d,y}$	Reactive power dispatch of distributed generation unit g
$p_{v,s}^{t,d,y}$	Real power generation of photovoltaic unit v
$q_{v,s}^{t,d,y}$	Reactive power generation of photovoltaic unit v
$p_{ch,e,s}^{t,d,y}$	Real power of BES unit e in charging mode
$p_{dc,e,s}^{t,d,y}$	Real power of BES unit e in discharging mode
$q_{e,s}^{t,d,y}$	Reactive power output of BES unit e
$p_{c,s}^{t,d,y}$	Real power demand of data center c
$p_{b,s}^{t,d,y}$	Real power flow in the distribution network branch b
$q_{b,s}^{t,d,y}$	Reactive power flow in the distribution network branch b
$U_{i,s}^{t,d,y}$	Squared voltage at bus i
$Z_{(.),s}^{t,d,y}$	Slack variables
$w_{c,s}^{t,d,y}$	Workload processed by data center c
$\pi_e^y, \pi_{c,s}^{t,d,y}$	Dual variables
$LS_{l,s}^{t,d,y}$	Demand curtailment

Parameters:

η	Annual discount rate
C_e	Investment cost of BES unit e
T_d	Total number of representatives
T_y	Total number of years
T_s	Total number of scenarios
T	Total number of hours
N_d	Number of days in representative d
$\tilde{P}_{v,s}^{t,d,y}$	Forecasted real power of photovoltaic unit v
$p_{l,s}^{t,d,y}$	Real power load in the distribution network
$q_{l,s}^{t,d,y}$	Reactive power load in the distribution network
$\phi_{b,s}^{t,d,y}$	Availability of the distribution network branch b;
	1 if a branch is available and 0 otherwise
r_{ij}^{b}	Resistance of branch b connecting buses i and j
x_{ij}^{b}	Reactance of branch b connecting buses i and j
S_b^{max}	Maximum apparent power of distribution branch b
V_i^{max}	Maximum acceptable bus voltage
V_i^{min}	Minimum acceptable bus voltage
pr_s	Probability of scenario s
$\Delta_s^{t,d,y}$	Total workload received from the end-users
$\lambda_g, \beta_g, \gamma_g$	Coefficients in the quadratic cost function of
	distributed generation unit g
w_c^{max}	Maximum workload in data center c
p_c^{max}	Maximum real power consumption of data center c
p_e^{max}	Maximum real power dispatch of BES unit e
q_e^{max}	Maximum reactive power dispatch of BES unit e
E_e^{max}	Maximum stored energy in BES unit e
E_e^{min}	Minimum stored energy in BES unit e
E_e^{0}	Initial stored energy in BES unit e
$\rho_{f,s}^{t,d,y}$	Hourly price of energy supplied by the main feeder f
ρ_e	Operation cost of BES unit e

δ_f	Minimum power factor for feeder f
$A_{(.)}$	Bus-unit incidence matrix
$D_{(.)}$	Bus-demand incidence matrix
B	Bus-branch incidence matrix
$EENS_y^{max}$	Acceptable annual expected energy not supplied
$VOLL$	Value of lost load

3.2 Problem Formulation

Fig. 3.2 shows the structure of the proposed stochastic expansion planning problem for the BES in distribution networks that captures the interactions between the DCO and DNO to solve this problem. As shown in this figure, DNO solves the BES expansion planning problem (master problem) to determine the location, capacity, and time of BES installations. Here, the objective is to minimize the investment cost of the BES units. Once the initial expansion decisions are determined, DNO solves the distribution network operation sub-problem. The objective of this sub-problem is to minimize the expected operation cost of the distribution network while satisfying the network constraints. Here, DNO checks for the feasibility and optimality of the expansion decisions considering the imposed uncertainties in the long-term operation horizon. If the expansion decisions are not feasible or optimal in the distribution network, the operation signal in the form of a Benders cut is sent to the expansion planning problem to revise the expansion decisions. Once the expansion decisions are optimal and feasible for the distribution network, the distribution network reliability is evaluated by solving the distribution network reliability evaluation sub-problem. If the expansion plans do not satisfy the system reliability, a reliability signal (Benders cut) is sent to the expansion planning problem.

Once the expansion decisions satisfy the reliability constraint in the distribution network, the power supplied to the data center is passed to the data center feasibility sub-problem solved by the DCO. Similarly, the interaction between DNO and DCO is captured using the Benders decomposition technique. Here, DCO checks for the feasibility of serving the end-users' stochastic workloads given the energy allocated to the data centers by the DNO. If the solution provided by the DNO is infeasible in the data center sub-problem and the

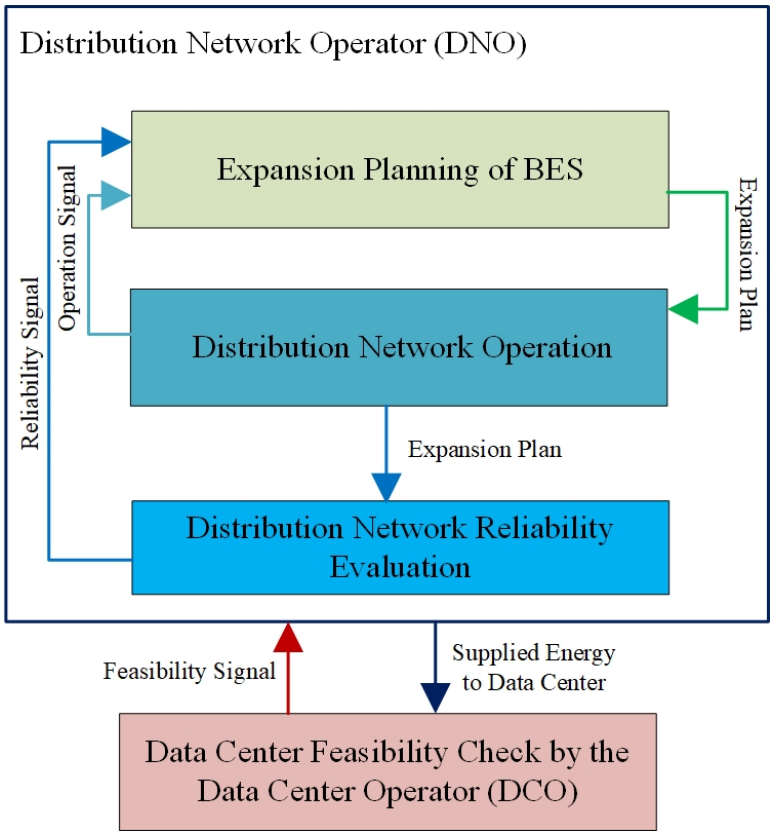

Figure 3.2: The proposed stochastic framework for the BES expansion planning.

quality of service cannot be guaranteed, a feasibility Benders cut is generated and sent to the distribution operation sub-problem to change the operational decisions and update the allocated energy to the data centers. This process continues until the solution provided by the DNO is feasible for the DCO in the data network.

The problem formulations for the master problem and sub-problems are discussed in detail in the following subsections.

3.2.1 BES Expansion Planning Problem – Master Problem (MP)

The master problem is formulated as a MILP problem (3.1)-(3.5). The objective function is shown in (3.1). The first term in (3.1) is the installation cost of the BES units which is formulated in (3.2) considering the annual discount rate. The second term in (3.1) is a positive variable that represents the total expected distribution network operation cost. The

auxiliary variable (α) is non-negative as shown in (3.3). It is assumed that only one BES unit is installed at each candidate bus in the planning horizon as enforced by (3.4)-(3.5).

$$min \quad Z_{lower} = IC + \alpha \tag{3.1}$$

s.t.

$$IC = \sum_{y=1}^{T_y} (1+\eta)^{1-y} \cdot \Big(\sum_{i \in \Omega_i} \sum_{e} C_e \cdot (Y_e^{i,y})\Big) \tag{3.2}$$

$$\alpha \geq 0 \tag{3.3}$$

$$\sum_{y=1}^{T_y} \sum_{e} Y_e^{i,y} \leq 1 \quad ; \forall i \in \Omega_i \tag{3.4}$$

$$\mu_e^{i,y} - \mu_e^{i,y-1} = Y_e^{i,y} \quad ; \forall i \in \Omega_i \tag{3.5}$$

The solution to this problem ($\hat{\mu}_e^{i,y}$) is passed to the distribution network operation problem (SP1) presented below.

3.2.2 Distribution Network Operation Sub-Problem (SP1)

This sub-problem is formulated as a linear programming (LP) problem (3.6)-(3.35). The objective function in SP1 is presented in (3.6). The distribution operation decisions minimize the expected operation cost of BES units, the expected cost of supplying energy from the upstream power network through the main distribution feeder, the expected operation cost of distributed generation assets, and the expected cost associated with the curtailed demand (CU) as shown in the first, second, third, and fourth terms of (3.6), respectively. The fifth term in (3.6) is the penalty associated with the mismatch in the nodal reactive power balance, where M is a large scalar. The expected operation cost of BES units, the expected cost of energy purchased from the main distribution feeder, and the expected operation cost of distributed generation units are computed by (3.7), (3.8), and (3.9), respectively. In this

chapter, the quadratic cost function in (3.9) is linearized using the piece-wise linearization technique. The expected cost associated with the demand curtailment is formulated as shown in (3.10) where $VOLL$ is the value of lost load. The demand curtailment ($LS_{l,s}^{t,d,y}$) is limited by the total demand in the distribution network as shown in (3.11). The real and reactive power balance at each bus is enforced by (3.12) and (3.13). Here, the mismatch between the nodal reactive power generation and demand is captured by introducing the slack variables in (3.13). The mismatch in the nodal real power balance is handled by demand curtailment ($LS_{l,s}^{t,d,y}$) in (3.12). Here, it is assumed that the reactive power requirement of the data center is compensated by on-site capacitor banks, and therefore, the reactive power consumption of the data center is ignored. The slack variables are non-negative as presented in (3.14).

$$min \;\; S_1 = OC_e + OC_f + OC_g + CU + \sum_{s}\sum_{y}\sum_{d}\sum_{t} M \cdot (Z_{1,s}^{t,d,y} + Z_{2,s}^{t,d,y}) \tag{3.6}$$

$$OC_e = \sum_{s}^{T_s} pr_s \cdot \left(\sum_{y=1}^{T_y} (1+\eta)^{(1-y)} \cdot \left[\sum_{d=1}^{T_d} N_d \times \sum_{t=1}^{T} \sum_{e} \left(\rho_e \cdot (p_{ch,e,s}^{t,d,y} + p_{dc,e,s}^{t,d,y}) \right) \right] \right) \tag{3.7}$$

$$OC_f = \sum_{s}^{T_s} pr_s \cdot \left(\sum_{y=1}^{T_y} (1+\eta)^{(1-y)} \cdot \left[\sum_{d=1}^{T_d} N_d \times \sum_{t=1}^{T} \sum_{f} \left(\rho_{f,s}^{t,d,y} \cdot p_{f,s}^{t,d,y} \right) \right] \right) \tag{3.8}$$

$$OC_g = \sum_{s}^{T_s} pr_s \cdot \left(\sum_{y=1}^{T_y} (1+\eta)^{(1-y)} \cdot \left[\sum_{d=1}^{T_d} N_d \times \sum_{t=1}^{T} \sum_{g} \left(\lambda_g . (p_{g,s}^{t,d,y})^2 + \beta_g \cdot p_{g,s}^{t,d,y} + \gamma_g \right) \right] \right) \tag{3.9}$$

$$CU = \sum_{s}^{T_s} pr_s \cdot \left(\sum_{y=1}^{T_y} (1+\eta)^{(1-y)} \cdot \left[\sum_{d=1}^{T_d} N_d \times \sum_{t=1}^{T} \sum_{l} \left(VOLL \cdot (LS_{l,s}^{t,d,y}) \right) \right] \right) \tag{3.10}$$

$$0 \leq LS_{l,s}^{t,d,y} \leq p_{l,s}^{t,d,y} \tag{3.11}$$

$$A_g \cdot p_{g,s}^{t,d,y} + A_v \cdot p_{v,s}^{t,d,y} + A_e \cdot (p_{dc,e,s}^{t,d,y} - p_{ch,e,s}^{t,d,y}) + A_f \cdot p_{f,b,s}^{t,d,y} = B \cdot p_{b,s}^{t,d,y} + D_l \cdot (p_{l,s}^{t,d,y} - LS_{l,s}^{t,d,y}) + D_c \cdot p_{c,s}^{t,d,y} \tag{3.12}$$

$$A_g \cdot q_{g,s}^{t,d,y} + A_v \cdot q_{v,s}^{t,d,y} + A_e \cdot q_{e,s}^{t,d,y} + A_f \cdot q_{f,b,s}^{t,d,y} + Z_{1,s}^{t,d,y} - Z_{2,s}^{t,d,y} = B \cdot q_{b,s}^{t,d,y} + D_l \cdot q_{l,s}^{t,d,y} \tag{3.13}$$

$$Z_{1,s}^{t,d,y}, Z_{2,s}^{t,d,y} \geq 0 \tag{3.14}$$

The charging and discharging real power of the BES unit are limited by their maximum values as shown in (3.15) and (3.16), respectively. The charging and discharging modes of the BES unit are mutually exclusive as the operation cost of the BES unit is minimized in the objective function [108]. The reactive power output of the BES unit is limited by (3.17). The stored energy in the BES unit is limited by the maximum and minimum values shown in (3.18). The start and final stored energies in the BES unit are equal to the initial stored energy (E_e^0) as shown in (3.19). The hourly stored energy in the BES unit is constrained by (3.20) where τ_e^{ch} and τ_e^{dc} are the charging and discharging efficiencies, respectively. Here, the planning decision of installing BES units ($\mu_e^{i,y}$) is a continuous variable that is fixed to the solution obtained from the MP ($\hat{\mu}_e^{i,y}$) as shown in (3.21).

$$0 \leq p_{ch,e,s}^{t,d,y} \leq \mu_e^{i,y} \cdot p_e^{max} \tag{3.15}$$

$$0 \leq p_{dc,e,s}^{t,d,y} \leq \mu_e^{i,y} \cdot p_e^{max} \tag{3.16}$$

$$-\mu_e^{i,y} \cdot q_e^{max} \leq q_{e,s}^{t,d,y} \leq \mu_e^{i,y} \cdot q_e^{max} \tag{3.17}$$

$$\mu_e^{i,y} \cdot E_e^{min} \leq E_{e,s}^{t,d,y} \leq \mu_e^{i,y} \cdot E_e^{max} \tag{3.18}$$

$$E_{e,s}^{1,t,y} = E_{e,s}^{T,d,y} = \mu_e^{i,y} \cdot E_e^0 \tag{3.19}$$

$$E_{e,s}^{t,d,y} = E_{e,s}^{t-1,d,y} + (\tau_e^{ch} \cdot p_{ch,e,s}^{t,d,y} - \frac{p_{dc,e,s}^{t,d,y}}{\tau_e^{dc}}) \tag{3.20}$$

$$\mu_e^{i,y} = \hat{\mu}_e^{i,y} \qquad : \pi_e^{i,y} \tag{3.21}$$

The real and reactive power dispatches of the distributed generation units are restricted by (3.22) and (3.23), respectively. The real power generation of the PV unit is restricted by the forecasted PV generation as shown in (3.24). The reactive power supply of the PV unit is limited by the PV inverters' capacity as shown in (3.25). The capacity of the main distribution feeder is restricted by (3.26) and (3.27), considering the minimum power factor (δ_f) at the upstream network interconnection. The squared nodal voltage is constrained by the upper and lower bounds as shown in (3.28). The linearized distribution flow (DistFlow) model is used to represent the power flow in the distribution network branch as shown in (3.29)-(3.30) [109]. Here, the Big-M method is used to address the availability of the distribution branch. The real and reactive power flows in a distribution network branch are affected by the availability of the branch as shown in (3.31) and (3.32) respectively. Once a distribution branch is not available, (3.29) and (3.30) are relaxed and the real and reactive power flow of the branch is equal to zero as enforced by (3.31) and (3.32). Hexagon approximation [110] is used to enforce the capacity limitation of the distribution branch in

(3.33)-(3.35). The capacity of the distribution branch is limited by the maximum apparent power in (3.36). Equation (3.36) is a circular constraint with a radius of the maximum apparent power (S_b^{max}). This quadratic constraint is approximated by an n sided convex polygon with (S_b^*) calculated as (3.37). Using hexagon approximation i.e., $n = 6$, the circular constraint (3.36) is replaced with (3.33)-(3.35) as discussed in [110]. Similar constraints are used to enforce the apparent power capacity of the main distribution feeder.

$$p_g^{min} \leq p_{g,s}^{t,d,y} \leq p_g^{max} \tag{3.22}$$

$$-q_g^{max} \leq q_{g,s}^{t,d,y} \leq q_g^{max} \tag{3.23}$$

$$p_{v,s}^{t,d,y} \leq \tilde{P}_{v,s}^{t,d,y} \tag{3.24}$$

$$-q_v^{max} \leq q_{v,s}^{t,d,y} \leq q_v^{max} \tag{3.25}$$

$$-p_f^{max} \leq p_{f,s}^{t,d,y} \leq p_f^{max} \tag{3.26}$$

$$-\tan(\delta_f) \cdot p_{f,s}^{t,d,y} \leq q_{f,s}^{t,d,y} \leq \tan(\delta_f) \cdot p_{f,s}^{t,d,y} \tag{3.27}$$

$$(V_i^{min})^2 \leq U_{i,s}^{t,d,y} \leq (V_i^{max})^2 \tag{3.28}$$

$$U_{i,s}^{t,d,y} - U_{j,s}^{t,d,y} \leq 2(r_{ij}^b \cdot p_{b,s}^{t,d,y} + x_{ij}^b \cdot q_{b,s}^{t,d,y}) + M \cdot (1 - \phi_{b,s}^{t,d,y}) \tag{3.29}$$

$$U_{i,s}^{t,d,y} - U_{j,s}^{t,d,y} \geq 2(r_{ij}^b \cdot p_{b,s}^{t,d,y} + x_{ij}^b \cdot q_{b,s}^{t,d,y}) - M \cdot (1 - \phi_{b,s}^{t,d,y}) \tag{3.30}$$

$$-M \cdot \phi_{b,s}^{t,d,y} \leq p_{b,s}^{t,d,y} \leq M \cdot \phi_{b,s}^{t,d,y} \tag{3.31}$$

$$-M \cdot \phi_{b,s}^{t,d,y} \leq q_{b,s}^{t,d,y} \leq M \cdot \phi_{b,s}^{t,d,y} \tag{3.32}$$

$$-\sqrt{3} \cdot (p_{b,s}^{t,d,y} + S_b^*) \leq q_{b,s}^{t,d,y} \leq -\sqrt{3} \cdot (p_{b,s}^{t,d,y} - S_b^*) \tag{3.33}$$

$$-\frac{\sqrt{3}}{2} \cdot S_b^* \leq q_{b,s}^{t,d,y} \leq \frac{\sqrt{3}}{2} \cdot S_b^* \tag{3.34}$$

$$\sqrt{3} \cdot (p_{b,s}^{t,d,y} - S_b^*) \leq q_{b,s}^{t,d,y} \leq \sqrt{3} \cdot (p_{b,s}^{t,d,y} + S_b^*) \tag{3.35}$$

$$(p_{b,s}^{t,d,y})^2 + (q_{b,s}^{t,d,y})^2 \leq (S_b^{max})^2 \tag{3.36}$$

$$S_b^* = S_b^{max} \cdot \sqrt{\frac{(\frac{2\pi}{n})}{\sin(\frac{2\pi}{n})}} \tag{3.37}$$

Once SP1 is solved, the upper bound of the solution is calculated as (3.38). If the lower bound ($\hat{Z}_{lower}$) i.e., the solution to the MP, and the upper bound ($\hat{Z}_{upper}$) satisfy $\left|\frac{\hat{Z}_{upper}-\hat{Z}_{lower}}{\hat{Z}_{upper}+\hat{Z}_{lower}}\right| \geq \epsilon$, Benders cut (3.39) is generated and sent to the MP. Otherwise, the distribution network reliability evaluation sub-problem (SP2) will be formulated and solved.

$$Z_{upper} = I\hat{C} + \hat{S}_1 \tag{3.38}$$

$$\alpha \geq \hat{S}_1 + \sum_y \sum_e \sum_i \hat{\pi}_e^{i,y} \cdot (\mu_e^{i,y} - \hat{\mu}_e^{i,y}) \tag{3.39}$$

3.2.3 Distribution Network Reliability Evaluation Sub-Problem (SP2)

To ensure that the BES expansion decisions satisfy the minimum reliability requirements of the distribution network, the distribution network reliability evaluation sub-problem is formulated as an LP problem. The objective is to minimize the annual demand curtailment [111], [112]. The objective function (3.40) is subjected to the constraints (3.41)-(3.42) and (3.15)-(3.35). The reliability evaluation sub-problem is solved using the expansion planning decision ($\hat{\mu}_e^{i,y}$). Here, the power supplied to the data centers in (3.41) is fixed to the solution obtained from the distribution network operation sub-problem (SP1) i.e., ($\hat{p}_{c,s}^{t,d,y}$).

$$min\ S_{2,s}^{t,d,y} = \sum_{l}(LS_{l,s}^{t,d,y}) \tag{3.40}$$

s.t.

$$A_g \cdot p_{g,s}^{t,d,y} + A_v \cdot p_{v,s}^{t,d,y} + A_e \cdot (p_{dc,e,s}^{t,d,y} - p_{ch,e,s}^{t,d,y}) + A_f \cdot p_{f,b,s}^{t,d,y} = B \cdot p_{b,s}^{t,d,y} + D_l \cdot (p_{l,s}^{t,d,y} - LS_{l,s}^{t,d,y}) + D_c \cdot \hat{p}_{c,s}^{t,d,y} \tag{3.41}$$

$$A_g \cdot q_{g,s}^{t,d,y} + A_v \cdot q_{v,s}^{t,d,y} + A_e \cdot q_{e,s}^{t,d,y} + A_f \cdot q_{f,b,s}^{t,d,y} = B \cdot q_{b,s}^{t,d,y} + D_l \cdot q_{l,s}^{t,d,y} \tag{3.42}$$

After solving the distribution network reliability sub-problem, the annual EENS is calculated using (3.43). If the annual EENS violates (3.44), the reliability cut (3.45) is sent to the MP. Otherwise, the power supplied to the data center ($\hat{p}_{c,s}^{t,d,y}$) is passed to the data center feasibility sub-problem (SP3). Here, $\hat{\pi}_e^{i,y}$ is the dual variable associated with the expansion decision of the BES units ($\mu_e^{i,y}$) in (3.21).

$$EENS_y = \sum_{s}\sum_{d}\sum_{t} pr_s \cdot N_d \cdot \hat{S}_{2,s}^{t,d,y} \tag{3.43}$$

$$EENS_y \leq EENS_y^{max} \tag{3.44}$$

$$\sum_{s}\sum_{d}\sum_{t} pr_s \cdot N_d \cdot \hat{S}_{2,s}^{t,d,y} + \sum_{e}\sum_{i} \hat{\pi}_e^{i,y} \cdot (\mu_e^{i,y} - \hat{\mu}_e^{i,y}) \leq EENS_y^{max} \tag{3.45}$$

3.2.4 Data Center Feasibility Sub-Problem (SP3)

The data center feasibility sub-problem (SP3) is formulated as an LP problem as shown in (3.46)-(3.51). The objective is to minimize the mismatch between the total workload collected from the end-users in the data network and the workload processed in the data centers as shown in (3.46). The workload in the data network represents the end-users' requests in the form of computing resources including processing, memory usage, and storage [113]. Here, the energy-intensive processing demand is considered as the workload. Positive slack variables are included in (3.47) to represent the mismatch between the received and processed workloads. The power consumed by a data center is associated with the workload processed as shown in (3.48). The capacity of a data center to process the workloads is limited by (3.49). Constraint (3.50) enforces the supplied energy to the data center to be equal to the solution obtained from SP1. The slack variables are non-negative as shown in (3.51).

$$min\ S_3 = \sum_{s}\sum_{y}\sum_{d}\sum_{t}(Z_{3,s}^{t,d,y} + Z_{4,s}^{t,d,y}) \tag{3.46}$$

s.t.

$$\sum_{c} w_{c,s}^{t,d,y} + Z_{3,s}^{t,d,y} - Z_{4,s}^{t,d,y} = \Delta_s^{t,d,y} \tag{3.47}$$

$$w_{c,s}^{t,d,y} \cdot p_c^{max} = w_c^{max} \cdot p_{c,s}^{t,d,y} \tag{3.48}$$

$$w_{c,s}^{t,d,y} \leq w_c^{max} \tag{3.49}$$

$$p_{c,s}^{t,d,y} = \hat{p}_{c,s}^{t,d,y} \quad : \pi_{c,s}^{t,d,y} \tag{3.50}$$

$$Z_{3,s}^{t,d,y}, Z_{4,s}^{t,d,y} \geq 0 \tag{3.51}$$

In case of any mismatch in (3.46), Benders feasibility cut (3.52) is formed and added to SP1. Once the supplied energy to the data center is sufficient to process the workloads, i.e. $\hat{S}_3 = 0$, the process stops.

$$(\hat{Z}_{3,s}^{t,d,y} + \hat{Z}_{4,s}^{t,d,y}) + \sum_{c} \hat{\pi}_{c,s}^{t,d,y} \cdot (p_{c,s}^{t,d,y} - \hat{p}_{c,s}^{t,d,y}) \leq 0 \tag{3.52}$$

3.3 Solution Methodology

The flowchart of the proposed framework is shown in Fig. 3.3. The algorithm is composed of the following steps:

Step (a): Solve the MP and determine the lower bound of the solution ($\hat{Z}_{lower}$).

Step (b): Using the solution of MP ($\hat{\mu}_e^{i,y}$), solve the distribution network operation sub-problem (SP1). Go to step (c).

Step (c): Calculate the upper bound of the solution $\hat{Z}_{upper}$ using (3.38).

Step (d): If $\left|\frac{\hat{Z}_{upper}-\hat{Z}_{lower}}{\hat{Z}_{upper}+\hat{Z}_{lower}}\right| \geq \epsilon$, then add the Benders cut (3.39) to the MP and go to step (a). Otherwise, go to step (e).

Step (e): Solve the distribution network reliability evaluation sub-problem (SP2) for the given expansion plan ($\hat{\mu}_e^{i,y}$), calculate the annual EENS using (3.43), and go to step (f).

Step (f): If there is any violation in the annual EENS requirement (3.44), add the reliability cut (3.45) to the MP and go to Step (a). Otherwise, go to Step (g).

Step (g): Solve the data center feasibility sub-problem (SP3) for the given $\hat{p}_{c,s}^{t,d,y}$ obtained from SP1.

Step (h): If SP3 is feasible for the given $\hat{p}_{c,s}^{t,d,y}$, i.e. $\hat{S}_3 = 0$, then terminate the process. Otherwise, add the Benders feasibility cut (3.52) to SP1 and go to Step (b).

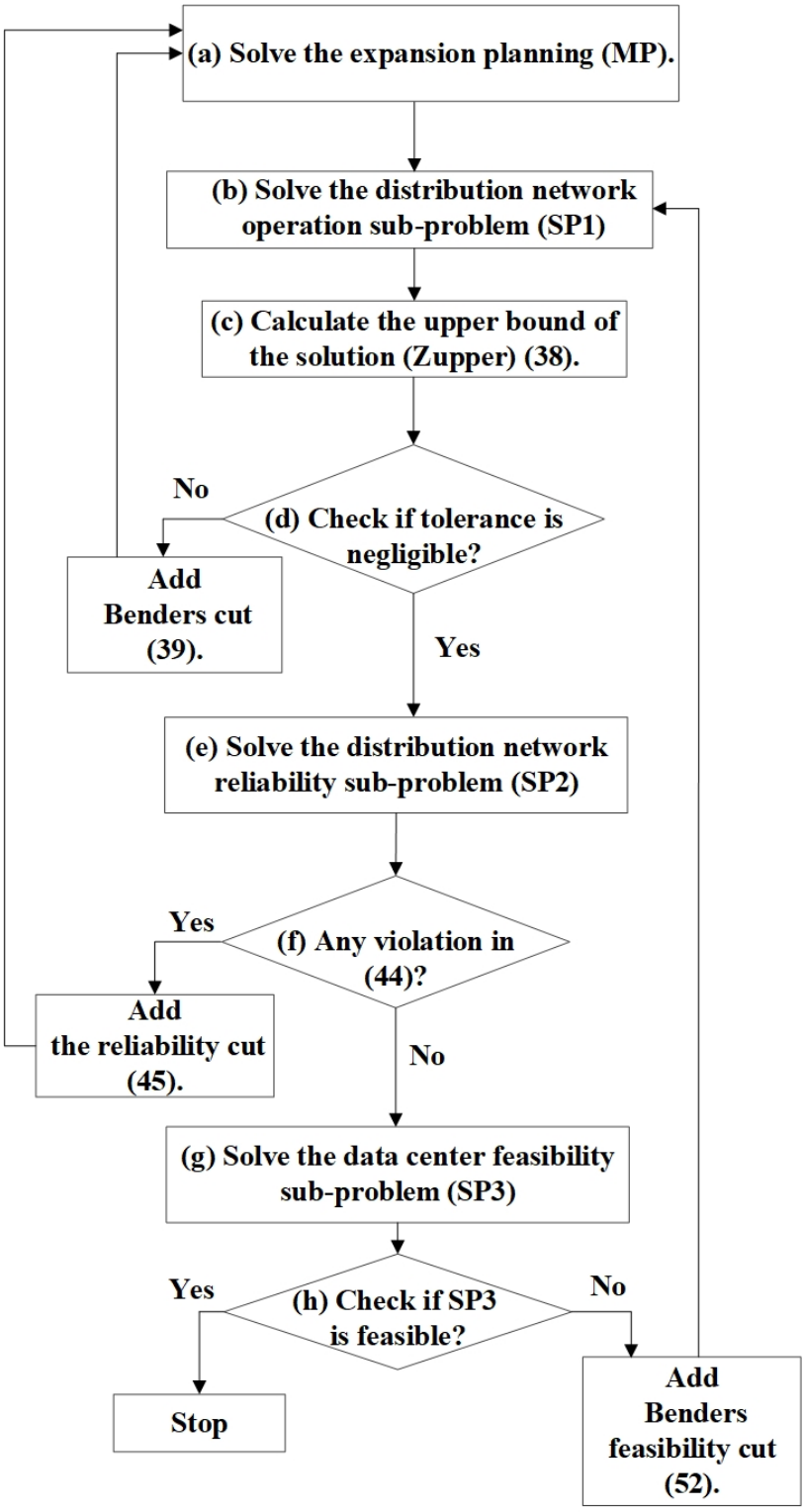

Figure 3.3: The flowchart of the proposed stochastic planning framework.

3.4 DS3 Algorithm

The uncertainties associated with the hourly demand, hourly electricity prices of the utility grid, the hourly power generation of the solar PV units, and the workloads received by the end-users in the data network are considered in this framework. To reduce the number of representative days and representative scenarios, the DS3 algorithm is used. This algorithm clusters the data points into a limited number of subsets. The subset is a set of data points that represents the original data set effectively. Each subset is formed using on a dissimilarity metric which is the Euclidean distance among the data points [114]. The pairwise distances between the n number of data points is used as a measure of dissimilarity as shown by matrix $\mathbf{A}$ in (3.53).

$$\mathbf{A} = \begin{bmatrix} a_{1,1} & a_{1,2} & \cdots & a_{1,n} \\ \vdots & \vdots & \ddots & \vdots \\ a_{n,1} & a_{n,2} & \cdots & a_{n,n} \end{bmatrix}_{n \times n} \tag{3.53}$$

where each entry $a_{j,k}$ in row j indicates how well the j-th data point in the data set represents the k-th data point. Having a small dissimilarity $a_{j,k}$ indicates a better representation while having a large dissimilarity shows a strong statistical independence between the j-th and k-th data points. Matrix $\mathbf{X}$ with the size of $n \times n$ is defined in (3.54) to store the linear dependence coefficients of all data points. Here, each non-zero column k indicates that the k-th data point is a representative.

$$\mathbf{X} = \begin{bmatrix} x_1^\top \\ \vdots \\ x_n^\top \end{bmatrix} = \begin{bmatrix} x_{1,1} & x_{1,2} & \cdots & x_{1,n} \\ \vdots & \vdots & \ddots & \vdots \\ x_{n,1} & x_{n,2} & \cdots & x_{n,n} \end{bmatrix}_{n \times n} \tag{3.54}$$

Each data point can be written as a linear combination of its corresponding representatives (i.e., corresponding non-zero columns). Each non-zero entry $x_{j,k} \in [0, 1]$ is the coefficient of the linear combination corresponding to the k-th data point that represents the j-th data point. If $x_{j,k} = 0$, the j-th data point is not represented by the k-th data point. Matrix $\mathbf{X}$ is not only to find the representatives but also to cluster the data points according to the representatives. That is, one can assume a cluster corresponding to each representative

with non-zero column in $\mathbf{X}$. To find the optimal representatives that best encode the data points corresponding to their clusters while minimizing the number of representatives, the DS3 algorithm solves the optimization problem (3.55), (3.56).

$$\min_{(x_{j,k})} \zeta . \sum_{j}^{n} \left\| x_j \right\|_2 + \sum_{k=1}^{n} \sum_{j=1}^{n} a_{j,k} \ . \ x_{j,k} \tag{3.55}$$

s.t.

$$\sum_{j=1}^{n} x_{j,k} = 1 \ , \forall k \tag{3.56}$$

Here, $\left\| x_j \right\|_2$ is the $L2$-norm of the j^{th} row of matrix $\mathbf{X}$. The objective function (3.55) has two terms. The first term represents the number of representative data points used in a linear combination to represent the j-th data point. Here, ζ is a regularization hyper-parameter that declines the number of representatives if increased. Having a small ζ (i.e., having a large number of representatives) would reduce the error in representing the original data and increase the process burden by handling more data samples. The expected distance between the representatives and the original data points in the data set is computed in the second term. If the representatives provide a powerful data encoding with a small error, the second term decreases; hence, optimizing the total error in (3.55). The constraint (3.56) limits the number of data points represented by one representative (i.e., k-th representative). This constraint leads to a better dimensionality reduction while enhancing the encoding quality when the data points are written as a linear combination of representatives. Once the DS3 optimization is solved, the non-zero columns of the optimal solution matrix $\mathbf{X}$ are considered as the representatives that best show the statistical characteristics of the entire data points.

3.5 Case Study

The modified IEEE-34 bus distribution network shown in Fig. 3.4 is used to validate the proposed planning approach. The network is equipped with 3 distributed generation (DG) units, 4 solar PV generation units, and 3 data centers in the distribution network. The capacity of the distribution feeder is 4.4 MVA with a minimum power factor of 0.8.

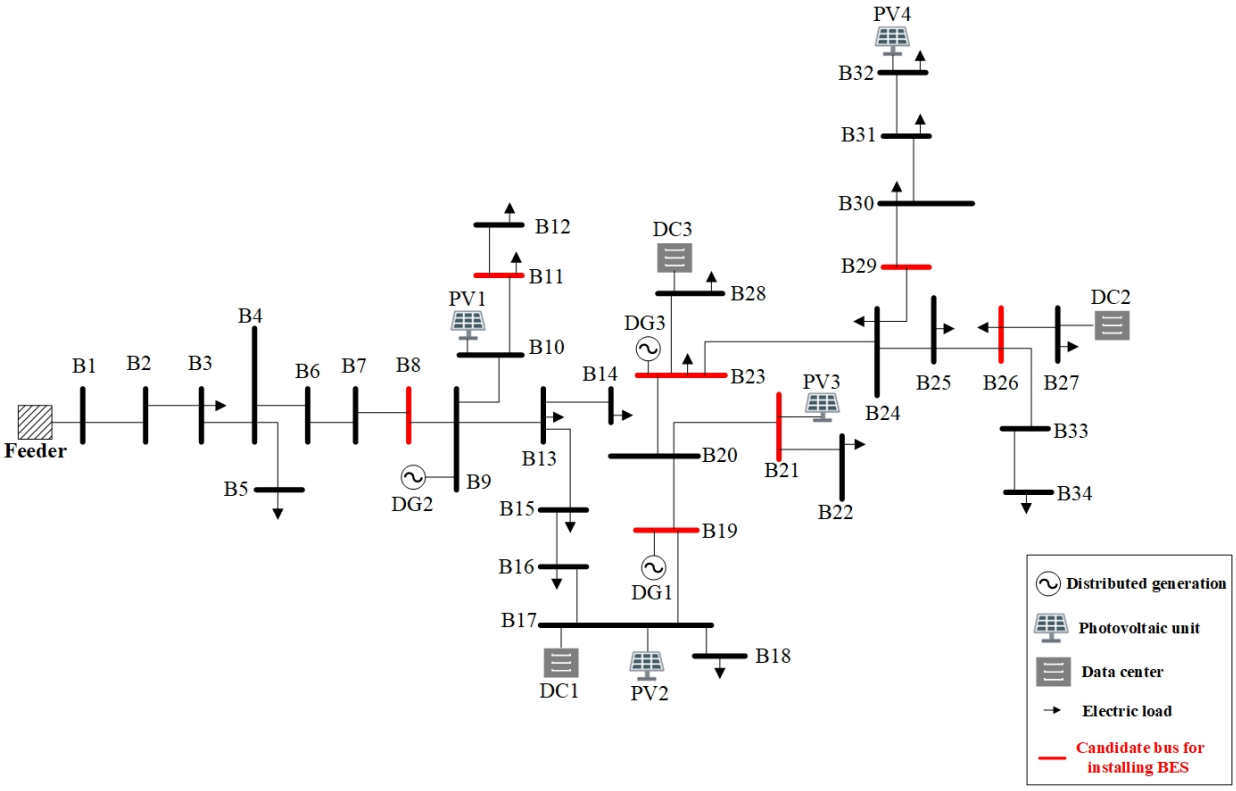

Figure 3.4: The modified IEEE-34 bus distribution network with data centers and PV generation units.

Table 3.2: Characteristics of distributed generation units

Unit	P_{max} (kW)	Q_{max} $(kVar)$	λ_g $(\$/kWh^2)$	β_g $(\$/kWh)$
DG1	300	150	0.00015	0.0025
DG2	150	75	0.00028	0.038
DG3	90	45	0.000778	0.00944

Table 3.3: Generation limits of PV units

Unit	Bus	P_{max} (kW)	Q_{max} (kVAR)
PV1	10	50	25
PV2	17	300	150
PV3	21	100	50
PV4	32	250	125

The characteristics of DG units and photovoltaic (PV) generation units are shown in Tables 3.2 and 3.3 respectively. The capacities of the data centers on buses B17, B27, and B28 are 100, 150, and 120 kW respectively. The characteristics of the BES units are shown in Table 3.4. Three types of Lithium-ion batteries are considered as the potential candidates. The characteristics of the BES units are obtained from [115] and their operation costs are calculated using the formulation in [116]. The charging and discharging efficiencies for the BES unit are 90%. As shown in Fig. 3.4, buses B8, B11, B19, B21, B23, B26, and B29 are considered as candidate buses to install the BES units. The minimum and the initial stored energy of all BES units are 15% and 50% of the maximum energy capacity, respectively.

The time horizon for the expansion planning is 10 years, the annual discount rate is 10%, and the annual growth of demand in the distribution network and data network is 5% [48]. The acceptable annual EENS is zero, and the convergence tolerance (ϵ) is 0.01%. The value of lost load is 10 \$/kWh. In the first year, the solar PV penetration which is defined as the ratio of the total PV generation to the total demand in the distribution network is

Table 3.4: Battery energy storage systems' characteristics.

Battery	P_{max} (kW)	Q_{max} $(kVar)$	E_{max} (kWh)	C_e $(\$/kWh)$	ρ_e $(\$/kWh)$
K1	100	60	400	450	0.18
K2	50	35	200	420	0.17
K3	25	15	100	380	0.15

17.21%, and the maximum demand of the data center is 20.49% of the peak demand in the distribution network. The following cases are considered:

Case 1 – Expansion planning of the BES units considering the forecasted demand, electricity prices, solar PV generation, and workload in the data network.

Case 2 – Expansion planning of the BES units considering the forecasted values with contingencies in the distribution network.

Case 3 – Expansion planning of the BES units with uncertainty in the forecasted demand, electricity prices, solar PV generation, and workload in the data network.

Case 4 – The impact of EENS on the expansion planning of the BES units.

3.5.1 Case 1 – Expansion planning of the BES units considering the forecasted demand, electricity prices, solar PV generation and workload in the data network

In this case, the distribution network with data centers is considered under normal operating conditions with no outages in the system. By applying the DS3 algorithm, the original data set which consists of 35040 data points are clustered into 3 representative data subsets consisting of 288 data points each year. Table 3.5 presents the number of representative days in each year ($R_{d,y}$). The normalized PV outputs for the three representative days in the first year are shown in Fig.3.5. Here, the maximum output for a PV unit is determined by multiplying the nominal capacity of each PV unit by the normalized PV output. Similarly, the demand profile and the hourly energy prices on the first representative day of the first year ($R_{1,1}$) are shown in Fig. 3.6. The workload in the data network for the first representative day of the first year is shown in Fig. 3.7.

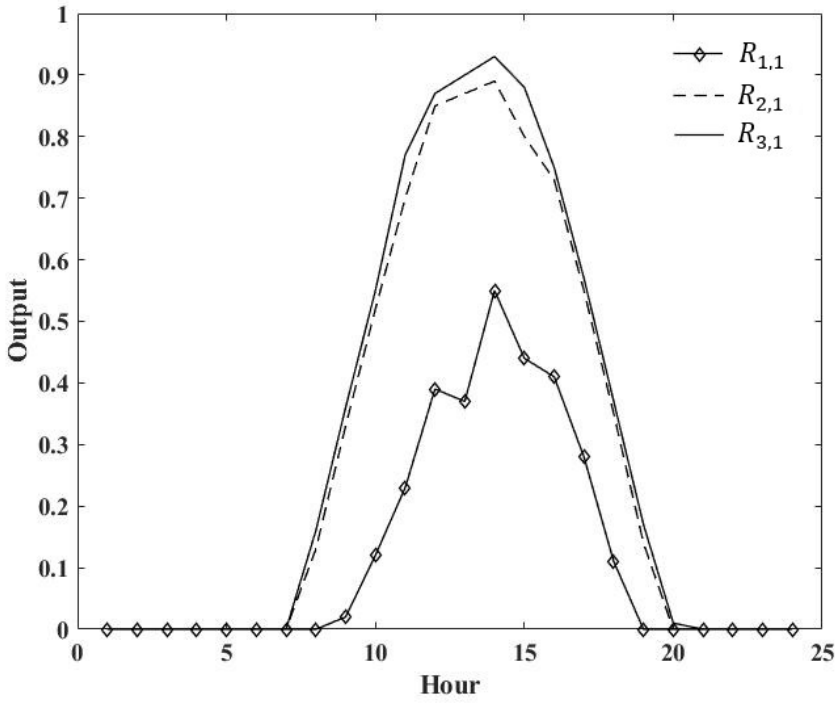

Figure 3.5: Normalized PV generation for the representative days 1-3 ($R_{1,1}, R_{2,1}, R_{3,1}$) in the first year.

Table 3.6 shows the installed BES in Case 1. As shown in this table, the expansion planning decision is to install three BES units type K2 with total capacity of 600 kWh. The location and installation time of the BES units are on buses B23, B26, B29 in the seventh, third, and fourth year, respectively. The installation and operation costs of BES units are \$163,588.86 and \$5,958.50, respectively. The cost of purchased energy from the main feeder and the operation cost of distributed generation units are \$417,642.92 and \$340,354.47, respectively. The total planning cost for this case is \$927,544.75. Fig. 3.8 shows the upper and lower bounds of the solution in each iteration. As shown in this figure, the upper and lower bounds of the solution converge as the number of iteration increases. The increase in the lower and upper bounds at 116th iteration is because of the feasibility cut passed from the data center feasibility sub-problem (SP3).

Table 3.5: Number of days in each representative days of each year

Year	Representative	Number of Days
1	$R_{1,1}$	265
	$R_{2,1}$	12
	$R_{3,1}$	88
2	$R_{1,2}$	131
	$R_{2,2}$	82
	$R_{3,2}$	152
3	$R_{1,3}$	265
	$R_{2,3}$	4
	$R_{3,3}$	96
4	$R_{1,4}$	232
	$R_{2,4}$	20
	$R_{3,4}$	113
5	$R_{1,5}$	130
	$R_{2,5}$	234
	$R_{3,5}$	1
6	$R_{1,6}$	136
	$R_{2,6}$	224
	$R_{3,6}$	5
7	$R_{1,7}$	258
	$R_{2,7}$	10
	$R_{3,7}$	97
8	$R_{1,8}$	216
	$R_{2.8}$	11
	$R_{3,8}$	138
9	$R_{1,9}$	147
	$R_{2,9}$	114
	$R_{3,9}$	104
10	$R_{1,10}$	179
	$R_{2,10}$	81
	$R_{3,10}$	105

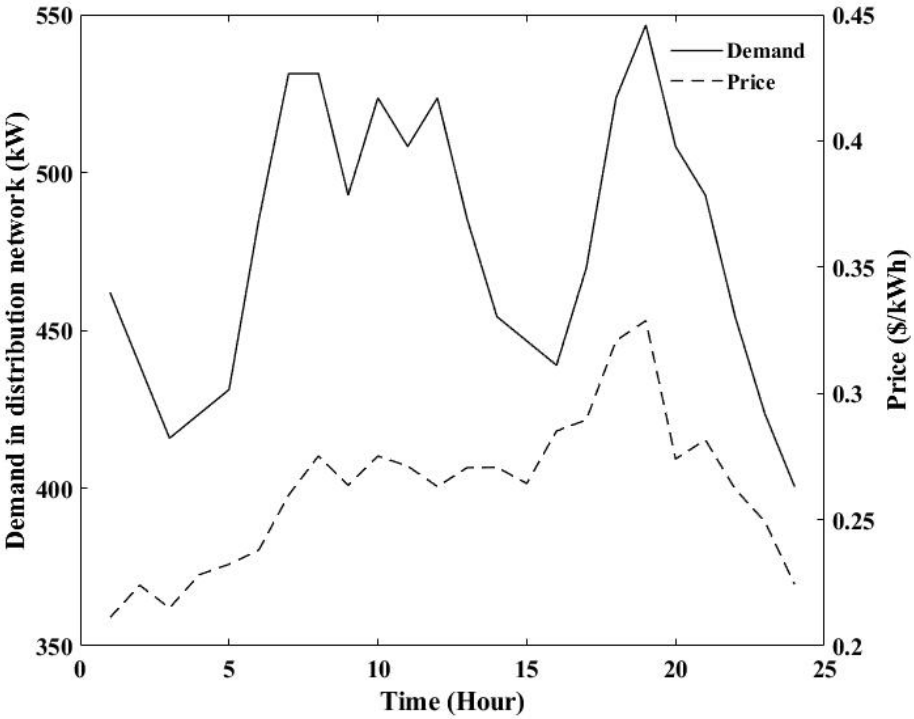

Figure 3.6: Total hourly demand in the distribution network and hourly energy price in the first representative day of the first year.

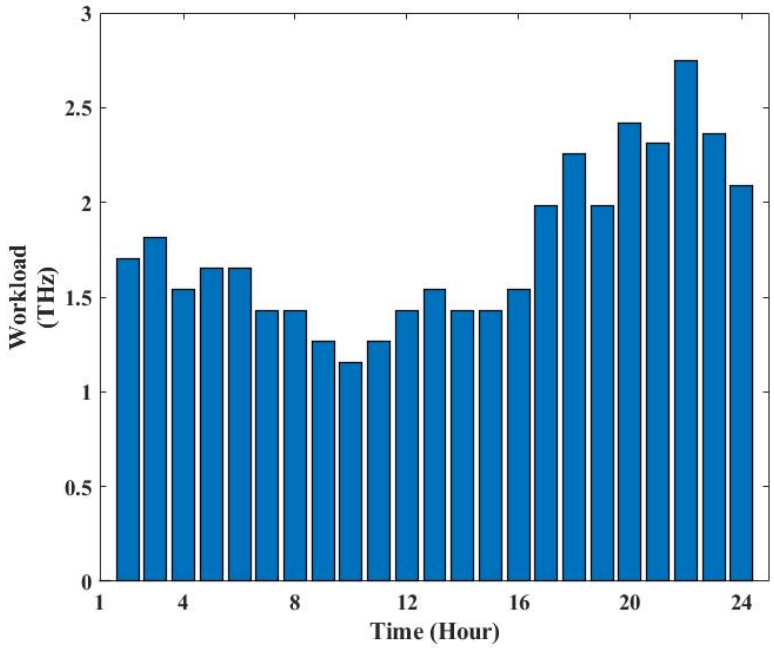

Figure 3.7: The total workload in the first representative day of the first year.

Table 3.6: The expansion decision for BES in Case 1

Bus	Year	Storage type
B23	7	K2
B26	3	K2
B29	4	K2

Table 3.7: Outages in the distribution lines

Line	Year	Representatives	Hour
B23-B24	5	R1	13:00
B20-B23	6	R2	16:00
B16-B17	7	R3	18:00
B25-B26	4	R2	12:00

3.5.2 Case 2 – Expansion planning of the BES units considering the forecasted values with contingencies in the distribution network

In this case, the impacts of outages in the distribution network on the expansion plans of the BES units are addressed. The outages in the branches between buses B23-B24, B20-B23, B16-B17, and B25-B26 are considered in the representative days of Case 1 as shown in Table 3.7. The expansion plans for the BES units are shown in Table 3.8. Compared to Case 1, three BES units are installed with total capacity of 600 kWh which is the same in Case 1. However, the location, year, and type of BES units are changed because of the branch outages in the distribution network. The planning decision is to install one BES unit type K1 at Bus B26 in the third year, and two BES unit type K3 at Bus B11 and B29 in the seventh and sixth year, respectively. The installed BES units will help to serve the demand once the distribution branches are on outage. The BES unit installed on bus B29 along with the PV generation at Bus B32 would supply the demand on buses B30, B31, and B32 during the outage of branch B20-B23. In Case 1, at hour 16:00 in the second representative day of the sixth year, the demands on buses B30, B31, and B32 along with demands on buses

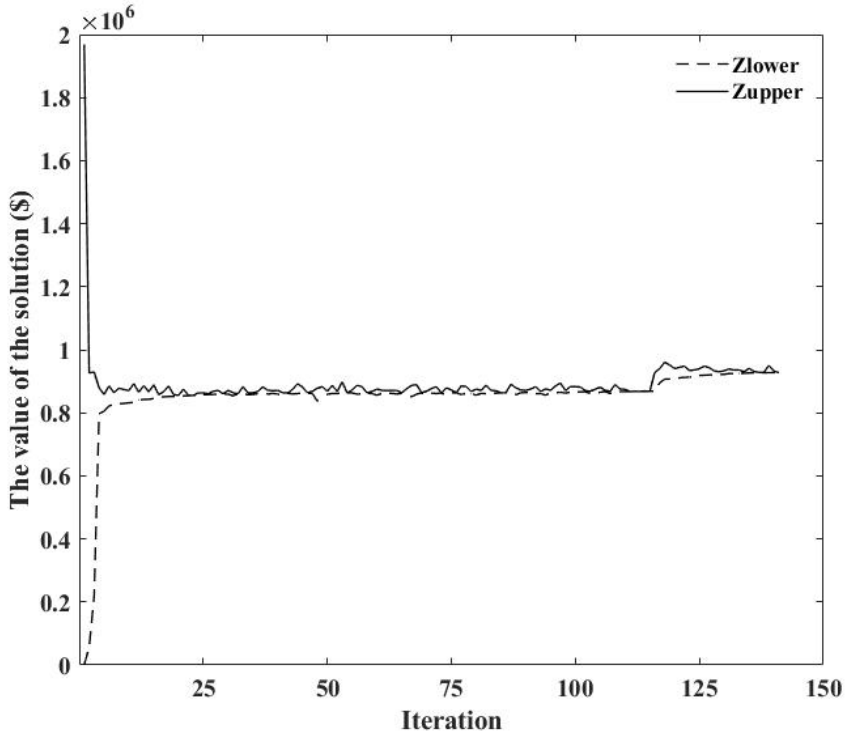

Figure 3.8: The upper and lower bounds of the solution at each iteration in Case 1.

Table 3.8: The expansion decisions for BES in Case 2

Bus	Year	Storage type
B11	7	K3
B26	3	K1
B29	6	K3

B23-B34 in the distribution network are supplied by branch B20-B23 that carries 168.566 kW, and by the distributed generations on bus B23 as well as the PV generation units on bus B21 and B32. During the same period in Case 2, branch B20-B23 is on outage, and the demands on buses B30, B31, and B32 are supplied by the BES unit type K3 on bus B29 along with PV generation unit on bus B32.

Furthermore, the outage in the distribution network would lead to changes in the work-

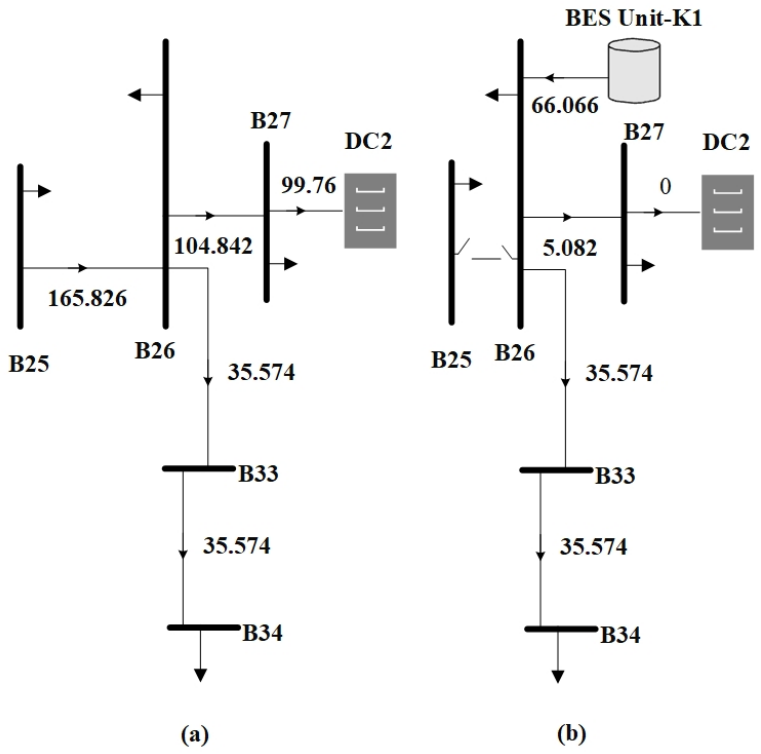

Figure 3.9: Power flow in the distribution network. (a) Case 1 (b) Case 2.

load process by the data centers. Fig. 3.9a. shows the power flow in a section of the distribution network at 12:00 on the second representative day of the fourth year in Case 1, while Fig. 3.9b. shows the power flow in the same period in Case 2 with branch B25-B26 on outage. As shown in Fig. 3.9a, the branch B25-B26 supplies the demand in the distribution network on buses B26, B27, and B34 as well as the demand of the data center DC2. The total power consumption of data center DC2 on bus B27 is 99.76 kW. However, in Fig. 3.9b, the power consumption of DC2 is zero and the workloads are redistributed among data centers DC1 and DC3. Here, because of the outage on branch B25-B26, the BES unit is installed on Bus B26 to merely serve the electric demand on buses B26, B27, and B34; and DC1 and DC3 serve the received workloads and increase their demand by 99.76 kW.

The total installation cost of the BES units is \$176,186.68 in this case which is higher than that in Case 1 by \$12,597.82. The operation cost of BES units is increased to \$14,816.52. The operation cost of distributed generation is increased to \$350,307.34 in this case because

of the increase in the power dispatch of DG1 and DG3 during the branch outages. The cost of the purchased power from the main feeder is reduced to $415,336.94. The total cost in this case is $956,647.48 which is $29,102.73 higher than that in Case 1. In Case 2, the branch outages lead to installing different types of BES units and increase the dispatch of the distributed generation units.

3.5.3 Case 3 – Expansion planning of the BES units with uncertainty in the forecasted demand, electricity prices, solar PV generation and workload in data network

The stochastic solution for the BES expansion planning is presented in this case. The uncertainties in the distribution network's demand, the PV generation, electricity prices, the workloads received by the data centers, and the outages of the distribution branches are considered. The forecast errors of the uncertain parameters are represented by the Gaussian probability distribution functions for which the mean values are the forecasted data used in Cases 1 and 2, and the standard deviations are 3% of the mean values. The mean time to failure (MTTF) and the mean time to repair (MTTR) for distribution branches B23-B24, B20-B23, B16-B17, and B25-B26 are 38,400 hours and 15 hours, respectively. Monte-Carlo simulation is used to generate 500 scenarios. Here, 8 matrices each with (500×87600) data points are generated to represent 8 uncertain parameters i.e. demand, electricity price, workload for the data centers, PV generation and the outage for four lines in 10 years. DS3 algorithm [114] is used to reduce the number of scenarios to 5 with associated probabilities shown in Table 3.9. Similarly, for each year in each scenario, 3 representative days are clustered using DS3 algorithm. Fig. 3.10 shows the number of days in each representative day in each year ($R_{d,y}$) for each scenario. After applying the DS3 algorithm, three representative days for each year are obtained in each scenario. Considering 10 years in the planning horizon, 30 representative days are considered in each scenario as shown in Fig. 3.10. Fig. 3.11 shows the normalized PV power generation in each scenario for the first representative day in the first year ($R_{1,1}$).

Table 3.10 shows the installation plan for the BES units. Compared to Case 1, an additional 200 kWh capacity of the BES units is installed. The expansion decision is installing one BES unit type K1 on bus B26 in the fourth year and two BES units type K2 on bus B29 and B23 in the fifth and eighth year, respectively. Compared to Case 1, the installation cost

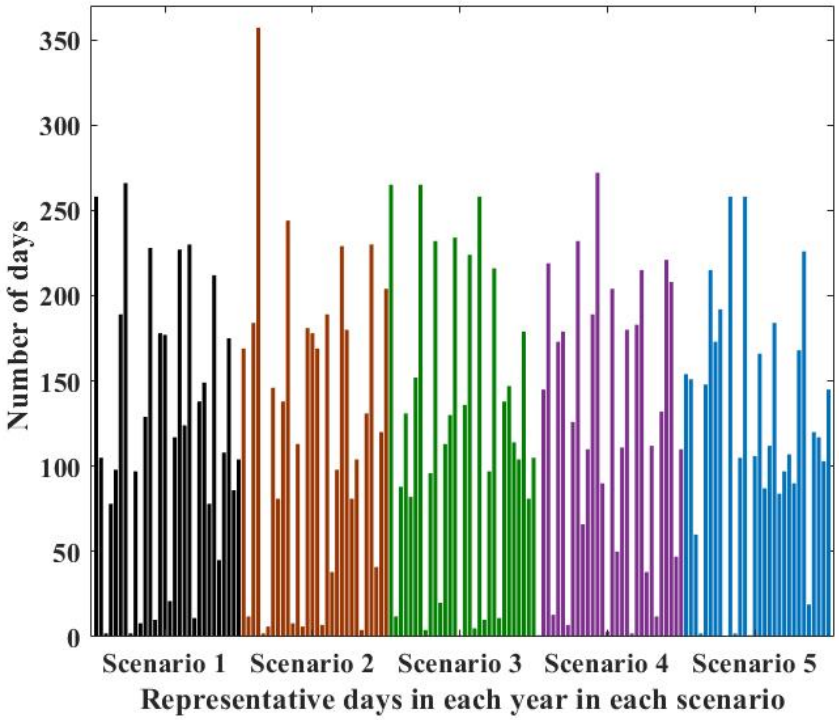

Figure 3.10: Number of days in the representative days in each year ($R_{d,y}$) for each scenario.

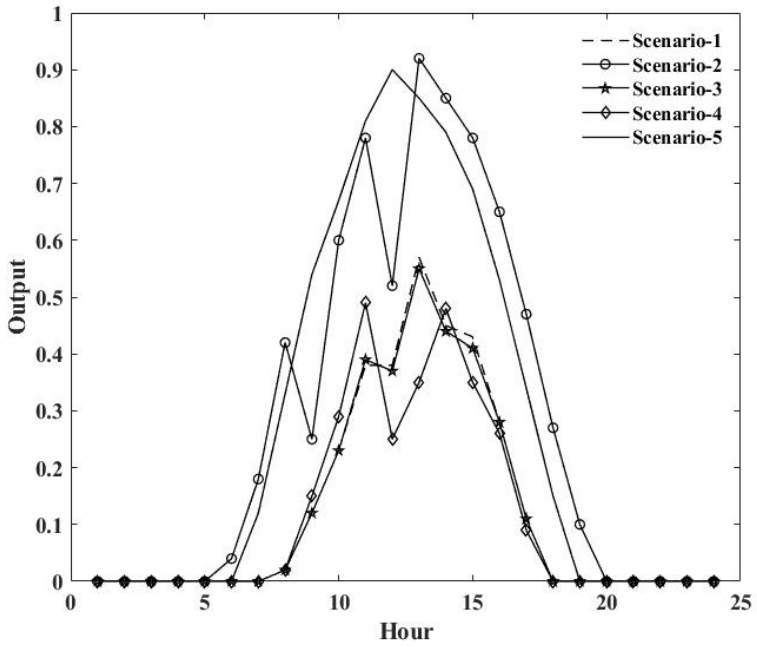

Figure 3.11: Normalized PV generation in each scenario for the first representative day in the first year ($R_{1,1}$) in Case 3.

Table 3.9: Probability of scenarios

Scenario	1	2	3	4	5
Probability (%)	28.2	33.6	34.6	0.4	3.2

of BES units is increased to $214,286.43. Furthermore, the total expected operation costs of the distributed generation and BES units are decreased to $338,424.69 and $3,831.28, respectively. The expected cost of the power supplied from the distribution feeder is $428,202.84 which is $10,559.92 higher than that in Case 1. Table 3.11 summarizes the solution outcomes in all cases. The total expansion and expected operation cost, in this case, is $984,745.24 which is 6.17% and 2.94% higher than the total expansion planning costs in Cases 1 and 2, respectively. Fig. 3.12 shows the mismatch between the total required and served workloads by the data center in each iteration for Cases 1-3. As shown in this figure, the mismatch reaches zero after two interactions (iterations) between the DNO and DCO in Cases 1 and 2. The workload mismatch in the data center converges to zero after four interactions between the DNO and DCO in Case 3.

Table 3.10: The expansion decisions for BES in Case 3

Bus	Year	Storage type
B23	8	K2
B26	4	K1
B29	5	K2

3.5.4 The impact of EENS on the expansion planning of BES

In this section, the impact of EENS on the expansion planning of BES units is evaluated in Case 3. Here, the acceptable EENS in the first year is 41.686 MWh which is 1% of the

Table 3.11: Summary of the planning solutions of all cases

#	Case 1	Case 2	Case 3
Total BES capacity (kWh)	600 kWh	600 kWh	800 kWh
Total investment cost ($)	$163,588.86	$176,186.68	$214,286.43
Total operation cost ($)	$763,955.89	$780,460.8	$770,458.81
Total planning cost ($)	$927,544.75	$956,647.48	$984,745.24

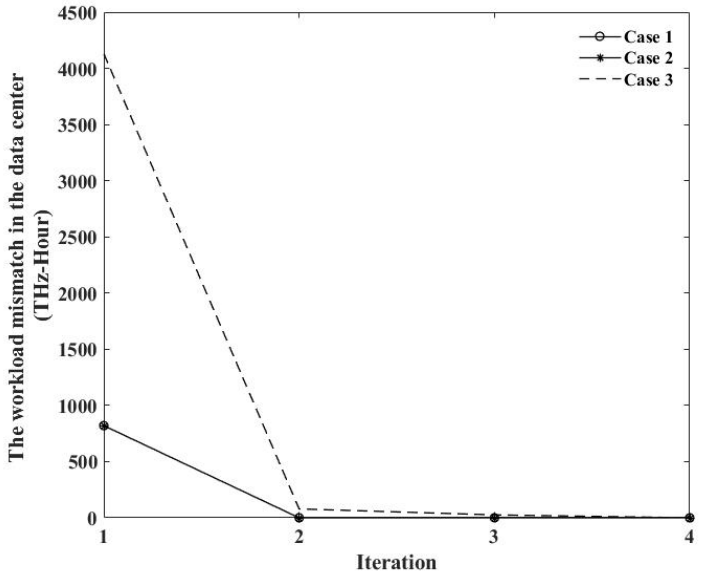

Figure 3.12: The mismatch between the required and served workloads by the data centers at each iteration in Cases 1-3.

total expected demand in the first year. The acceptable EENS increases by 5% annually. Therefore, the acceptable total EENS for the planning horizon is 524.32 MWh. The value of lost load is the same as in previous cases. Table 3.12 shows the expansion plans for the BES units in this case. The expansion planning decision is to install 500 kWh BES units, which is 300 kWh lower than the installed capacity once the acceptable total EENS is zero. Consequently, the investment cost for BES units is reduced to $139,983.58 with the total EENS of 4063.451 kWh. The penalty associated with the curtailed demand is $15,876.55

Table 3.12: The expansion decisions in Case 3 with the total acceptable EENS of 524.32 MWh

Bus	Year	Storage type
B23	7	K3
B26	3	K2
B29	4	K2

and total operation cost is $802,510.48. The total expansion planning cost is $958,370.61 which is 2.68% lower than that in Case 3 with zero acceptable total EENS.

The total EENS, the investment cost for the BES units, the total operation and planning costs as well as the cost associated with the curtailed demand for Case 3 are shown in Table 3.13 with the changes in the VOLL from $10/kWh to $50/kWh. As shown in this table, as the VOLL increases, the total EENS is reduced because of the increase in the penalty associated with the curtailed demand. Consequently, the operation cost is reduced. Moreover, the increase in the VOLL will increase the installed capacity of the BES units to reduce the total EENS. Consequently, the investment cost and the total planning cost are increased with the increase in the VOLL.

Table 3.13: The impact of VOLL on the investment, operation, and total planning costs

VOLL ($/kWh)	Total EENS (kWh)	Investment Cost ($)	Operation Cost ($)	Demand Curtailment Cost ($)	Total Planning Cost ($)
50	0	214,286	770,458	0	984,745
40	482	202,775	774,474	7,441	984,691
30	2390	163,588	788,395	27,650	979,634
20	2390	163,588	788,395	18,433	970,417
10	4063	139,983	802,510	15,876	958,370

3.6 Conclusion

A scenario based expansion planning framework is proposed in this chapter for optimal sizing and location the BES units in the distribution network with data center facilities. The planning algorithm seeks to minimize the installation cost, the operation cost of the distribution network while providing sufficient power supply to the data centers and ensuring the reliability of the distribution network. The proposed algorithm captures the interactions between DNO and DCO using the Bender decomposition technique. Monte Carlo simulation is used to generate a large number of scenarios based on the probability distribution functions representing the forecast errors in uncertain parameters. DS3 clustering technique is used to perform scenario reduction and select the effective scenarios. The modified IEEE-34 bus distribution network with three data centers is used to validate the effectiveness of the proposed algorithm. The numerical results show that incorporating the uncertainty in the availability of the distribution lines, electricity demand and prices, workloads in the data network, and generation of PV units will lead to an increase in the installed BES capacity in the distribution network. Moreover, the outages in the distribution branches lead to changes in the location and types of the BES units and consequently, changes in the expansion planning costs and resource allocation strategies in data centers to process the received workloads. The impact of EENS on the expansion planning decisions is evaluated. It is shown that the total expansion planning cost is reduced as the EENS increases. Moreover, as the VOLL increases, the total EENS decreases, and the investment cost and the total planning cost increase.

Chapter 4

Distributionally Robust Generation Expansion Planning of Gas-Fired Distributed Generation with Demand Response

This chapter proposes a distributionally robust expansion planning framework for the gas-fired distributed generation in the interconnected distribution and natural gas networks with demand response. The proposed formulation accounts for the uncertainties associated with the electricity demand, natural gas demand, PV generation outputs, and demand bidding price. The ambiguity sets for the uncertain variables are constructed based on the Wasserstein distance. The expansion planning decisions are obtained under the worst probability distributions of the uncertain parameters. The problem is decomposed using Benders decomposition and solved in multi-stages to preserve the autonomous operation of the independent networks. The expansion planning of the gas-fired distributed generation is determined in the master problem, and the feasibility and optimality of the decisions in the power and natural gas networks are ensured using the corresponding sub-problems. The modified IEEE 34-bus distribution network connected with a 11-node natural gas network and the modified IEEE 123-bus system with a 28-node natural gas network are used to validate the efficiency of the proposed planning framework. The contributions of this chapter are summarized as follows:

– The formulated expansion planning for GFDG is solved in a decentralized fashion using Benders decomposition to ensure the autonomous operation of DSO and natural gas supplier.

– The power distribution and natural network operation problems are formulated as DRO problems in which the empirical samples of electricity and natural gas demands, PV generation, and demand bids are used to form the empirical probability distributions. The Wasserstein distance is used as a measure to form the ambiguity set.

– The expansion planning problem is solved as a multi-stage optimization problem, and

Benders decomposition is used to coordinate the long-term expansion planning decisions with the robust short-term operation decisions. The short-term operation problems are reformulated into linear programming problems.

The rest of the paper is organized as follows: A list of symbols used in this chapter is presented in Section 4.1. The problem formulation is presented in Section 4.2, and the problem reformulation is discussed in Section 4.3. The solution methodology is presented in Section 4.4. Section 4.5 presents the numerical results and the conclusions are derived in Section 4.6.

4.1 List of Symbols

Indices and Sets:

b	Index of bus
d	Index of demand
e	Index of electricity network
f	Index of the distribution feeder
g	Index of the distributed generation unit other than the gas-fired distributed generation unit
h	Index of gas-fired distributed generating unit
i	Index of sample
j	Index of natural gas node
k	Index of cost function segment
l	Index of distribution branch
m	Index of responsive load block
p	Index of natural gas pipeline
r	Index of responsive load
s	Index of season
t	Index of hour
u	Index of natural gas supplier
v	Index of the PV generation unit
y	Index of year

q	Index of battery storage system
$\mathcal{D}$	Set of non-responsive loads in the power distribution network
$\mathcal{F}$	Set of the distribution feeders
$\mathcal{G}$	Set of distributed generation units
$\mathcal{L}$	Set of natural gas loads
$\mathcal{R}$	Set of responsive loads in the distribution network
$\mathcal{Q}$	Set of battery storage units in the distribution network
$\mathcal{U}$	Set of natural gas suppliers
$\Omega_{(.)}$	Set of candidate buses/nodes to install gas-fired distributed generation units

Variables:

$I_h^{b,y}$	Binary decision variable for installing the gas-fired distributed generation unit
$P_{(.),t}^{s,y}$	Real power dispatch of a unit
$Q_{(.),t}^{s,y}$	Reactive power dispatch of a unit
$P_{d,t}^{s,y}$	Real demand
$Q_{d,t}^{s,y}$	Reactive demand
$P_{l,t}^{s,y}$	Real power flow in a branch
$Q_{l,t}^{s,y}$	Reactive power flow in a branch
$U_{b,t}^{s,y}$	Squared of bus voltage
$L_{m,d,t}^{s,y}$	Responsive load in block m
$F_{u,t}^{s,y}$	Volume of natural gas supply
$f_{p,t}^{s,y}$	Natural gas flow in a pipeline
$\pi_h^{b,y}, \Gamma_{h,t}^{s,y}$	Dual variables
$s_i, \lambda, \gamma, \eta$	Auxiliary variables

Parameters:

$A_b^{(.)}$	Element of unit-bus incidence matrix
B_b^l	Element of line-bus incidence matrix $B_b^l \in \{-1, 0, 1\}$
C_h	Investment cost of gas-fired generating unit
C_k^g	Marginal generation cost at segment k

D_b^d	Element of demand-bus incidence matrix
$d_{m,d,t}^{s,y,max}$	Maximum responsive load in block m
E_j^u	Element of natural gas supply-node incidence matrix
G_j^p	Element of natural gas pipeline-node incidence matrix
H_j^d	Element of natural gas demand-node incidence matrix
N_s	Number of days in a season
NR	Number of blocks in responsive load
$P_{(.)}^{max}$	Maximum real power dispatch of a unit
$P_{(.)}^{min}$	Minimum real power dispatch of a unit
$Q_{(.)}^{max}$	Maximum reactive power dispatch of a unit
R_l	Resistance of distribution line l
S_l^{max}	The capacity of the distribution branch
$T_{(.)}$	Number of time steps
X_l	Inductive reactance of distribution line l
κ_q^{ch}	Efficiency of charging of battery storage units
κ_q^{dc}	Efficiency of discharging of battery storage units
$\rho_{f,t}^{s,y}$	Electricity price
$\rho_n^{s,y}$	Natural gas price
$\epsilon_{(.)}$	Wasserstein radius

Uncertain Parameters:

$\widetilde{\omega}_{(.),t}^{s,y}$	Forecast error of net load.
$\widetilde{\xi}_{m,t}^{s,y}$	Bidding price of the responsive load (\$/kWh).

4.2 Problem Formulation

In this section, the expansion planning problem is formulated in the power distribution and natural gas networks. The objective function is shown in (4.1), in which the first term represents the investment cost on GFDG considering the annual discount rate (ϑ). The second term represents the expected operation cost of the distribution network, considering the worst-case probability distribution of the net demand. The third term represents the negative demand surplus for the responsive load, considering the worst-case probability

distribution for the demand bids. The fourth term in (4.1) represents the expected operation cost of the natural gas network considering the worst-case probability distribution of the natural gas demand. The constraints of this problem are shown in (4.2)-(4.41). It is assumed that no more than one GFDG is installed on each bus of the power distribution network in the planning horizon as enforced by (4.2). The expected operation cost of the distributed generation units, the expected cost of feeder energy, the expected operation cost of battery storage units, the responsive demand surplus, and the expected cost of the natural gas network are shown in (4.3)-(4.7), respectively. In (4.5), the charging and discharging modes are denoted by *ch* and *dc*, respectively.

$$min \quad \sum_{y} (1+\vartheta)^{1-y}.(\sum_{b}\sum_{h} C_h.I_h^{b,y}) + \sup_{\mathbb{P}\in\mathcal{P}} E_{\mathbb{P}}\left\{\Psi_{\mathrm{g}}\left(x_g,\widetilde{\omega}_e\right) + \Psi_{\mathrm{f}}(x_f,\widetilde{\omega}_e) + \Psi_q(x_q,\widetilde{\omega}_e)\right\} - \sup_{\mathbb{Q}\in\mathcal{Q}} E_{\mathbb{Q}}\left\{\Psi_r(x_r,\widetilde{\xi})\right\} + \sup_{\mathbb{N}\in\mathcal{N}} E_{\mathbb{N}}\left\{\Psi_n(x_n,\widetilde{\omega}_n)\right\} \tag{4.1}$$

$$\sum_{y=1}^{T_y}\sum_{h} I_h^{b,y} \leq 1 \ ; \ \forall b \in \Omega_b \tag{4.2}$$

$$\Psi_g(x_g,\widetilde{\omega}_e) = \sum_{y=1}^{T_y}(1+\vartheta)^{1-y}.\left(\sum_{s=1}^{T_s} N_s.\sum_{t=1}^{T_t}\left(\left(\sum_{g\in\mathcal{H}}\left(\sum_{k=1}^{K} C_k^g.\left(P_{g,t}^{s,y}+\sigma_{g,t}^{s,y}.\widetilde{\omega}_{e,t}^{s,y}\right)\right)\right)\right)\right) = \sum_{y=1}^{T_y}\sum_{s=1}^{T_s}\sum_{t=1}^{T_t}\left(\left(\sum_{g\in\mathcal{G}}\left(\sum_{k=1}^{K}\left(a_{g,t}^{s,y}.\widetilde{\omega}_{e,t}^{s,y}+b_{g,t}^{s,y}\right)\right)\right)\right) \tag{4.3}$$

$$\Psi_f(x_f,\widetilde{\omega}_e) = \sum_{y=1}^{T_y}(1+\vartheta)^{1-y}.\left(\sum_{s=1}^{T_s} N_s.\sum_{t=1}^{T_t}\left(\sum_{f\in\mathcal{F}}\left(\rho_{f,t}^{s,y}.\left(P_{f,t}^{s,y}+\sigma_{f,t}^{s,y}.\widetilde{\omega}_{e,t}^{s,y}\right)\right)\right)\right) = \sum_{y=1}^{T_y}\sum_{s=1}^{T_s}\sum_{t=1}^{T_t}\left(a_{f,t}^{s,y}.\widetilde{\omega}_{e,t}^{s,y}+b_{f,t}^{s,y}\right) \tag{4.4}$$

$$\Psi_q(x_q,\widetilde{\omega}_e)=\sum_{y=1}^{T_y}(1+\vartheta)^{1-y}.\sum_{s=1}^{T_s}N_s.\left(\sum_{t=1}^{T_t}\sum_{q\in\mathcal{Q}}\rho_q.\left(P_{q,t}^{ch,s,y}+P_{q,t}^{dc,s,y}+\sigma_{q,t}^{s,y}.\widetilde{\omega}_{e,t}^{s,y}\right)\right)$$
$$=\sum_{y=1}^{T_y}\sum_{s=1}^{T_s}\sum_{t=1}^{T_t}\left(a_{q,t}^{s,y}.\widetilde{\omega}_{e,t}^{s,y}+b_{q,t}^{s,y}\right) \quad (4.5)$$

$$\Psi_r(x_r,\widetilde{\xi}) \;=\; \sum_{y=1}^{T_y}(1+\vartheta)^{1-y}.\left(\sum_{s=1}^{T_s}N_s.\sum_{t=1}^{T_t}\left(\left(\sum_{d\in\mathcal{R}}\sum_{m=1}^{NR}\widetilde{\xi}_{m,t}^{s,y}.L_{m,d,t}^{s,y}\right)\right)\right) \quad (4.6)$$

$$\Psi_n(x_n,\widetilde{\omega}_n)=\sum_{y=1}^{T_y}(1+\vartheta)^{1-y}.\left(\sum_{s=1}^{T_s}N_s.\sum_{t=1}^{T_t}\rho_n^{s,y}.\left(\left(\sum_{u\in\mathcal{U}}F_{u,t}^{s,y}+\sigma_{u,t}^{s,y}.\widetilde{\omega}_{n,t}^{s,y}\right)\right)\right)$$
$$=\sum_{y=1}^{T_y}\sum_{s=1}^{T_s}\sum_{t=1}^{T_t}\left(a_{n,t}^{s,y}.\widetilde{\omega}_{n,t}^{s,y}+b_{n,t}^{s,y}\right) \quad (4.7)$$

The distribution network operation constraints are presented in (4.8)-(4.35). The linearized power flow constraint is shown in (4.8). In (4.9), the nodal voltage is constrained by the upper and lower values. The capacity of the distribution branch is approximated by the linear approximation of the circular constraints [117] as shown in (4.10)-(4.12). The reactive power dispatch of PV generation unit is limited by the upper and lower bounds as shown in (4.13).

$$B_b^l.U_{b,t}^{s,y}=2.\left(R_l^{i,j}.P_{l,t}^{s,y}+X_l^{i,j}.Q_{l,t}^{s,y}\right);\ \forall t,\forall s,\forall y \quad (4.8)$$

$$\left(V_b^{min}\right)^2\le U_{b,t}^{s,y}\le\left(V_b^{max}\right)^2\ ;\forall b,\forall t,\forall s,\forall y \quad (4.9)$$

$$-\sqrt{3}.(P_{l,t}^{s,y}+S_l^{max})\le Q_{l,t}^{s,y}\le-\sqrt{3}.(P_{l,t}^{s,y}-S_l^{max});\forall l,\forall t,\forall s,\forall y \quad (4.10)$$

$$-\frac{\sqrt{3}}{2}.S_l^{max}\le Q_{l,t}^{s,y}\le\frac{\sqrt{3}}{2}.S_l^{max}\ ;\forall l,\forall t,\forall s,\forall y \quad (4.11)$$

$$\sqrt{3}.(P_{l,t}^{s,y}-S_l^{max})\le Q_{l,t}^{s,y}\le\sqrt{3}.(P_{l,t}^{s,y}+S_l^{max})\ ;\forall l,\forall t,\forall s,\forall y \quad (4.12)$$

$$-Q_v^{max}\le Q_{v,t}^{s,y}\le Q_v^{max}\ ;\forall v,\forall t,\forall s,\forall y \quad (4.13)$$

The uncertainties in electricity demand and the PV generation are represented by net demand forecast error ($\widetilde{\omega}_t^{s,y}$) shown in (4.14) where $\tilde{P}_{(.),t}^{s,y}$ and $\overline{P}_{(.),t}^{s,y}$ are the actual and forecasted values. In (4.15)-(4.18), the affine rules for the power adjustment of distributed generation units other than GFDG as well as the feeder in response to the total net demand forecast error are shown. The nodal real and reactive power balances are shown in (4.19) and (4.20), respectively. The real and reactive power outputs of a distributed generating unit other than the GFDG unit, are limited to the unit's capacity, as shown in (4.21) and (4.22), respectively. Similarly, in (4.23) and (4.24), the real and reactive power outputs of the installed GFDG unit are limited by their maximum and minimum values. The real and reactive power dispatch of the main distribution feeder is limited by (4.25)-(4.26), considering the minimum power factor.

$$\widetilde{\omega}_{e,t}^{s,y} = \sum_{b} \left(\sum_{d \in \mathcal{D} \cup \mathcal{R}} \left(\tilde{P}_{d,t}^{s,y} - \overline{P}_{d,t}^{s,y} \right) - \sum_{v} \left(\tilde{P}_{v,t}^{s,y} - \overline{P}_{v,t}^{s,y} \right) \right); \forall t, \forall s, \forall y \tag{4.14}$$

$$0 \leq \sigma_{g,t}^{s,y} \leq 1 \ ; \forall g, \forall t, \forall s, \forall y \tag{4.15}$$

$$0 \leq \sigma_{f,t}^{s,y} \leq 1; \forall f, \forall t, \forall s, \forall y \tag{4.16}$$

$$0 \leq \sigma_{q,t}^{s,y} \leq 1; \forall q, \forall t, \forall s, \forall y \tag{4.17}$$

$$\sum_{g} \sigma_{g,t}^{s,y} + \sum_{f} \sigma_{f,t}^{s,y} + \sum_{q} \sigma_{q,t}^{s,y} = 1 \ ; \forall t, \forall s, \forall y \tag{4.18}$$

$$\sum_{f} A_b^f . (P_{f,t}^{s,y} + \sigma_{f,t}^{s,y} . \widetilde{\omega}_{e,t}^{s,y}) + \sum_{g} A_b^g . (P_{g,t}^{s,y} + \sigma_{g,t}^{s,y} . \widetilde{\omega}_{e,t}^{s,y}) + \sum_{h} A_b^h . P_{h,t}^{s,y} + \sum_{v} A_b^v . \tilde{P}_{v,t}^{s,y} + \sum_{l} B_b^l . P_{l,t}^{s,y}$$
$$+ \sum_{q} A_b^q . (P_{q,t}^{dc,s,y} - P_{q,t}^{ch,s,y} + \sigma_{q,t}^{s,y} . \widetilde{\omega}_{e,t}^{s,y}) = \sum_{d \in \mathcal{D}} D_b^d . \tilde{P}_{d,t}^{s,y} + \sum_{d \in \mathcal{R}} D_b^d . \sum_{m=1}^{NR} L_{m,d,t}^{s,y} \ ; \ \forall b, \forall t, \forall s, \forall y \tag{4.19}$$

$$\sum_{f} A_b^f.Q_{f,t}^{s,y} + \sum_{g} A_b^g.Q_{g,t}^{s,y} + \sum_{h} A_b^h.Q_{h,t}^{s,y} + \sum_{v} A_b^v.Q_{v,t}^{s,y} + \sum_{l} B_b^l.Q_{l,t}^{s,y} + \sum_{q} A_b^q.Q_{q,t}^{s,y}$$
$$= \sum_{d\in\mathcal{D}} D_b^d.\left(\tan(\cos^{-1}\theta_d).\tilde{P}_{d,t}^{s,y}\right) + \sum_{d\in\mathcal{R}} D_b^d.\tan(\cos^{-1}\theta_d).\sum_{m=1}^{NR} L_{m,d,t}^{s,y}\ ;\ \forall b,\forall t,\forall s,\forall y \quad (4.20)$$

$$P_g^{min} \le P_{g,t}^{s,y} + \sigma_{g,t}^{s,y}.\widetilde{\omega}_{e,t}^{s,y} \le P_g^{max}; \forall g,\forall t,\forall s,\forall y \quad (4.21)$$

$$-Q_g^{max} \le Q_{g,t}^{s,y} \le Q_g^{max}; \forall g,\forall t,\forall s,\forall y \quad (4.22)$$

$$P_h^{min}.I_h^{b,y} \le P_{h,t}^{s,y} \le P_h^{max}.I_h^{b,y}; \forall h,\forall t,\forall s,\forall y \quad (4.23)$$

$$-Q_h^{max}.I_h^{b,y} \le Q_{h,t}^{s,y} \le Q_h^{max}.I_h^{b,y}; \forall h,\forall t,\forall s,\forall y \quad (4.24)$$

$$P_f^{min} \le P_{f,t}^{s,y} + \sigma_{f,t}^{s,y}.\widetilde{\omega}_{e,t}^{s,y} \le P_f^{max}; \forall f,\forall t,\forall s,\forall y \quad (4.25)$$

$$-\tan(\theta_f)\ .P_{f,t}^{s,y} \le Q_{f,t}^{s,y} \le \tan(\theta_f)\ .P_{f,t}^{s,y}; \forall f,\forall t,\forall s,\forall y \quad (4.26)$$

The operation constraints for the battery storage units are given in (4.27)-(4.32). Since the expected operation cost of the battery storage units is minimized in the objective function (4.1), the discharging and charging states are mutually exclusive [118, 119]. The available hourly energy of the battery storage is limited by the battery capacity limits as shown in (4.27) and determined using the hourly charging and discharging power as enforced by (4.28). The starting and final values of the stored energy in the battery storage are equal to an initial value as enforced by (4.29). The limits on discharging and charging of the battery storage units are presented in (4.30) and (4.31), respectively. Here, the battery participation factor in response to the net demand uncertainty is considered [120]. The reactive power of the battery storage units is within the limits as enforced by (4.32).

$$E_q^{min} \le E_{q,t}^{s,y} \le E_q^{max} \quad (4.27)$$

$$E_{q,t}^{s,y} = E_{q,t-1}^{s,y} + (\kappa_q^{ch} \cdot p_{q,t}^{ch,s,y} - \frac{p_{q,t}^{dc,s,y}}{\kappa_q^{dc}}) \quad (4.28)$$

$$E_{q,1}^{s,y} = E_{q,T_t}^{s,y} = E_q^{ini} \quad (4.29)$$

$$0 \le p_{q,t}^{dc,s,y} + \sigma_{q,t}^{s,y}.\widetilde{\omega}_{e,t}^{s,y} \le p_q^{max} \quad (4.30)$$

$$0 \leq p_{q,t}^{ch,s,y} - \sigma_{q,t}^{s,y}.\widetilde{\omega}_{e,t}^{s,y} \leq p_q^{max} \tag{4.31}$$

$$-Q_q^{max} \leq Q_{q,t}^{s,y} \leq Q_q^{max} \tag{4.32}$$

Demand response (DR) programs provide several benefits in the planning and operation of the electricity network, including savings in customers' energy costs, reduction in the energy production costs, improving system reliability, and reducing the risk of unexpected outages [121, 122]. The capacity of the responsive load is restricted by the total load as shown in (4.33) [123]. The responsive load at each block of the bidding curve is limited by the upper and lower bounds as enforced by (4.34). The total daily deployed demand response is limited by an upper bound ($ED_{d,s,y}^{max}$) as shown in (4.35).

$$0 \leq \sum_{m=1}^{NR} L_{m,d,t}^{s,y} \leq \tilde{P}_{d,t}^{s,y} \; ; \forall d \in \mathcal{R}, \forall t, \forall s, \forall y \tag{4.33}$$

$$0 \leq L_{m,d,t}^{s,y} \leq d_{m,d,t}^{s,y,max} \; ; \forall d \in \mathcal{R}, \forall m, \forall t, \forall s, \forall y \tag{4.34}$$

$$\sum_{t} (\tilde{P}_{d,t}^{s,y} - \sum_{m=1}^{NR} L_{m,d,t}^{s,y}) \; \leq ED_{d,s,y}^{max} \; ; \forall d \in \mathcal{R}, \forall s, \forall y \tag{4.35}$$

The operation constraints of the natural gas network are presented in (4.36)-(4.41). The uncertainty in the natural gas demand is represented by the forecast error ($\widetilde{\omega}_{n,t}^{s,y}$) in (4.36). Constraints (4.37)-(4.38) present the affine rules for adjusting the natural gas supply in response to the forecast error in natural gas demand. To reduce the complexity of the long-term expansion planning problem, the nodal demand and supply balance and the limitation on the natural gas flow in the pipelines are considered [49,50,53]. The nodal supply and demand balance for the natural gas network is enforced by (4.39). The natural gas consumption of the GFDG unit is determined using its power output as shown in (4.39), where ζ_h is the energy conversion efficiency of the unit. The natural gas supply is limited by the minimum and maximum limits as shown in (4.40). The natural gas flow in the pipeline is limited by the pipeline capacity as enforced by (4.41).

$$\widetilde{\omega}_{n,t}^{s,y} = \sum_{d \in \mathcal{L}} (\tilde{P}_{d,t}^{s,y} - \overline{P}_{d,t}^{s,y}); \; \forall t, \forall s, \forall y \tag{4.36}$$

$$0 \leq \sigma_{u,t}^{s,y} \leq 1;\ \forall u, \forall t, \forall s, \forall y \tag{4.37}$$

$$\sum_{u} \sigma_{u,t}^{s,y} = 1;\ \forall u, \forall t, \forall s, \forall y \tag{4.38}$$

$$\sum_{u} E_j^u.(F_{u,t}^{s,y} + \sigma_{u,t}^{s,y}.\widetilde{\omega}_{n,t}^{s,y}) = \sum_{p} G_j^p.f_{p,t}^{s,y} + \sum_{d \in \mathcal{L}} H_j^d.\tilde{P}_{d,t}^{s,y} + \sum_{d \in \Omega_j} H_j^d.(\zeta_h.P_{h,t}^{s,y})\ ; \forall j, \forall t, \forall s, \forall y \tag{4.39}$$

$$F_u^{min} \leq F_{u,t}^{s,y} + \sigma_{u,t}^{s,y}.\widetilde{\omega}_{n,t}^{s,y} \leq F_u^{max};\ \forall u, \forall t, \forall s, \forall y \tag{4.40}$$

$$f_p^{min} \leq f_{p,t}^{s,y} \leq f_p^{max};\ \forall p, \forall t, \forall s, \forall y \tag{4.41}$$

4.3 Problem Reformulation

In order to reformulate the problem, first we define the ambiguity set using the Wasserstein distance metric, and later we reformulate the problem into an MILP problem. Given the probability distributions $\mathbb{P}_1, \mathbb{P}_2 \in M(\Xi)$, where $M(\Xi)$ is the space of all probability distributions $\mathbb{P}$ and Ξ is the support set, the Wasserstein distance between the probability distributions $\mathbb{P}_1$ and $\mathbb{P}_2$ is defined as (4.42) [62, 63, 65, 66, 124]. Here, $\|.\|$ can represent any norm on $\mathbb{R}^m$ and Π is the joint probability distribution of the uncertain variables ξ_1 and ξ_2 with marginal probability distributions $\mathbb{P}_1$ and $\mathbb{P}_2$ respectively. In this chapter, the 1-Wasserstein distance metric [124], i.e., the L_1-norm distance is used. The Wasserstein distance-based ambiguity set is defined in (4.43) in which the empirical distribution $\mathbb{P}_{\mathrm{N}}$ is centered in the Wasserstein ball with radius $\epsilon(\mathrm{N})$. The radius $\epsilon(\mathrm{N})$ is calculated using (4.44) and (4.45) [62,63], [65] given the confidence level β, the sample size N, and the mean value of samples μ. The Wasserstein-based ambiguity set has the following properties [124]: a) finite sample guarantee, b) the solution of the data-driven converges to the stochastic solution as N tends to ∞, and c) tractable reformulation.

$$d_w\left(\mathbb{P}_1, \mathbb{P}_2\right) = \inf \left\{ \int_{\Xi^2} \|\xi_1 - \xi_2\| \quad \Pi(\mathrm{d}\xi_1, d\xi_2) \right. \tag{4.42}$$

$$\Xi := \{\mathbb{P} \in M(\Xi) \ \mid d_w\left(\mathbb{P}_N, \mathbb{P}\right) \leq \epsilon(\mathrm{N})\} \tag{4.43}$$

$$\epsilon(\mathrm{N}) = D.\sqrt{\frac{2}{N}\log(\frac{1}{1-\beta})} \tag{4.44}$$

$$D = \min_{\delta \geq 0} 2\sqrt{\frac{1}{2.\delta}\left(1 + ln\left(\frac{1}{N}\sum_{i=1}^{N} e^{\delta(\|\widehat{\xi}_i - \mu\|)}\right)\right)} \tag{4.45}$$

The second and third terms in the objective function (4.1) are piece-wise affine functions. Assuming that the uncertainty set of the net demand is represented by a polytope, the uncertainty set is given as: $\Xi = \widetilde{\omega}_e \in \mathbb{R}^m : C_e.\widetilde{\omega}_e \leq d_e$. Using the Corollary 5.1 in [124], the worst-case expected operation cost of distributed generation is determined by formulating (4.46a)-(4.46c), where $\gamma^e_{i,k}$ is a positive variable and $\widetilde{\omega}^{s,y}_{e,t}$ in (4.14) is simplified to $\widetilde{\omega}_e$. Here, L_∞ norm in (4.46c) is represented by a set of linear constraints (4.46d)-(4.46f) [64]. Similar formulation is used to determine the worst-case expected operation cost of the main distribution feeder considering the worst-case probability distribution of the net demand.

$$\sup_{\mathbb{P}\in\mathcal{P}} E_{\mathbb{P}}\left\{\Psi_g(x_g, \widetilde{\omega}_e)\right\} = \inf_{\lambda, s_i, \gamma_{i,k}} (\lambda_e.\ \epsilon_e + \frac{1}{N_e}\sum_{i=1}^{N_e} s^e_i) \tag{4.46a}$$

$$s.t\ \ \Psi_g\left(x_g, \widehat{\omega}^i_e\right) + \gamma^{e,\intercal}_{i,k}.\left(d_e - C_e.\widehat{\omega}^i_e\right) \leq s^e_i,\ \forall i \leq N_e, k \leq K \tag{4.46b}$$

$$\left\|{C_e}^T \gamma^e_{i,k} - a^e_k\right\|_\infty \leq \lambda_e,\ \forall i \leq N_e, k \leq K \tag{4.46c}$$

$$\eta_e \leq \lambda_e \tag{4.46d}$$

$$\eta_e \geq {C_e}^T \gamma^e_{i,k} - a^e_k,\ \forall i \leq N_e, k \leq K \tag{4.46e}$$

$$\eta_e \geq -({C_e}^T \gamma^e_{i,k} - a^e_k),\ \forall i \leq N_e, k \leq K \tag{4.46f}$$

The fourth term in the objective function is the demand surplus which is a concave function. Assuming that the uncertainty set of demand bids is a polytope $\Xi = \widetilde{\xi} \in \mathbb{R}^m : C_r.\widetilde{\xi} \leq d_r$. According to Corollary 5.4 in [124], the worst-case expected demand surplus in the fourth term of (4.1) is determined by formulating (4.47a)-(4.47c) where x_r is the responsive demand in each block and γ^r_i is a positive variable.

$$\sup_{\mathbb{Q}\in\mathcal{Q}} E_{\mathbb{Q}}\left\{\Psi_r(x_r, \widetilde{\xi})\right\} = \inf_{\lambda, s_i, \gamma_i} (\lambda_r.\ \epsilon_r + \frac{1}{N_r}\sum_{i=1}^{N_r} s^r_i) \tag{4.47a}$$

$$s.t\ \ -\Psi_r\left(x_r, \widehat{\xi}_i\right) + \gamma^{r,\intercal}_i.\left(d_r - C_r.\widehat{\xi}_i\right) \leq s^r_i,\ \forall i \leq N_r \tag{4.47b}$$

$$\left\| x_r - {C_r}^T \gamma_i^r \right\|_\infty \leq \lambda_r, \ \forall i \leq N_r \tag{4.47c}$$

The expected operation cost of the natural gas network under the worst-case PDF of natural gas demand is shown in the fifth term of the objective function (4.1). This term is a piece-wise affine function with $k = 1$, as shown in (4.7). The uncertain natural gas load is within a polytope defined by $\Xi = \widetilde{\omega}_n \in \mathbb{R}^m : C_n.\widetilde{\omega}_n \leq d_n$. Therefore, the worst-case expected operation cost for the natural gas network is determined by solving (4.48a)-(4.48c), (4.36)-(4.41) where, $\widetilde{\omega}_{n,t}^{s,y}$ in (4.36) is simplified to $\widetilde{\omega}_n$.

$$\sup_{\mathbb{N} \in \mathcal{N}} E_{\mathbb{N}} \left\{ \Psi_n(x_n, \widetilde{\omega}_n) \right\} \ = \ \inf_{\lambda, s_i, \gamma_{i,k}} \ (\lambda_n.\ \epsilon_n + \frac{1}{N_n} \sum_{i=1}^{N_n} s_i^n) \tag{4.48a}$$

$$s.t \quad \Psi_n \left(x_n, \widehat{\omega}_n^i \right) + \gamma_{i,k}^{n,\intercal}. \left(d_n - C_n.\widehat{\omega}_n^i \right) \leq s_i^n, \ \forall i \leq N_n, k = 1 \tag{4.48b}$$

$$\left\| {C_n}^T \gamma_{i,k}^n - a_k^n \right\|_\infty \leq \lambda_n, \ \forall i \leq N_n, k = 1 \tag{4.48c}$$

By incorporating the above reformulations, the problem (4.1)-(4.41) is reformulated in (4.49), (4.2)-(4.7), (4.46b),(4.46d)-(4.46f), (4.47b)-(4.47c), (4.48b)-(4.48c), the distribution operation constraints (4.8)-(4.35), and the natural gas operation constraints (4.36)-(4.41).

$$\begin{aligned} min \quad & \sum_y (1+\vartheta)^{1-y}.(\sum_i \sum_h C_h.I_h^{b,y}) + \lambda_e.\epsilon_e \\ & + \frac{1}{N_e} \sum_{i=1}^{N_e} s_i^e + \lambda_r.\epsilon_r + \frac{1}{N_r} \sum_{i=1}^{N_r} s_i^r + \lambda_n.\epsilon_n + \frac{1}{N_n} \sum_{i=1}^{N_n} s_i^n \end{aligned} \tag{4.49}$$

4.4 Solution Methodology

This section presents the decentralized framework to solve the GFDG expansion planning problem in the interconnected power distribution and natural gas networks. Here, the dispatch of the GFDG unit, i.e., $P_{h,t}^{s,y}$ is shared between the DSO and the natural gas supplier, and the decentralized framework is solved in the following stages.

4.4.1 Master Problem

The expansion planning problem is formulated as a master problem (MP) (4.50a)-(4.50b), and (4.2). The objective is to minimize the lower bound of the solution, which is the investment costs of GFDG as shown in (4.50b). Once the MP is solved, the expansion decisions, i.e., $\hat{I}_h^{b,y}$, are sent to the distribution network feasibility check subproblem (SP1).

$$\min \quad Z_{lower} \tag{4.50a}$$

$$Z_{lower} \geq \sum_{y} (1+\vartheta)^{1-y}.(\sum_{b}\sum_{h} C_h.I_h^{b,y}) \tag{4.50b}$$

4.4.2 Sub-Problems

The distribution network feasibility sub-problem (SP1) is formulated in (4.51a)-(4.51d) and the distribution network operation constraints (4.8)-(4.18) and (4.21)-(4.35). The objective of SP1 (4.51a) is to minimize the mismatch in electricity generation and demand in the distribution network. The slack variables are introduced in the real and reactive power balance constraints (4.51b) and (4.51c) to capture the mismatch in real and reactive power generation and demand. The expansion planning decisions are fixed to the solution obtained from the MP using (4.51d). Here, the planning decision ($I_h^{b,y}$) is a continuous variable in the sub-problems.

$$\min \quad W_1 = \sum_{y}\sum_{s}\sum_{t}\sum_{b}(Z_{b,t}^{1,s,y} + Z_{b,t}^{2,s,y} + Z_{b,t}^{3,s,y} + Z_{b,t}^{4,s,y}) \tag{4.51a}$$

$$\begin{aligned}\sum_{f} A_b^f.(P_{f,t}^{s,y} + \sigma_{f,t}^{s,y}.\widetilde{\omega}_{e,t}^{s,y}) + \sum_{g} A_b^g.(P_{g,t}^{s,y} + \sigma_{g,t}^{s,y}.\widetilde{\omega}_{e,t}^{s,y}) + \sum_{h} A_b^h.P_{h,t}^{s,y} + \sum_{v} A_b^v.\tilde{P}_{v,t}^{s,y} + \sum_{l} B_b^l.P_{l,t}^{s,y} \\ + \sum_{q} A_b^q.(P_{q,t}^{dc,s,y} - P_{q,t}^{ch,s,y} + \sigma_{q,t}^{s,y}.\widetilde{\omega}_{e,t}^{s,y}) + Z_{b,t}^{1,s,y} - Z_{b,t}^{2,s,y} \\ = \sum_{d\in\mathcal{D}} D_b^d.\tilde{P}_{d,t}^{s,y} + \sum_{d\in\mathcal{R}} D_b^d.\sum_{m=1}^{NR} L_{m,d,t}^{s,y} \;;\; \forall b, \forall t, \forall s, \forall y\end{aligned} \tag{4.51b}$$

$$\sum_{f} A_b^f.Q_{f,t}^{s,y} + \sum_{g} A_b^g.Q_{g,t}^{s,y} + \sum_{h} A_b^h.Q_{h,t}^{s,y} + \sum_{v} A_b^v.Q_{v,t}^{s,y} + \sum_{l} B_b^l.Q_{l,t}^{s,y} + \sum_{q} A_b^q.Q_{q,t}^{s,y}$$
$$+ Z_{b,t}^{3,s,y} - Z_{b,t}^{4,s,y} = \sum_{d\in\mathcal{D}} D_b^d.\Big(\tan(\cos^{-1}\theta_d).\tilde{P}_{d,t}^{s,y}\Big)$$
$$+ \sum_{d\in\mathcal{R}} D_b^d.\tan(\cos^{-1}\theta_d).\sum_{m=1}^{NR} L_{m,d,t}^{s,y} \;;\; \forall b,\forall t,\forall s,\forall y \quad (4.51c)$$

$$I_h^{b,y} = \hat{I}_h^{b,y} \;\; : \pi_h^{b,y} \;\; ;\forall h,\forall b,\forall y \quad (4.51d)$$

If the SP1 is infeasible, the feasibility cut in (4.52) is formed and sent to the MP.

$$\hat{W}_1 + \sum_{y}\sum_{b}\sum_{h} \widehat{\pi}_h^{b,y} .(I_h^{b,y} - \hat{I}_h^{b,y}\;) \leq 0 \quad (4.52)$$

Next, the natural gas network feasibility sub-problem (SP2) is presented in (4.53a)-(4.53c), (4.36)-(4.38) and (4.40)-(4.41). The objective is to minimize the natural gas supply and demand mismatch in the natural gas network. Here, slack variables are introduced in the natural gas nodal balance constraint (4.53b) to capture mismatch in the nodal supply and demand. The dispatch for the GFDG units is fixed to the solution of the sub-problem SP1 as shown in (4.53c).

$$\min \sum_{y}\sum_{s}\sum_{t} W_{2,t}^{s,y} = \sum_{y}\sum_{s}\sum_{t}\sum_{j} (Z_{j,t}^{1,s,y} + Z_{j,t}^{2,s,y}) \quad (4.53a)$$

$$\sum_{u} E_j^u.(F_{u,t}^{s,y} + \sigma_{u,t}^{s,y}.\widetilde{\omega}_{n,t}^{s,y}) = \sum_{p} G_j^p.f_{p,t}^{s,y} + \sum_{d\in\mathcal{L}} H_j^d.\tilde{P}_{d,t}^{s,y}$$
$$+ Z_{j,t}^{1,s,y} - Z_{j,t}^{2,s,y} + \sum_{d\in\Omega_j} H_j^d.(\zeta_h.P_{h,t}^{s,y}) \;;\forall j,\forall t,\forall s,\forall y \quad (4.53b)$$

$$P_{h,t}^{s,y} = \hat{P}_{h,t}^{s,y} : \Gamma_h^{s,y}; \forall h,\forall t,\forall s,\forall y \quad (4.53c)$$

If the SP2 is infeasible, the feasibility cut (4.54) is generated and sent to the sub-problem SP1 solved by the DSO.

$$\hat{W}_{2,t}^{s,y} + \sum_{h} \widehat{\Gamma}_{h,t}^{s,y} .(P_{h,t}^{s,y} - \hat{P}_{h,t}^{s,y}) \leq 0; \forall t, \forall s, \forall y \tag{4.54}$$

Once the sub-problems SP1 and SP2 are feasible, the DSO solves the distribution network optimality sub-problem (SP3) in (4.55a)-(4.55b), (4.3)-(4.6), (4.8)-(4.35), (4.46b),(4.46d)-(4.46f), (4.47b)-(4.47c), and (4.51d). If the solution obtained from the MP, i.e., $\hat{I}_h^{b,y}$ is not optimal, the optimality cut (4.56) is added to the MP.

$$min \;\; W_3 \tag{4.55a}$$

$$W_3 \geq \lambda_e.\epsilon_e + \frac{1}{N_e}\sum_{i=1}^{N_e} s_i^e + \lambda_r.\epsilon_r + \frac{1}{N_r}\sum_{i=1}^{N_r} s_i^r \tag{4.55b}$$

$$Z_{lower} \geq \sum_{y} (1+\vartheta)^{1-y}.(\sum_{i}\sum_{h} C_h.I_h^{b,y}) + \hat{W}_3 + \sum_{y}\sum_{b}\sum_{h} \widehat{\pi}_h^{b,y} .(I_h^{b,y} - \hat{I}_h^{b,y}) \tag{4.56}$$

Subsequently, the natural gas supplier solves the natural gas optimality sub-problem (SP4) (4.57), (4.7), (4.36)-(4.41), (4.48b)-(4.48c), and (4.53c). If the solution procured by the DSO in the sub-problem SP3, i.e., $\hat{P}_{h,t}^{s,y}$, is not optimal in the sub-problem SP4, the optimality cut in (4.58) is sent to the sub-problem SP3.

$$\min \;\; \mathrm{W}_4 = \lambda_n.\epsilon_n + \frac{1}{N_n}\sum_{i=1}^{N_n} s_i^n \tag{4.57}$$

$$W_3 \geq \lambda_e.\epsilon_e + \frac{1}{N_e}\sum_{i=1}^{N_e} s_i^e + \lambda_r.\epsilon_r + \frac{1}{N_r}\sum_{i=1}^{N_r} s_i^r + \hat{W}_4 + \sum_{y}\sum_{s}\sum_{t}\sum_{h} \widehat{\Gamma}_{h,t}^{s,y} . \left(P_{h,t}^{s,y} - \hat{P}_{h,t}^{s,y}\right) \tag{4.58}$$

4.4.3 Proposed Algorithm

The implementation of the proposed algorithm for solving the natural gas expansion planning in the interconnected distribution and natural gas networks is as follows:

Step 0: Initialization:

- Obtain the forecasted values and empirical samples of the historical data for each

uncertain variable.

- Calculate the Wasserstein radius for each uncertain parameter according to (4.44)-(4.45).

- Set count iteration $\tau = 0$.

- Set the predefined tolerance ϵ.

Step 1: Solve the MP and update the expansion decision $\hat{I}_h^{b,y}$ and $Z_{lower}^{(\tau)}$.

Step 2: Solve the SP1 for the procured planning decision $\hat{I}_h^{b,y}$ from the MP.

Step 3: Solve the SP2 for the procured GFDG dispatch $\hat{P}_{h,t}^{s,y}$ from the SP1.

Step 4: Check if SP2 is feasible, i.e., $\sum_y \sum_s \sum_t \hat{W}_{2,t}^{s,y} = 0$, then go to Step 5. Otherwise, add feasibility cut (4.54) to the SP1 and go to Step 2.

Step 5: Check if SP1 is feasible, i.e., $\hat{W}_1 = 0$, then go to Step 6. Otherwise, add feasibility cut (4.52) to the MP and go to Step 1.

Step 6: Solve the SP3 for the procured planning decision $\hat{I}_h^{b,y}$ from the MP.

Step 7: Solve the SP4 for the procured GFDG dispatch $\hat{P}_{h,t}^{s,y}$ from the SP3.

Step 8: Calculate the upper and lower bounds of the operation solution UB and LB according to (4.59) and (4.60) respectively.

$$UB = \widehat{\lambda}_e.\epsilon_e + \frac{1}{N_e}\sum_{i=1}^{N_e} \hat{s}_i^e + \widehat{\lambda}_r.\epsilon_r + \frac{1}{N_r}\sum_{i=1}^{N_r} \hat{s}_i^r + \widehat{\lambda}_n.\epsilon_n + \frac{1}{N_n}\sum_{i=1}^{N_n} \hat{s}_i^n \tag{4.59}$$

$$LB = \hat{W}_3 \tag{4.60}$$

Step 9: If $\frac{|UB-LB|}{|UB+LB|} \leq \varepsilon$ is satisfied, then go to Step 10; otherwise, generate the optimality cut (4.58) and add it to SP3 and go to Step 6.

Step 10: Calculate the upper bound of the planning solution ($Z_{upper}^{(\tau)}$) using (4.61).

$$Z_{upper}^{(\tau)} = \sum_y (1+\vartheta)^{1-y}.(\sum_b \sum_h C_h.\hat{I}_h^{b,y}) + \hat{W}_3 \tag{4.61}$$

Step 11: If $\frac{\left|Z_{upper}^{(\tau)} - Z_{lower}^{(\tau)}\right|}{Z_{upper}^{(\tau)} + Z_{lower}^{(\tau)}} \leq \varepsilon$, then terminate the algorithm. Otherwise, send the optimality cut (4.56) to the MP, increase the iteration index $\tau = \tau + 1$, and go to Step 1. The flowchart of the proposed framework is shown in Fig. 4.1.

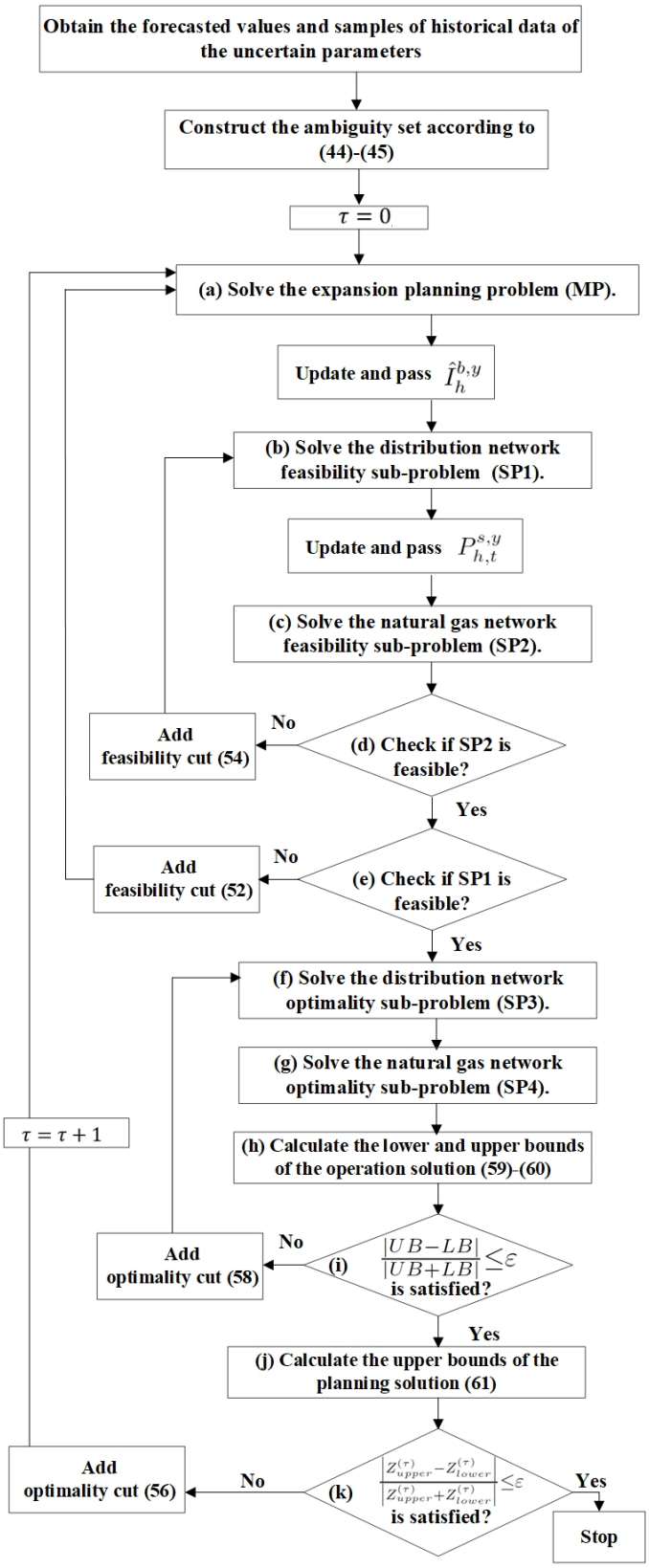

Figure 4.1: The flowchart of the proposed algorithm.

Table 4.2: GFDG Units' Characteristics

Type	P_{max} (kW)	Q_{max} (kvar)	IC ($/kW)	ζ_h (%)
GF1	350	175	710	32%
GF2	250	125	650	31%

Table 4.3: Distributed Generation Units' Characteristics

Units	Bus	P_{max} (kW)	Q_{max} $(kvar)$	$\$/kWh^2$	$\$/kWh$
DG1	B9	260	180	0.00015	0.0025
DG2	B20	200	100	0.00028	0.038

4.5 Numerical Results

In this section, the modified IEEE 34-bus distribution network interconnected with the 11-node natural gas network [51] is used to evaluate the effectiveness of the proposed expansion planning framework. The network topology is shown in Fig. 4.2. The maximum capacity of the main distribution feeder is 1.6 MVA with a minimum power factor of 0.8. As shown in Fig. 4.2, the gas supplier is at node 4 and has a capacity of 6000 m^3/h [51]. There are two potential candidates for the GFDG units as shown in Table 4.2 [125]. The characteristics of other distributed generation and photovoltaic generation units are shown in Tables 4.3 and 4.4, respectively. The battery storage units' characteristics are shown in Table 4.5 [126] and the battery operation costs are estimated using the formulation in [127]. The efficiency of discharging and charging of the battery storage units is 90%. The seasonal values of the natural gas demand and price are the average of the monthly values in a season, which are obtained from [128] and [129], respectively. The conversion efficiencies (ζ_h) of GFDG units are 32% and 31% for types GF1 and GF2, respectively. Buses B19, B21, B23, B24, B29, and B33 are the candidate buses for installing GFDG units.

The historical data for the hourly energy prices and normalized electricity demand pro-

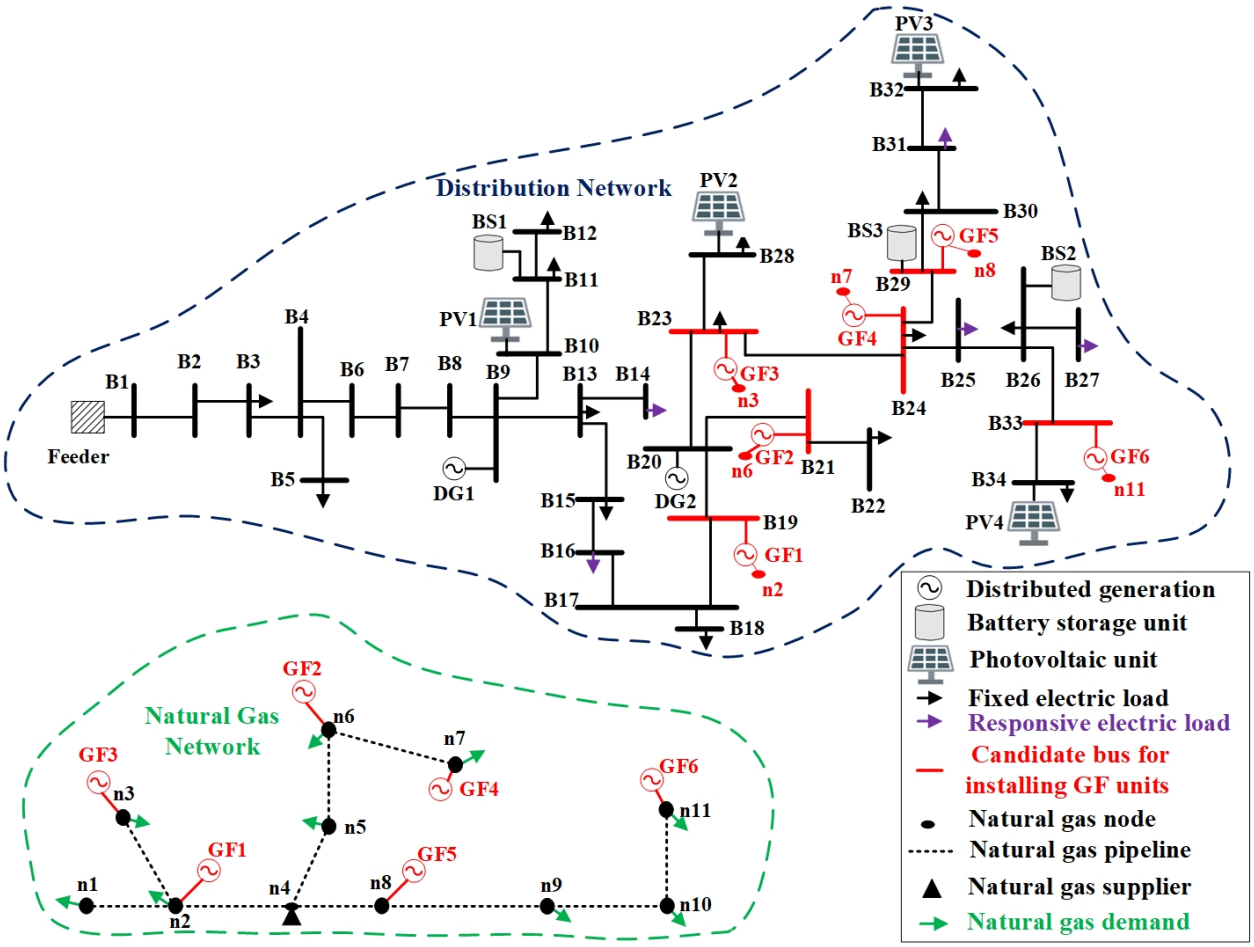

Figure 4.2: The modified IEEE 34-bus distribution network interconnected with an 11-node natural gas network.

Table 4.4: PV units' Characteristics

PVs	Bus	P_{max} (kW)	Q_{max} $(kvar)$
PV1	B10	150	75
PV2	B28	300	150
PV3	B32	160	80
PV4	B34	250	125

Table 4.5: Characteristics of battery storage units

Battery	Bus	ρ_q $(\$/kWh)$	E_{max} (kWh)	P_{max} (kW)	Q_{max} $(kvar)$
BS1	11	0.18	400	100	60
BS2	26	0.17	200	50	35
BS3	29	0.15	100	25	15

file are obtained from [130], and the hourly normalized photovoltaic output is obtained from [131]. Five responsive demands at buses B14, B16, B25, B27, and B31 with three bidding blocks for each responsive demand are considered. The annual input data consists of electricity price, electricity demand, PV power outputs, prices for demand bid in each block, natural gas demand, and natural gas price. Three representative days are considered in each year where each day represents a typical day in a season, i.e., spring/fall, summer, and winter [78, 79]. The number of days in each season is 92, 91, 92, and 90 for spring, fall, summer, and winter, respectively [79]. Therefore, the representative days capture 183, 92, and 90 days in spring/fall, summer, and winter, respectively. The empirical distributions of the samples are assumed to follow multivariate normal distribution functions, where the mean values are shown in Fig. 4.3, and the standard deviation is assumed to be 3% of the mean values [74, 75]. The annual growth rate is 3% for the electricity and natural gas demands. The hourly electricity prices and demand bids in each block on the first representative day in the fall/spring season in the first year are shown in Fig. 4.4. The normalized

photovoltaic power profiles, electricity demand, and natural gas demand profiles in the three representative days of the first year are shown in Fig. 4.3. The proposed expansion planning is performed for 10 years, where the annual discount rate is 10%. The optimality gap (ε) in step 12 is 0.01%. The allowable $ED^{max}_{d,s,y}$ is 5% of the total forecast daily load d in this period. The allowable $ED^{max}_{d,s,y}$ increases by 3% annually. The case studies are simulated on a server with dual 14 Core Intel Xeon 2.6 GHz, 380 GB of memory, and Cplex 12.8 is used as the solver. Two case studies are considered. First, the deterministic solution is presented where the forecast values of the uncertain parameters are used. Second, the distributionally robust expansion planning decisions are presented using 20 hourly samples of each uncertain parameter. Finally, the performance of the proposed algorithm is evaluated. The performance of the proposed DRO solution is compared to the solution to the SP problem solved using the Sample Average Approximation (SAA) approach.

4.5.1 Case 1 – Expansion planning deterministic solution

In this case, the forecasted values of electricity demand, demand bidding prices, photovoltaic power generation outputs, and natural gas demand are considered. To evaluate the impact of DR program on the expansion planning decision, DR program is ignored in this case. The expansion planning decisions, in this case, are to install three GFDG with 750 kW. The three units of type GF2 are installed at buses B21, B23, and B19 in the eighth, ninth, and tenth years, respectively. The investment cost is \$207,374.09, and the total planning and operation costs is \$2,632,777.98. Considering the DR program in expansion planning problem, the expansion planning decision is to install one GFDG of type GF2 at bus B33 in the tenth year. The hourly regulation of the responsive demand using the DR program reduced the installed capacity of GFDG units from 750 kW in the case without DR to 250 kW in the case with DR. Hence, the investment cost for GFDG is reduced to \$62,650.78. The total operation cost of the distribution and natural gas networks is \$2,458,370.38, where the main distribution feeder cost, the distributed generation operation cost, the operation cost of the battery storage units, and the natural gas operation cost are \$1,682,687.74, \$311,775.68, \$29,104.55. and \$434,802.41, respectively. Furthermore, the DR flattens the hourly demand profile, e.g., the electric demands at the peak periods of hours 18-20 during the fall/spring

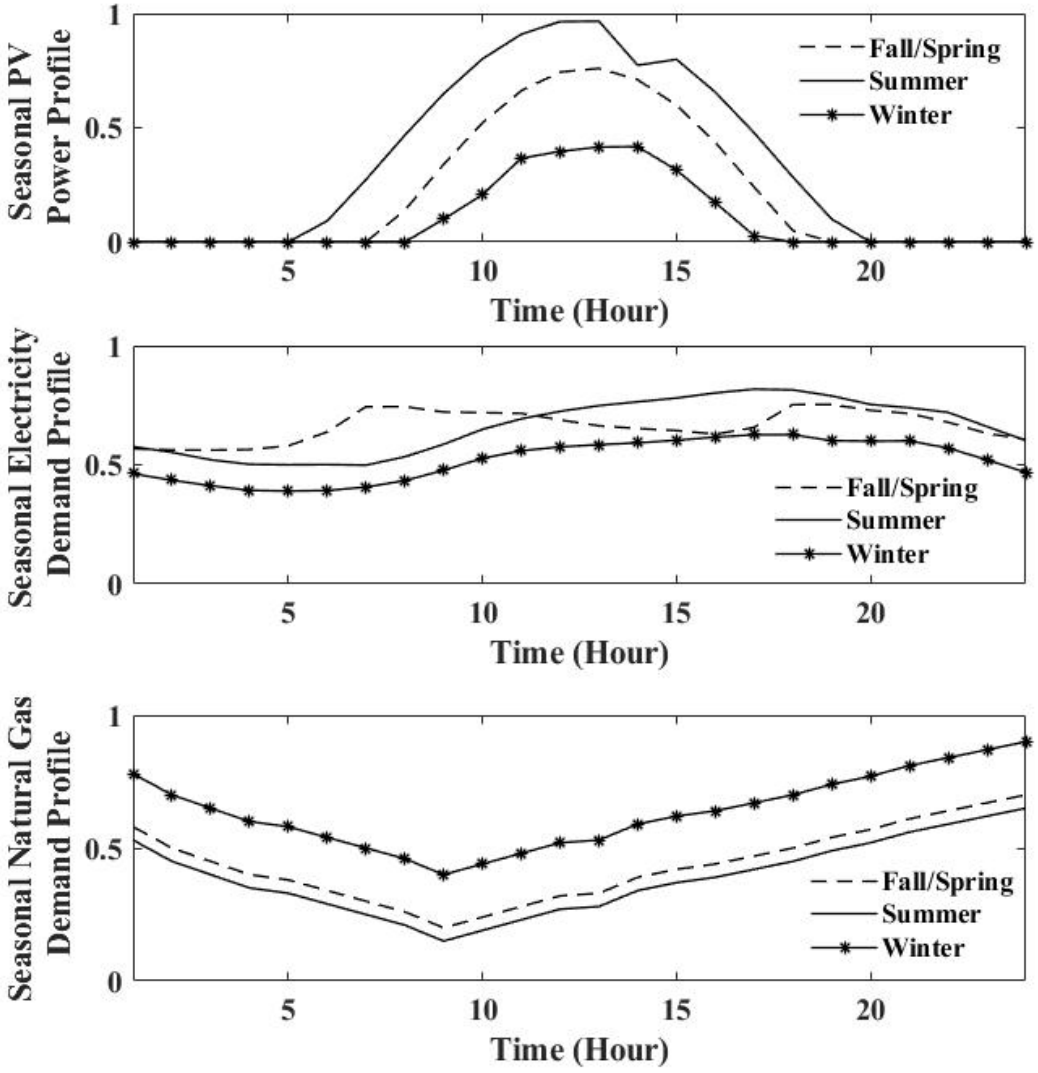

Figure 4.3: The normalized photovoltaic power, electricity demand, and natural gas demand profiles in the three seasons of the first year.

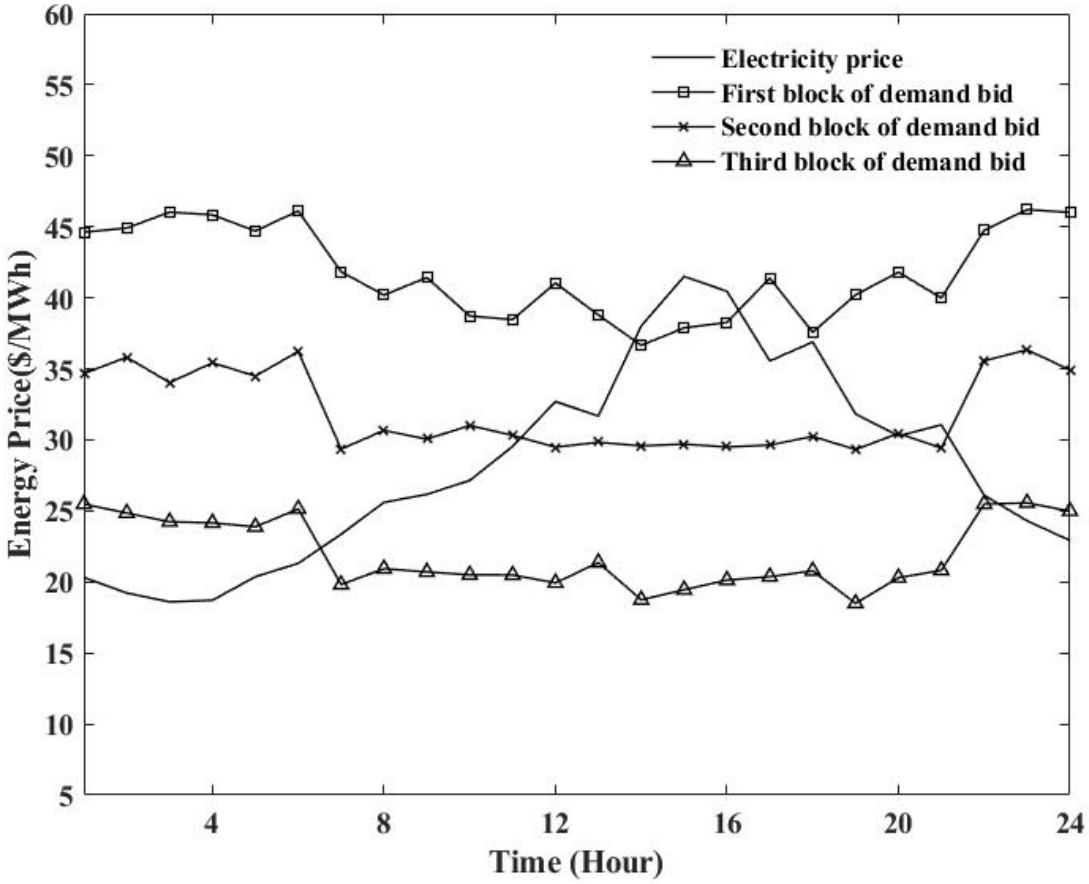

Figure 4.4: The hourly electricity prices and demand bid in each block of the first representative day (i.e., fall/spring season) in the first year.

season in the first year are reduced by 57.939 kW, 100.953 kW, and 51.161 kW, respectively. Moreover, installing gas-fired unit GF2 at buses B33 is delayed for two years compared to the case without the DR program. Incorporating DR program into the planning framework reduces the total expansion planning and operation costs from $2,632,777.98 to $2,521,021.16. Hence, incorporating DR program in the planning decision not only reduced the installed capacity of GFDG and the total planning and operation costs but also postponed the expansion decisions in the distribution network and reduced the reliance on the natural gas network.

4.5.2 Case 2 – Distributionally Robust Expansion Planning

In this case, the solution to the formulated distributionally robust expansion planning problem is presented. The empirical data include 20 hourly samples of uncertain variables, i.e., 1440 samples in each year, and the uncertain variables include electricity demand, PV power output, demand bid in each block, and natural gas demand. The Wasserstein radius for uncertain variable is obtained by solving (4.44)-(4.45) [62]. The expansion planning decisions, in this case, are to install 3 GFDG units with a total power capacity of 750 kW, which is 500 kW higher than the installed capacity in Case 1. The three GFDG units of type GF2 are installed at buses B29, B24, and B23 in the eighth, ninth, and tenth years, respectively. Compared to Case 1, the investment cost on GFDG units is increased to $207,374.09, and the total expected operation cost is $2,412,512.53. Here, the expected distribution and natural gas network operation costs are $1,967,606.27 and $444,906.26, respectively. The total expansion planning and expected operation cost is $2,619,886.62. The expansion planning solution is feasible for the power distribution and natural gas networks after 8 iterations, and the solution is optimal for both networks after 3 iterations.

The in-sample performance of the formulated DRO problem is compared to the SP counterpart solved using the Benders decomposition technique. Here, the solution to the SP problem provides less conservative planning decisions, i.e., installing 2 GFDG units with a total power capacity of 500 kW on Bus B29 and B21 in the ninth and tenth years, respectively. The solution time of the DRO and SP problems that are solved for the same optimality gap (ε=0.01%) are 6h-21min-56s and 3h-46min- 35s, respectively. However, the

solution to the SP problem is not hedged against unseen scenarios that will be discussed in the next subsection.

4.5.3 Performance Evaluation

This section compares the solution to the proposed decentralized DRO framework with the solution to the SP problem procured using the SAA approach. The size of empirical samples for each uncertain variable is 100, and a total number of 72,000 samples in the planning horizon for each uncertain variable is considered. The data is split 50/50 holdout method, i.e., 50 hourly samples are used to evaluate the in-sample performance of the two approaches. The other set of samples with 50 hourly samples is used to assess the out-of-sample performance.

The in-sample and out-of-sample performance of Case 2 are shown in Table 4.6 and the Wasserstein radius for each uncertain parameter in each set of samples is shown in Table 4.7. As shown in this table, the in-sample cost of DRO yields a higher total cost compared to the solution to the SP problem. Table 4.6 shows that the DRO formulation provides a more conservative solution compared to the SP formulation. As the number of samples increases to the infinity, the solution to the DRO and SP problems would eventually converge [124]. However, increasing the number of samples for each uncertain parameter would increase the complexity of the long-term planning problem. The out-of-sample performance of DRO and SP formulations for Case 2 are presented in Table 4.6. Here, the robustness of the GFDG expansion decisions obtained by solving the DRO and SP problems are evaluated considering the unseen scenarios. These decisions include the expansion decisions ($I_h^{b,y}$), the maximum natural gas demand for GFDG unit in each season ($\sum_t P_{h,t}^{s,y}$), and the maximum amount of demand response in each season ($\sum_t \tilde{P}_{d,t}^{s,y} - \sum_m L_{m,d,t}^{s,y}$). As shown in the fourth and fifth columns in Table 4.6, using 20 samples, the out-of-sample expected operation cost obtained by solving the DRO problem is reduced by \$547,524.16 compared to the solution to the SP problem. Therefore, the DRO solution is more robust to the unseen scenarios compared to the solution procured using the SAA approach. Moreover, the solution to the SP problem leads to 105.85 kWh expected non-responsive demand curtailment due to insufficient generation capacity in the unseen scenarios. Considering 15\$/kWh as the value

Table 4.6: The expected operation cost used to evaluate the in-sample and out-of-sample performance of DRO and SP formulations

N	In-sample		Out-of-sample	
	DRO ($)	SP ($)	DRO ($)	SP ($)
20	2,619,886.62	2,525,770.13	2,339,901.75	2,887,425.91
30	2,624,905.24	2,526,966.65	2,343,275.38	2,884,631.09
40	2,628,182.29	2,526,580.35	2,324,054.16	2,882,957.07
50	2,629,003.87	2,526,486.03	2,324,598.69	2,882,266.32

Table 4.7: The Wasserstein radius for each uncertain parameter in each set of samples

N	Wasserstein radius		
	ϵ_e	ϵ_r	ϵ_n
20	3.7095	0.7227	1.0378
30	2.9288	0.5996	0.8535
40	2.6124	0.5087	0.7404
50	2.3595	0.4496	0.6844

of the lost load, this leads to a $1,587.75 penalty for the demand curtailment. However, the DRO solution provides adequate generation capacity to serve the non-responsive loads, and the demand curtailment is zero. The probability distributions of the out-of-sample operation cost of SP and DRO are compared in Fig. 4.5. As shown in this figure, the mean and standard deviation of the operation costs for the DRO solution (i.e., $M2.3246 and $6041.1) are lower than those for the SAA (i.e., $M2.8823 and $8562.0). This indicates that the DRO solution is more robust when unseen scenarios are realized.

4.5.4 Scalability of the Proposed Expansion Planning Framework

In this section, the scalability of the proposed expansion planning framework is evaluated using the modified IEEE 123-bus distribution network interconnected with the 28-node natural gas network as shown in Fig. 4.6 [51]. The maximum capacity of the main distribution feeder is 1.65 MVA with a minimum power factor of 0.8. The gas supplier is at node 18 and

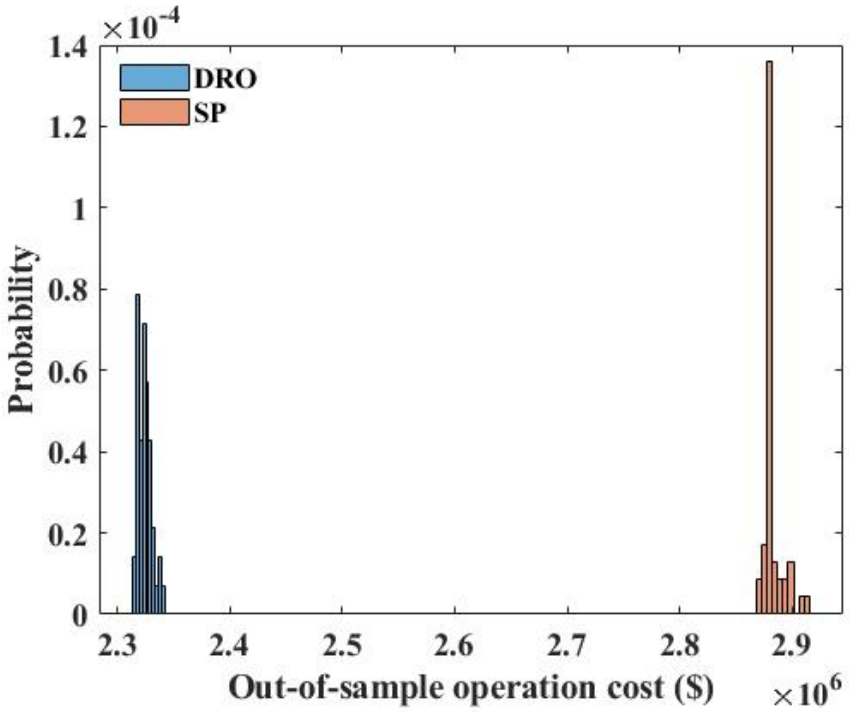

Figure 4.5: The out-of sample performance of DRO and SP solutions.

has a capacity of 6000 m^3/h. The potential candidates for the GFDG units are shown in Table 4.2 and the candidate buses for installing GFDG units are B62, B80, B89, B97, B109, and B116. The characteristics of other distributed generation and photovoltaic generation units are shown in Tables 4.8 and 4.9, respectively. The battery storage units' characteristics are shown in Table 4.10, and the efficiency of discharging and charging the battery storage units is 90%. Five responsive demands at buses B34, B42, B53, B99, and B112, with two bidding blocks for each responsive demand, are considered. The optimality gap is 5%. The annual input data profiles, demand growth, planning horizon, and annual discount rate are similar to the previous case. To address the increase in the marginal cost of natural gas and distribution generations, the annual inflation rate is 5%. The uncertain variables include electricity demand, PV power output, demand bid in each block, and natural gas demand. The empirical data include 15 hourly samples of uncertain variables, i.e., 1080 samples each year.

In this case, the expansion planning decisions are installing four GFDG units with a

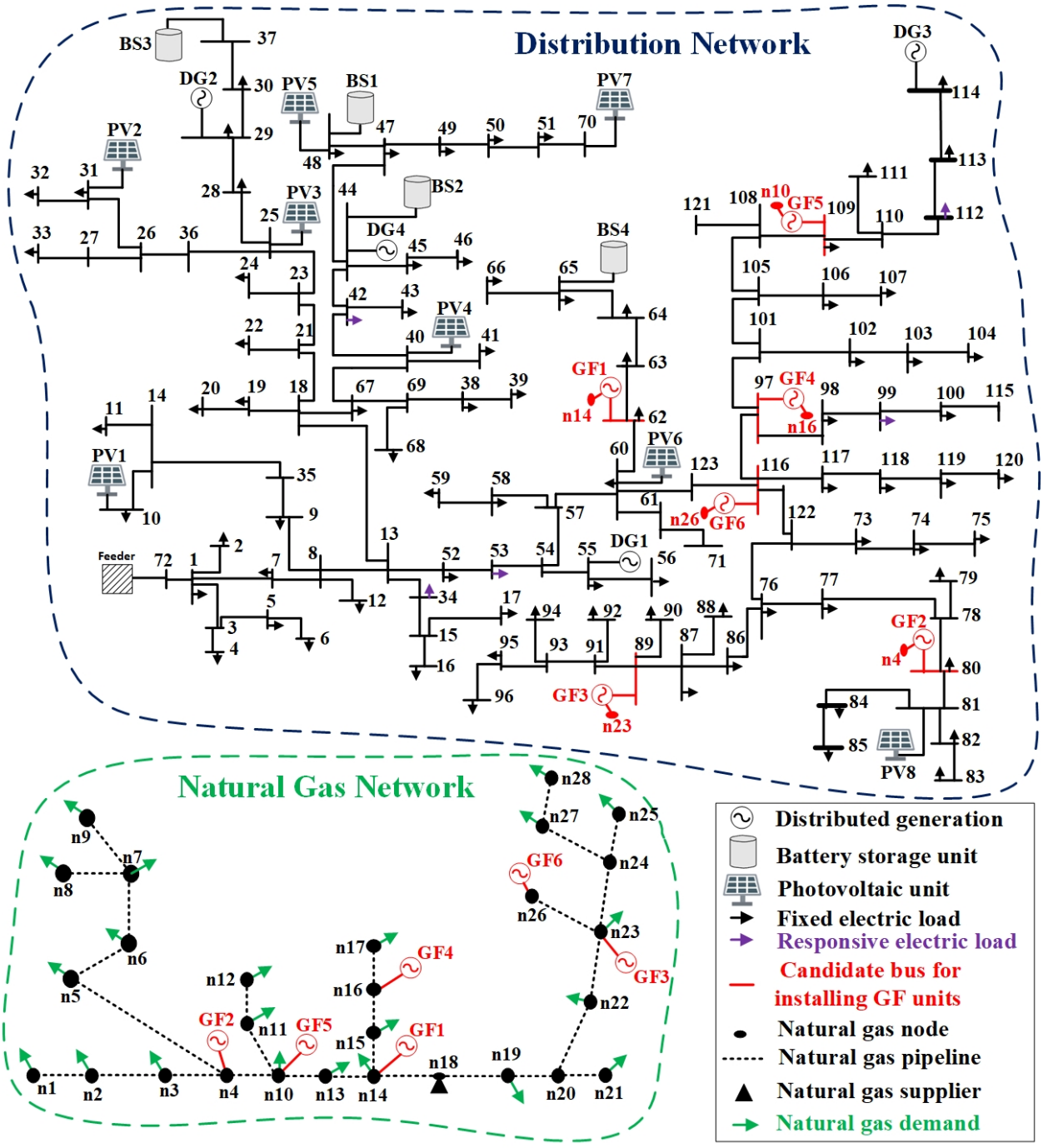

Figure 4.6: The modified IEEE 123-bus distribution network connected to a 28-node natural gas network.

Table 4.8: Distributed Generation Units' Characteristics

Units	Bus	P_{max} (kW)	Q_{max} $(kvar)$	$\$/kWh^2$	$\$/kWh$
DG1	B55	260	180	0.00015	0.0025
DG2	B29	200	100	0.00028	0.038
DG3	B114	300	150	0.00015	0.0025
DG4	B44	150	75	0.00028	0.038

total power capacity of 1200 kW. Two GFDGs of type GF1 are installed on Buses B97 and B116 in the first and third years, respectively. Two GFDG units of type GF2 are installed on Buses B109 and B62 in the ninth and tenth years, respectively. The investment cost on GFDG units, the expected distribution network operation cost, and the expected natural gas network operation cost are \$544,177.47, \$2,395,442.06, and \$605,516.49, respectively. The total planning and operation cost for this case is \$3,545,136.02. The expansion planning solution is feasible for the power distribution and natural gas networks after 3 iterations, and the optimal solution is obtained after 8 iterations. Compared with the solution to the SP problem, the total planning and expected operation cost procured by solving the SP problem is \$3,282,787.84, which is 7.4% less than the total planning and expected operation cost obtained by solving the DRO formulation. Comparing the out-of-sample performance of DRO and SP problems, the total planning and expected operation costs obtained by solving the DRO and SP problems are \$3,084,245.22 and \$3,828,741.01, respectively. Hence the DRO problem yields less expected planning and operation costs compared to the solution to the SP problem when facing unseen scenarios. The solution time of the DRO and SP problems that are solved using the proposed Benders decomposition algorithm for the same optimality gap (ε=5%) are 22h-40min-56s and 3h-47min-47s, respectively. As shown here, the solution to the SP problem is not hedged against unseen scenarios. Here, the total planning and expected operation cost for the out-of-sample solution of the SP problem is 24.14% higher than the total expected operation cost procured by solving the DRO problem.

Table 4.9: PV units' Characteristics

PVs	Bus	P_{max} (kW)	Q_{max} $(kvar)$
PV1	B10	50	25
PV2	B31	300	150
PV3	B25	100	50
PV4	B40	250	125
PV5	B48	100	50
PV6	B60	50	25
PV7	B70	100	50
PV8	B81	150	75

Table 4.10: Characteristics of battery storage units

Battery	Bus	ρ_q $(\$/kWh)$	E_{max} (kWh)	P_{max} (kW)	Q_{max} $(kvar)$
BS1	48	0.18	400	100	60
BS2	44	0.17	200	50	35
BS3	37	0.15	100	25	15
BS4	65	0.17	200	50	35

4.6 Conclusion

This chapter proposes a Wasserstein distance-distributionally robust optimization for GFDG units in the interconnected distribution and natural gas networks incorporating demand response program. The uncertainties in electricity demand, PV generation, demand bidding price, and natural gas demands are considered. The solution for the formulated generation expansion planning problem addresses the worst-case probability distribution of the uncertain parameters in the planning horizon. The DRO problem is reformulated to a tractable linear formulation which is solved in a decentralized fashion using the Benders decomposition. The proposed solution framework facilitates the autonomous operation of the DSO and natural gas supplier. The problem is decomposed into a master problem and feasibility and optimality subproblems in the power distribution and natural gas networks.

The numerical results show that the solution to the formulated DRO problem outperforms the solution to the SP problem in two domains. First, DRO formulation can obtain a more robust solution compared to the SP with a limited number of samples. Furthermore, solving the DRO problem would reduce the complexity and size of the planning problem compared to the SP counterpart. Second, the numerical results show that the expected operation cost obtained by solving the DRO problem is lower than that obtained by solving the SP problem when facing the unseen scenarios. Moreover, the merits of DR in the expansion planning practices are shown. The results show the effect of the DR program on flatting the demand profile and reducing the overall planning and expected operating costs of the interconnected distribution and natural gas network. It is shown that incorporating demand response would not only delay the installation time of natural gas distributed generation but also reduce the installed capacity, change the planning expansion decisions, and reduce the reliance on the natural gas network.

Chapter 5

Distributionally Robust Decentralized Operation of Distribution networks with Hydrogen Refueling Stations

This chapter proposes a distributionally robust coordinated operation of the distribution network with hydrogen refueling stations. The proposed operation framework determines the optimal operation of the integrated power and hydrogen system, considering the worst-case probability distribution of the electricity demand, PV output, hydrogen demand, and hydrogen supply. A decentralized operation framework is proposed for the hydrogen refueling stations that capture the interactions between the autonomous station operators and the DSO. Benders decomposition is used to coordinate the operational decisions among the DSO and hydrogen refueling station operators to serve the BEVs and HFCVs. The contributions of this chapter are outlined as follows:

– The coordinated operation problems for the distribution network with hydrogen refueling stations are formulated as DRO problems. The ambiguity set is constructed using the Wasserstein distance metric, where the empirical samples of electricity demand, PV generation, hydrogen demand, and hydrogen supply are leveraged to form the empirical probability distributions.

– The optimal dispatch of generation units in the distribution network and hydrogen production and storage facilities in the hydrogen refueling stations are coordinated in a decentralized manner using the Benders decomposition algorithm to minimize the total operation cost while preserving the privacy of the autonomous operators.

The rest of the chapter is organized as follows: A list of symbols used in this chapter is presented in Section 5.1. The problem description and formulation are presented in Section 5.2 and Section 5.3, respectively. The solution methodology is presented in Section 5.4. Section 5.5 presents the numerical results, and the conclusions are summarized in Section 5.6.

5.1 List of Symbols

Indices and Sets:

e	Index of electricity network
c	Index of hydrogen refueling station
s	Index of hydrogen storage
d	Index of demand
b	Index of bus
t	Index of hour
g	Index of the distributed generation
f	Index of the distribution feeder
l	Index of distribution line
v	Index of the PV generation unit
k	Index of cost function segment
i	Index of sample
$\mathcal{G}$	Set of distributed generation units
$\mathcal{F}$	Set of the distribution feeders

Variables:

$U_{b,t}$	Squared of bus voltage
$P_{(.),t}$	Real power dispatch of a unit
$Q_{(.),t}$	Reactive power dispatch of a unit
$P_{l,t}$	Real power flow in a branch
$Q_{l,t}$	Reactive power flow in a branch
$\tilde{P}_{d,t}$	Real power demand
$Q_{d,t}$	Reactive power demand
$I_{c,t}^{EH}$	Binary variable indicating the operating status of electrolyzers; 1 if the power flow from the distribution network to electrolyzers and 0 otherwise
$I_{c,t}^{HE}$	Binary variable indicating the operating status of the fuel cells; 1 if the power flow from the fuel cells to the distribution

	network and 0 otherwise
$P_{c,t}^{-}$	The real power consumed by electrolyzers
$P_{c,t}^{+}$	The real power supplied to the distribution network by fuel cells
$E_{c,t}$	The hydrogen production by electrolyzers
$F_{c,t}$	The hydrogen consumed by fuel cells
$\tilde{q}_{c,}$	The hydrogen supply to the hydrogen storage by hydrogen supply chain
$H_{s,t}^{c}$	The available hydrogen in the hydrogen storage
$h_{s,t}^{c}$	The discharge of the hydrogen storage
$\tilde{L}_{c,t}^{HV}$	The hydrogen demand consumed by hydrogen-based vehicles
$\tilde{L}_{c,t}^{EV}$	The hydrogen demand consumed by fuel cells to supply electric vehicles
$\mu_t/Z_t^{(.)}$	Auxiliary positive variables
$\gamma, \lambda, s_i,$	Auxiliary variables
$\Gamma_{c,t}^{+}, \Gamma_{c,t}^{-}$	Dual variables

Parameters:

A_b^l	Element of line-bus incidence matrix
L_b^d	Element of demand-bus incidence matrix
$B_b^{(.)}$	Element of unit-bus incidence matrix
R_l	Resistance of distribution line l
X_l	Inductive reactance of distribution line l
S_l^{max}	The capacity of the distribution branch
$\rho_{f,t}$	Electricity price
C_k^g	Marginal generation cost at segment k
$P_{(.)}^{max}$	Maximum real power dispatch of a unit
$P_{(.)}^{min}$	Minimum real power dispatch of a unit
$Q_{(.)}^{max}$	Maximum reactive power dispatch of a unit
α_{EH}	The electricity to hydrogen conversion
η^{EH}	The efficiency of the electrolyzers
α_{HE}	The hydrogen to electricity conversion

η^{HE}	The efficiency of the fuel cell
$\epsilon_{(.)}$	Wasserstein radius

Uncertain Parameters:

$\widetilde{\xi}_{(.),t}$	Forecast error of net load.

5.2 Problem Description

The physical and control layouts of the distribution network and hydrogen refueling stations are presented in Fig. 5.1. Each hydrogen refueling station operator manages the electrolyzers, fuel cells, and hydrogen tanks in the station and communicates with the DSO. The DSO operates the generation resources and communicates with the hydrogen refueling stations to ensure the secure and reliable operation of the distribution network. The hydrogen refueling stations coordinate with the DSO to either convert power to hydrogen through electrolyzers during light load in the distribution network or transform hydrogen to power using fuel cells during peak load in the distribution network to reduce the burden on the distribution network. Meanwhile, the hydrogen supply and demand balance is maintained considering the uncertainty in the hydrogen supply and the hydrogen and electricity demand imposed by HFCVs and BEVs, respectively. As shown in Fig. 5.1 limited information will be shared among the operators of the hydrogen refueling stations and DSO to preserve the privacy of the operators and coordinate the power exchange between the refueling stations and distribution network. The problem formulation for each operator and the coordination scheme among the operators are presented in the next section.

5.3 Problem Formulation

This section presents the problem formulation for the operation of the distribution network with hydrogen refueling stations. The problem is formulated as a DRO problem that captures the worst-case probability distribution of net electricity loads and net hydrogen demands. The objective function is formulated in (5.1), where the first term represents the expected operation cost of the distribution network, and the second term represents the expected operation cost of the hydrogen refueling stations. The expected operation cost of the distribution network includes the expected operation costs of the distributed generation

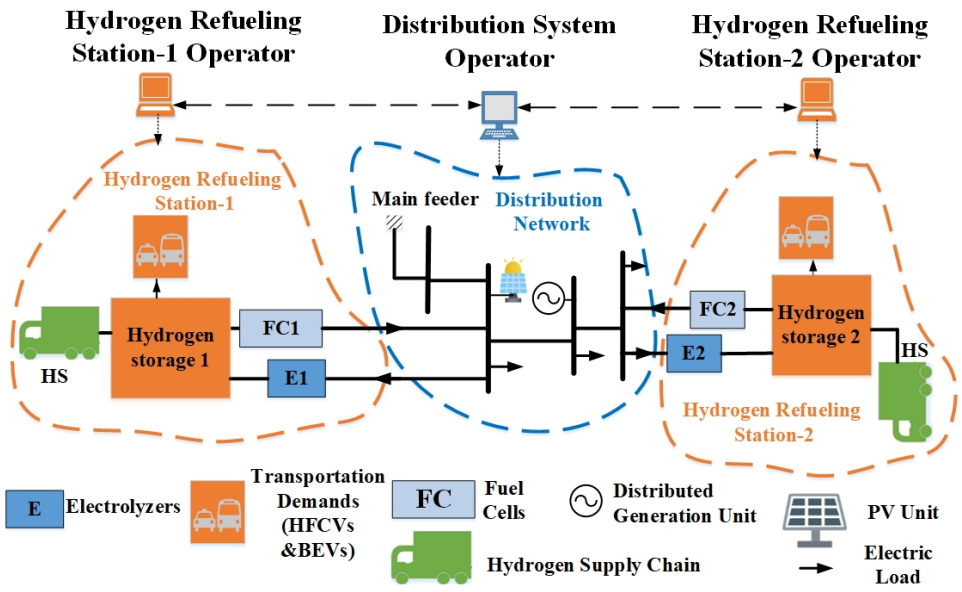

Figure 5.1: The physical and control layouts of the distribution network and hydrogen refueling stations.

units and the main distribution feeder that are formulated in (5.33) and (5.34), respectively. The expected operation cost of the hydrogen refueling stations is formulated in (5.35). The constraints for the distribution network operation with the hydrogen refueling station are presented in (5.2)-(5.32).

$$\min_{x_g,x_f,x_c} \left\{ \sup_{\mathbb{P}\in\mathcal{P}} E_{\mathbb{P}} \left\{ \Psi_{\mathrm{g}}\left(x_g,\widetilde{\xi}_e\right) + \Psi_{\mathrm{f}}(x_f,\widetilde{\xi}_e) \right\} + \sup_{\mathbb{H}\in\mathcal{H}} E_{\mathbb{H}}\Big\{ \sum_{c} \Psi_{\mathrm{c}}\big(x_c,\widetilde{\xi}_{c,t}\big)\Big\} \right\} \tag{5.1}$$

The capacity of the distribution branch is restricted by the linear equation sets as shown in (5.2)-(5.4) [110]. The reactive power output of the PV unit is restricted by the maximum capacity of the PV inverters, as shown in (5.5). The voltage at each distribution bus is constrained by an upper and a lower value, as shown in (5.6). The linearized representation of the distribution power flow (DistFlow) model is presented in (5.7).

$$-\sqrt{3}.(P_{l,t}+S_l^{max}) \le Q_{l,t} \le -\sqrt{3}.(P_{l,t}-S_l^{max}) \;;\; \forall l, \forall t \tag{5.2}$$

$$-\frac{\sqrt{3}}{2}.S_l^{max} \leq Q_{l,t} \leq \frac{\sqrt{3}}{2}.S_l^{max};\ \forall l, \forall t \tag{5.3}$$

$$\sqrt{3}.(P_{l,t} - S_l^{max}) \leq Q_{l,t} \leq \sqrt{3}.(P_{l,t} + S_l^{max});\ \forall l, \forall t \tag{5.4}$$

$$-Q_v^{max} \leq Q_{v,t} \leq Q_v^{max}; \forall v, \forall t \tag{5.5}$$

$$\left(V_b^{min}\right)^2 \leq U_{b,t} \leq (V_b^{max})^2\ \ ;\ \forall b, \forall t \tag{5.6}$$

$$B_b^l.U_{i,t} = 2.\left(r_l^{i,j}.P_{l,t} + x_l^{i,j}.Q_{l,t}\right)\ \ ;\ \forall l\ \forall t \tag{5.7}$$

The forecast error of the total net demand ($\widetilde{\xi}_{e,t}$) in (5.8) represents the uncertainties in electricity demand and the PV generation. The affine rules for the power adjustment of distributed generating units and main distribution feeder in response to the total net forecasted demand errors are presented in (5.9)-(5.11). The nodal real and reactive power balances are shown in (5.12) and (5.13), respectively. Constraints (5.14)-(5.16) ensure that each hydrogen refueling station either consumes electricity from the distribution network or supplies power to the distribution network at each hour. In other words, each hydrogen refueling station either converts electricity to hydrogen to charge the hydrogen storage or converts the hydrogen to electricity and discharges the hydrogen storage. The main distribution feeder is restricted by its capacity as shown in (5.17)-(5.18), considering the minimum power factor (θ_f). The real and reactive power of the distributed generating unit is limited to its capacity, as shown in (5.19) and (5.20), respectively.

$$\widetilde{\xi}_{e,t} = \sum_b \left(\sum_d \left(\tilde{P}_{d,t} - \overline{P}_{d,t} \right) - \sum_v \left(\tilde{P}_{v,t} - \overline{P}_{v,t} \right) \right); \forall t \tag{5.8}$$

$$0 \leq \mu_{f,t} \leq 1; \forall f, \forall t \tag{5.9}$$

$$0 \leq \mu_{g,t} \leq 1\ ; \forall g, \forall t \tag{5.10}$$

$$\sum_g \mu_{g,t} + \sum_f \mu_{f,t} = 1\ ; \forall t \tag{5.11}$$

$$\sum_{f} B_b^f.(P_{f,t} + \mu_{f,t}.\widetilde{\xi}_{e,t}) + \sum_{g} B_b^g.(P_{g,t} + \mu_{g,t}.\widetilde{\xi}_{e,t}) + \sum_{C} B_b^C.P_{c,t}^+ - \sum_{C} B_b^C.P_{c,t}^- + \sum_{v} B_b^v.\tilde{P}_{v,t} + \sum_{l} A_b^l.P_{l,t} = \sum_{d} L_b^d.\tilde{P}_{d,t} \;;\; \forall b, \forall t \quad (5.12)$$

$$\sum_{f} B_b^f.Q_{f,t} + \sum_{g} B_b^g.Q_{g,t} + \sum_{v} B_b^v.Q_{v,t} + \sum_{l} A_b^l.Q_{l,t} = \sum_{d} L_b^d.\tan(\cos^{-1}(\theta_d)).\tilde{P}_{d,t} \quad ;\; \forall b, \forall t \quad (5.13)$$

$$-P_c^{max}.I_{c,t}^{EH} \leq P_{c,t}^+ \leq P_c^{max}.I_{c,t}^{EH} \quad ;\; \forall c, \forall t \quad (5.14)$$

$$-P_c^{max}.I_{c,t}^{HE} \leq P_{c,t}^- \leq P_c^{max}.I_{c,t}^{HE} \quad ;\; \forall c, \forall t \quad (5.15)$$

$$I_{c,t}^{EH} + I_{c,t}^{HE} \leq 1;\; \forall c, \forall t \quad (5.16)$$

$$P_f^{min} \leq P_{f,t} + \mu_{f,t}.\widetilde{\xi}_{e,t} \leq P_f^{max}; \forall f, \forall t \quad (5.17)$$

$$-\tan(\theta_f)\ .P_{f,t} \leq Q_{f,t} \leq \tan(\theta_f)\ .P_{f,t}; \forall f, \forall t \quad (5.18)$$

$$P_g^{min} \leq P_{g,t} + \mu_{g,t}.\widetilde{\xi}_{e,t} \leq P_g^{max}; \forall g, \forall t \quad (5.19)$$

$$-Q_g^{max} \leq Q_{g,t} \leq Q_g^{max}; \forall g, \forall t \quad (5.20)$$

The constraints for each hydrogen refueling station are shown in (5.21)-(5.32). The total net demand forecast errors ($\widetilde{\xi}_{c,t}$) shown in (5.21) represent the uncertainties in the hydrogen demand and supply. Here, the hydrogen demand includes the demand for HFCVs and fuel cells that serve BEVs. The affine rules that adjust the output of the hydrogen storage in response to the forecast error of the net hydrogen demand are shown in (5.22)-(5.23). The hydrogen supply and demand balance is enforced by (5.24). The hydrogen discharge is limited by the maximum and minimum values as shown in (5.25). The available hydrogen in the hydrogen storage tank is shown in (5.26) [82, 83]. The stored hydrogen is restricted by the minimum and maximum capacity limits as enforced by (5.27). The initially stored hydrogen is equal to the stored hydrogen in the final operation period, as shown in (5.28). Here, the hydrogen supply within a time window is an uncertain parameter as it relies on the hydrogen supply chain [83]. The hydrogen production from the electrolyzer is given in (5.29), considering the electricity to hydrogen conversion factor and the efficiency of the electrolyzer. The capacity of the produced hydrogen by the electrolyzer is limited by (5.30).

The hydrogen consumption of the fuel cell is given by (5.31) considering the hydrogen to electricity conversion factor and the efficiency of the fuel cell. The hydrogen consumption of the fuel cell is limited by its capacity as enforced by (5.32).

$$\widetilde{\xi}_{c,t} = (\tilde{L}^{HV}_{c,t} - \overline{L}^{HV}_{c,t}) + (\tilde{L}^{EV}_{c,t} - \overline{L}^{EV}_{c,t}) - (\tilde{q}_{c,t} - \overline{q}_{c,t}); \forall t, \forall c \tag{5.21}$$

$$0 \leq \mu^{s}_{c,t} \leq 1 \ ; \forall c, \forall s, \forall t \tag{5.22}$$

$$\sum_{s} \mu^{s}_{c,t} = 1 \ ; \forall c, \forall t \tag{5.23}$$

$$\sum_{s} (h^{c}_{s,t} + \mu^{c}_{s,t}.\widetilde{\xi}_{c,t}) = F_{c,t} + \tilde{L}^{HV}_{c,t} + \tilde{L}^{EV}_{c,t} \ ; \forall c, \forall t \tag{5.24}$$

$$h^{min}_{c} \ \leq h^{c}_{s,t} + \mu^{c}_{s,t}.\widetilde{\xi}_{c,t} \leq h^{max}_{c} \ ; \ \forall c, \forall s, \forall t \tag{5.25}$$

$$H^{c}_{s,t} = H^{c}_{s,t-1} + \tilde{q}_{c,t} + E_{c,t} - (h^{c}_{s,t} + \mu^{c}_{s,t}.\widetilde{\xi}_{c,t}); \forall c, \forall s, \forall t \tag{5.26}$$

$$H^{min}_{c} \ \leq H^{c}_{s,t} \leq H^{max}_{c} \ ; \ \forall c, \forall s, \forall t \tag{5.27}$$

$$H^{c}_{s,1} = H^{c}_{s,T} = H_{c}^{\ ini} \tag{5.28}$$

$$E_{c,t} = \alpha_{EH}.P^{-}_{c,t}.\eta^{EH} \ ; \forall c, \forall t \tag{5.29}$$

$$E_{c,t} \leq E^{max}_{c}.I^{EH}_{c,t} \ \ ; \ \forall c, \forall t \tag{5.30}$$

$$F_{c,t} = \beta_{HE}.P^{+}_{c,t} \ / \eta^{HE}; \forall c, \forall t \tag{5.31}$$

$$F_{c,t} \leq F^{max}_{c}.I^{HE}_{c,t}; \ \forall c, \forall t \tag{5.32}$$

$$\begin{aligned} \Psi_{g}(x_{g}, \widetilde{\xi}_{e}) &= \sum_{t=1}^{T} \left(\left(\sum_{g \in \mathcal{G}} \left(\sum_{k=1}^{K} C^{g}_{k}. \left(P_{g,t} + \mu_{g,t}.\widetilde{\xi}_{e,t} \right) \right) \right) \right) \\ &= \sum_{t=1}^{T} \left(\left(\sum_{g \in \mathcal{G}} \left(\sum_{k=1}^{K} \left(a_{g,t}.\widetilde{\xi}_{e,t} + b_{g,t} \right) \right) \right) \right) \end{aligned} \tag{5.33}$$

$$\Psi_{f}(x_{f}, \widetilde{\xi}_{e}) = \sum_{t=1}^{T} \left(\sum_{f \in \mathcal{F}} \left(\rho_{f,t}. \left(P_{f,t} + \mu_{f,t}.\widetilde{\xi}_{e,t} \right) \right) \right) = \sum_{t=1}^{T} \left(a_{f,t}.\widetilde{\xi}_{e,t} + b_{f,t} \right) \tag{5.34}$$

$$\Psi_{\mathrm{c}}\left(x_c,\widetilde{\xi}_c\right)=\sum_{t=1}^{T}\left(\sum_{s}\left(\mu_{c,t}^{s}.\widetilde{\xi}_{c,t}\right)\right)=\sum_{t=1}^{T}\left(a_{c,t}.\widetilde{\xi}_{c,t}\right) \tag{5.35}$$

The DRO problem (5.1)-(5.32) considers the ambiguity set formed by the Wasserstein distance metric using the empirical samples [63,65,66,124]. The Wasserstein distance-based ambiguity set is defined in (5.36), where the empirical distribution $\mathbb{P}_{\mathrm{N}}$ is centered in the Wasserstein ball with radius $\epsilon(\mathrm{N})$. The radius $\epsilon(\mathrm{N})$ is calculated using (5.37) and (5.38) considering the confidence level ϑ, the sample size N, and the mean value of samples π [63], [65].

$$\Xi:=\left\{\mathbb{P}\in M(\Xi)\ \mid d_w\left(\mathbb{P}_N,\mathbb{P}\right)\leq\epsilon(\mathrm{N})\right\} \tag{5.36}$$

$$\epsilon(\mathrm{N})=R.\sqrt{\frac{2}{N}\log(\frac{1}{1-\vartheta})} \tag{5.37}$$

$$R=\min_{\phi\geq 0}2\sqrt{\frac{1}{2.\phi}\left(1+ln\left(\frac{1}{N}\sum_{i=1}^{N}e^{\phi(\|\widehat{\xi}_i-\pi\|)}\right)\right)} \tag{5.38}$$

The objective functions in (5.1) are piecewise affine functions. The uncertainty set for the net electricity demand is a polytope, i.e., $\Xi=\widetilde{\xi}_e\in\mathbb{R}^m:C_e.\widetilde{\xi}_e\leq d_e$. The worst-case expected cost for the distributed generation in the first term of (5.1) can be reformulated as (5.39a)-(5.39d). Similar formulations are used to reformulate the second and third terms in the objective function that determine the worst-case expected cost for feeder energy and the worst-case expected operation cost of the hydrogen refueling station, respectively.

$$\sup_{\mathbb{P}\in\mathcal{P}}E_{\mathbb{P}}\left\{\Psi(x_e,\widetilde{\xi}_e)\right\}=\inf_{\lambda,s_i,\gamma_{i,k}}\left(\lambda_e.\ \epsilon_e+\frac{1}{N_e}\sum_{i=1}^{N_e}s_i^e\right) \tag{5.39a}$$

$$s.t\ \ \Psi\left(x_e,\widehat{\xi}_e^i\right)+\gamma_{i,k}^{e,\intercal}.\left(d_e-C_e.\widehat{\xi}_e^i\right)\leq s_i^e,\ \forall i\leq N_e,k\leq K \tag{5.39b}$$

$$\left\|{C_e}^T\gamma_{i,k}^e-a_k^e\right\|_\infty\leq\lambda_e\forall i\leq N_e,k\leq K \tag{5.39c}$$

$$\gamma_{i,k}^e\geq 0\ \forall i\leq N_e,k\leq K \tag{5.39d}$$

Finally, the problem in (5.1)-(5.32) is reformulated to (5.40),(5.33)-(5.35), and (5.39a)-(5.39d) for distributed generation, feeder, and hydrogen refueling station costs, subjected to the distribution network operation constraints (5.2)-(5.20), and hydrogen refueling sta-

tion operation constraints (5.21)-(5.32).

$$min \;\; \lambda_e.\epsilon_e + \frac{1}{N_e}\sum_{i=1}^{N_e} s_i^e \;\; + \sum_c \left(\lambda_c.\epsilon_c + \frac{1}{N_c}\sum_{i=1}^{N_c} s_i^c\right) \tag{5.40}$$

5.4 Solution Framework

In this section, the decentralized framework to solve the coordinated operation of the distribution network with hydrogen refueling stations is presented. The information related to the power consumption of electrolyzers and the power generation of fuel cells, i.e., $P_{c,t}^-, P_{c,t}^+$ are shared between the DSO and refueling station operators. The decentralized framework leverages Benders decomposition to solve the problem. The problem is decomposed into a master problem solved by the DSO and two sub-problems solved by hydrogen refueling stations. The master problem and sub-problems are formulated in the next subsections.

5.4.1 Master Problem

First, the operation problem of the distribution network is formulated as the master problem (MP) in (5.41a)-(5.41b), (5.39b)-(5.39d), (5.33)-(5.34), and (5.2)-(5.20). Once the MP is solved, the decisions related to the power consumption of electrolyzers and the power generation of fuel cells, i.e., $P_{c,t}^-, P_{c,t}^+$, are sent to the hydrogen refueling station feasibility sub-problem (SP1).

$$\min \;\; Z_{lower} \tag{5.41a}$$

$$Z_{lower} \geq \lambda_e.\epsilon_e + \frac{1}{N_e}\sum_{i=1}^{N_e} s_i^e \tag{5.41b}$$

5.4.2 Sub-Problems

The hydrogen feasibility sub-problem (SP1) is formulated for each hydrogen refueling station. Here, each hydrogen refueling station operator will solve SP1 to ensure the feasibility of the determined power flow between the hydrogen storage and distribution network in the MP. The SP1 is formulated in (5.42a)-(5.42d), (5.21)-(5.23), and (5.25)-(5.32). The objective is

to minimize the mismatch in the hydrogen supply-demand balance in the hydrogen refueling station. The positive slack variables are introduced in the hydrogen supply-demand balance constraint as shown in (5.42b). Constraints (5.42c)-(5.42d) fix the power flow decisions to the solution obtained from the MP.

$$\min \;\; W_1^c = \sum_t (Z_{c,t}^1 + Z_{c,t}^2) \tag{5.42a}$$

$$\sum_s (h_{s,t}^c + \mu_{s,t}^c . \widetilde{\xi}_{c,t}) + Z_{c,t}^1 - Z_{c,t}^2 = F_{c,t} + \tilde{L}_{c,t}^{HV} + \tilde{L}_{c,t}^{EV}; \forall c, \forall t \tag{5.42b}$$

$$P_{c,t}^+ = \hat{P}_{c,t}^+ : \;\; \Gamma_{c,t}^+ \;\; \forall c, \forall t \tag{5.42c}$$

$$P_{c,t}^- = \hat{P}_{c,t}^- : \;\; \Gamma_{c,t}^- \;\; \forall c, \forall t \tag{5.42d}$$

If SP1 is infeasible, the feasibility cut in (5.43) is formed for each hydrogen refueling station and sent to the MP.

$$\hat{W}_1^c + \widehat{\Gamma}_{c,t}^+ . (P_{c,t}^+ - \hat{P}_{c,t}^+) + \widehat{\Gamma}_{c,t}^- . (P_{c,t}^- - \hat{P}_{c,t}^-) \leq 0; \forall c, \forall t \tag{5.43}$$

Once SP1 is feasible for each hydrogen station, the hydrogen refueling optimality subproblem SP2 is solved to ensure the optimality of the procured solution in the MP. SP2 is formulated as (5.44a)-(5.44b), (5.39b)-(5.39d), (5.42c)-(5.42d), and (5.21)-(5.32). If the solution procured by the DSO in the MP, i.e., $\hat{P}_{c,t}^-, \hat{P}_{c,t}^+$, is not optimal, the optimality cut in (5.45) is formed and sent to the MP.

$$\min \;\; W_2 \tag{5.44a}$$

$$W_2 \geq \lambda_c . \epsilon_c + \frac{1}{N_c} \sum_{i=1}^{N_c} s_i^c \tag{5.44b}$$

$$Z_{lower} \geq \lambda_e . \epsilon_e + \frac{1}{N_e} \sum_{i=1}^{N_e} s_i^e \;\; + \sum_c \left(\widehat{\lambda}_c . \epsilon_c + \frac{1}{N_c} \sum_{i=1}^{N_c} \hat{s}_i^c + \widehat{\Gamma}_{c,t}^+ . (P_{c,t}^+ - \hat{P}_{c,t}^+) + \widehat{\Gamma}_{c,t}^- . (P_{c,t}^- - \hat{P}_{c,t}^-) \right) \tag{5.45}$$

5.4.3 Implementation

The implementation of the proposed algorithm for solving the operation problem of the distribution network with hydrogen refueling stations is as follows:

Step 0: Initialization:

- Obtain the forecasted values and samples from the historical data for each uncertain parameter.

- Calculate the Wasserstein radius for each uncertain parameter according to (5.37)-(5.38).

- Set the predefined optimality gap ϵ.

Step 1: Solve the MP and update the power consumption decisions for the electrolyzers and the power generation decisions for the fuel cells $\hat{P}^{-}_{c,t}, \hat{P}^{+}_{c,t}$ and $\hat{Z}_{lower}$.

Step 2: Solve the feasibility sub-problem SP1 for each hydrogen refueling station given the power consumption and power generation decisions $\hat{P}^{-}_{c,t}, \hat{P}^{+}_{c,t}$ obtained from the MP.

Step 3: If SP1 is feasible for each hydrogen refueling station, i.e., $\hat{W}^{c}_{1,t} = 0$, then go to Step 4. Otherwise, add feasibility cut (5.43) to the MP and go to Step 1.

Step 4: Solve the optimality sub-problem SP2 for each hydrogen refueling station considering the power flow decisions between the distribution network and the hydrogen refueling station $\hat{P}^{-}_{c,t}, \hat{P}^{+}_{c,t}$ obtained from the MP.

Step 5: Calculate the upper bound of the solution (Z_{upper}) using (5.46).

$$Z_{upper} = \widehat{\lambda}_e.\epsilon_e + \frac{1}{N_e}\sum_{i=1}^{N_e}\hat{s}^{e}_{i} + \sum_{c}\left(\widehat{\lambda}_c.\epsilon_c + \frac{1}{N_c}\sum_{i=1}^{N_c}\hat{s}^{c}_{i}\right) \tag{5.46}$$

Step 6: If $\frac{|\hat{Z}_{upper} - \hat{Z}_{lower}|}{|\hat{Z}_{upper} + \hat{Z}_{lower}|} \leq \varepsilon$, then terminate the algorithm. Otherwise, send the optimality cut (5.45) to the MP, and go to Step 1.

5.5 Numerical Results

In this section, the modified IEEE 34-bus distribution network with two hydrogen refueling stations, shown in Fig. 5.2, are used to evaluate the performance of the proposed decentralized operation framework. The maximum capacity of the main distribution feeder is 1.8 MVA with a minimum power factor of 0.8. The characteristics and location of the

Table 5.2: Distributed Generation Unit Characteristics

Units	Bus	P_{max} (kW)	Q_{max} $(kvar)$	$\$/kWh^2$	$\$/kWh$
DG1	B12	360	180	0.00015	0.0025
DG2	B21	300	150	0.00028	0.038
DG3	B26	200	100	0.00015	0.0025

distributed generation and photovoltaic power generation units are shown in Tables 5.2 and 5.3, respectively. The hydrogen supply is 350kg for each hydrogen refueling station. Here, the hydrogen supply is refueling each hydrogen station in a certain time window (7:00-9:00 AM) [83]. The capacity of alkaline electrolyzers is 1100kW (330kg H_2) for hydrogen refueling stations. The electricity to hydrogen conversion is considered as 33.33 kWh/kg [132, 133], and the efficiency of the electrolyzer is 60% [84, 132]). The capacity of the hydrogen storage is 850kg for hydrogen refueling stations. The capacity of fuel cells [133] is 80kW and 100kW for hydrogen refueling station-1 and station-2, respectively, where α_{HE} is the hydrogen to electricity conversion (0.03 kg/kWh) and η_{HE} is the efficiency of the fuel cell (55%) [133]. The empirical distributions of the samples are assumed to follow multivariate normal distribution functions, where the mean values are shown in Fig. 5.3, and the standard deviation is assumed to be 3% of the mean values [74, 75]. The normalized electricity demand, photovoltaic power, and hydrogen demand, including the demand profile for BEVs and HFCVs for each refueling station, are shown in Fig. 5.3. The peak demand for BEVs is 300kW, and the peak demand for HFCVs is 45kg/hr H_2. It is assumed that each BEV requires 10kW, and the number of BEVs is 30 BEVs. It is assumed that each HFCV requires 1kg/hr H_2, and the number of HFCVS is 45 HFCVS. The optimality gap (ε) in step 6 is 1%. The case studies are simulated using GAMS on a server with dual 14 Core Intel Xeon 2.6 GHz, 380 GB of memory, and CPlex 12.8 is used as the solver. In this section, two case studies are performed. First, the deterministic solution for the operation problem is presented, which considers the forecast values of the uncertain parameters. Second, the solution to the proposed distributionally robust operation problem is presented using five hourly samples of each uncertain parameter.

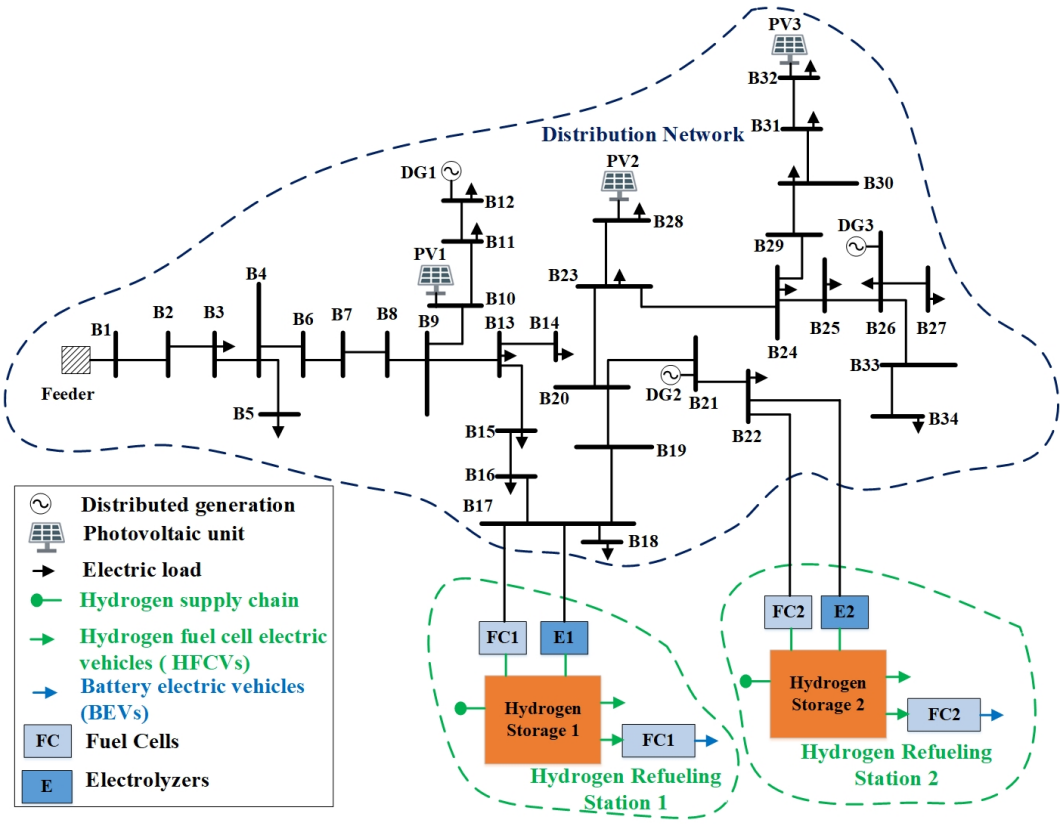

Figure 5.2: The modified IEEE 34-bus distribution network with two hydrogen refueling stations.

Table 5.3: PV units' Characteristics

PVs	Bus	P_{max} (kW)	Q_{max} $(kvar)$
PV1	B10	150	75
PV2	B28	300	150
PV3	B32	160	80

5.5.1 Case 1 – Deterministic Solution

In this case, the solution to the operation problem of the distribution network with two hydrogen refueling stations is presented considering the forecasted values of electricity demands, PV power output, HFCV, and BEV demands. Here, the total energy consumption of hydrogen refueling stations are 108.694 kWh in the operation horizon. The total energy supply to the distribution network from hydrogen refueling station-1 and station-2 are 1920.00 kWh and 2200.00 kWh, respectively. The operation cost of the distributed generation and the cost of the main feeder are \$1,424.35 and \$3,844.49, respectively. The total operation cost of the distribution network with two hydrogen stations is \$5,268.84. The operation decisions are feasible for the distribution and hydrogen refueling stations after two iterations, and the solution is optimal after one iteration.

5.5.2 Case 2 – The Proposed Distributionally Robust Problem

In this case, the worst-case probability distributions of electricity demand, PV generation, hydrogen demand, and hydrogen supply are determined by formulating the operation problem as a distributionally robust optimization problem. The empirical data include five hourly samples of the uncertain parameters, which include electricity demand, PV power output, hydrogen demands, and the hydrogen supply. The Wasserstein radius for each uncertain parameter is obtained using (5.37) and (5.38) [63, 65]. Here, the total expected energy consumption of hydrogen refueling station-1 and station-2 in the operation horizon are 251.042 kWh and 330.847 kWh, respectively. Compared to the deterministic solution, the expected energy consumption of hydrogen refueling stations is increased by 473.195 kWh in response to the net hydrogen load uncertainty. The total expected energy supplied to

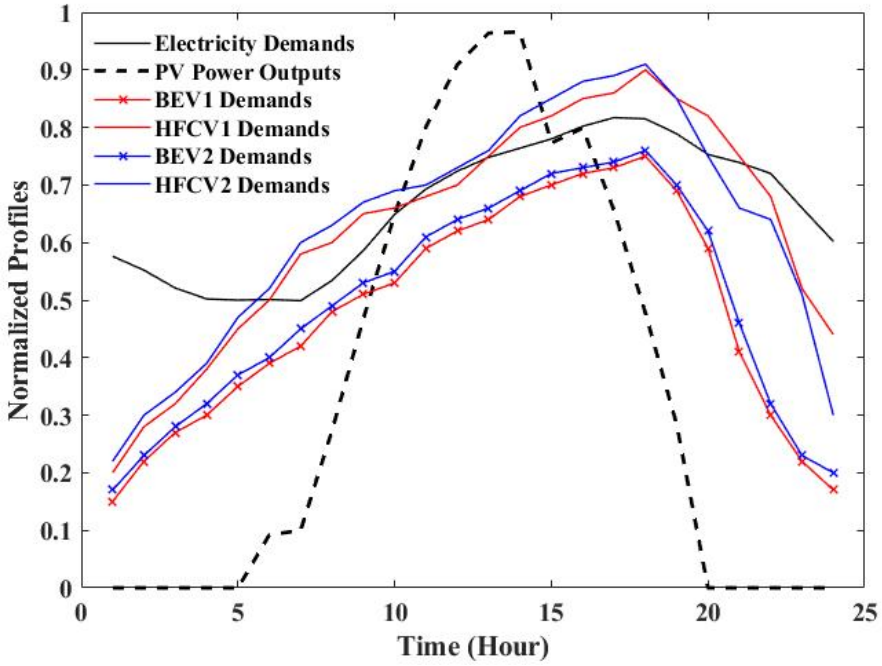

Figure 5.3: The normalized power profiles for electricity demands, PV power, electric vehicles and hydrogen vehicles demands for station-1, and electric vehicles and hydrogen vehicles demands for station-2.

the distribution network by hydrogen refueling station-1 is reduced to 1600.00 kWh. The total expected energy supplied to the distribution network by hydrogen refueling station-2 is 2200.00 kWh which is similar to the energy supplied to the distribution network from hydrogen refueling station-2 in Case 1. The expected operation costs of the distributed generation and the main feeder are \$1,382.97 and \$4,034.54, respectively. The total expected operation cost of the distribution network with two hydrogen stations is \$5,442.69, which is \$173.85 higher than the total operation cost in Case 1. Compared to Case 1, the expected operation cost of hydrogen station-1 and station-2 are increased by \$15.61 and \$9.57, respectively. The operation decisions are feasible for the distribution and hydrogen refueling stations after 55 iterations, and the solution is optimal for the distribution and hydrogen refueling stations after one iteration.

5.5.3 Performance Evaluation

This section evaluates the performance of the solution to the DRO problem compared to its SP counterpart. The size of hourly empirical samples for each uncertain parameter is 28. The data is divided using the holdout method, i.e., 14 hourly samples are used to evaluate the in-sample performance of the DRO and SP problems. The other set of samples with 14 hourly samples is used to evaluate the out-of-sample performance of the DRO and SP problems.

The in-sample performance of the proposed DRO problem is compared to the SP counterpart solved using the Benders decomposition algorithm. Here, the solution to the SP problem provides less conservative operational decisions with the total expected operation cost of \$5,409.88, which is \$32.81 lower than the expected operation cost in the proposed DRO problem. The total expected energy consumption of hydrogen refueling station-1 and station-2 are 366.242 kWh and 55.646 kWh, respectively. The total expected energy consumption of the hydrogen refueling stations in the solution to the SP problem is 160.001 kWh lower than the total expected energy consumption of hydrogen refueling stations determined by solving the DRO problem. The total expected energy supplied to the distribution network by hydrogen refueling station-1 and station-2 are 1440.00 kWh and 2093.779 kWh, respectively. The total expected energy supplied to the distribution network by the hydrogen refueling stations using the SP formulation is 266.221 kWh lower than the solution to the DRO problem.

The in-sample performance of the DRO solution in Case 2 and the Wasserstein radius corresponding to the number of samples for each uncertain parameter are presented in Table 5.4. As shown in this table, the DRO solution provides a higher expected operation cost compared to its SP counterpart. The proposed DRO formulation provides more conservative operational decisions compared to the SP formulation; however, as shown in Table 5.4, the difference between the solutions to the DRO and SP problems decreases as the number of samples increases [124].

The out-of-sample performance of DRO and SP formulations for Case 2 are shown in Table 5.5. Here, the operational decisions procured by solving the DRO and SP problems are assessed when facing the unseen scenarios. These decisions related to the power con-

Table 5.4: The expected operation cost for the in-sample sets of the uncertain parameters using DRO and SP formulations

N	Wasserstein radius			DRO ($)	SP ($)
	ϵ_e	ϵ_{c_1}	ϵ_{c_2}		
5	6.5849	0.424	0.4435	5,442.69	5,409.88
8	6.0265	0.4214	0.4418	5,448.76	5,413.11
11	5.0279	0.4077	0.4273	5,457.21	5,420.79
14	4.7749	0.3868	0.4057	5,459.01	5,420.28

Table 5.5: The expected operation cost for the out-of-sample sets of the uncertain parameters using DRO and SP formulations

N	DRO ($)	SP ($)
5	5,160.15	5,184.82
8	5,163.48	5,192.14
11	5,159.80	5,176.78
14	5,155.44	5,180.32

sumption decisions for the electrolyzers and the power generation decisions for the fuel cells, i.e., $\hat{P}^{-}_{c,t}, \hat{P}^{+}_{c,t}$ are fixed. As shown in this table, using 5 samples, the out-of-sample expected operation costs for the DRO and SP solutions are \$5,160.15 and \$5,184.82, respectively. As expected, the DRO solution is more robust against the unseen scenarios since the out-of-sample expected operation cost of DRO solution is \$24.67 lower than the out-of-sample expected operation cost of SP solution. The probability distributions of the out-of-sample operation cost of SP and DRO are compared in Fig. 5.4. As presented in this figure, the mean of the expected operation costs for the DRO solution is lower than the SP.

5.6 Conclusion

This chapter proposes a coordinated operation framework for the distribution network operation and hydrogen refueling stations formulated as distributionally robust optimization

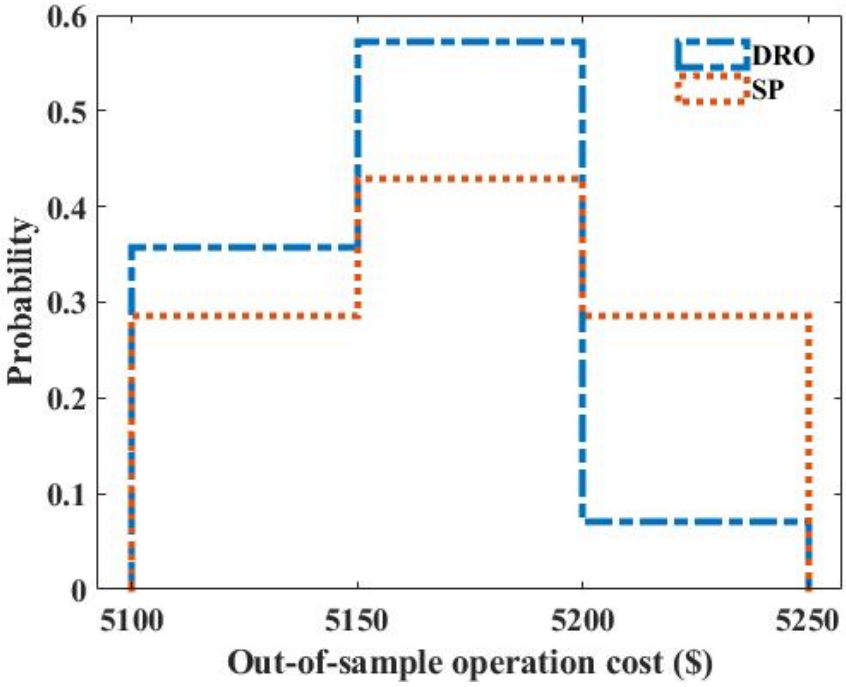

Figure 5.4: The probability distributions of the out-of-sample operation cost of SP and DRO.

problems. The proposed formulation determines the worst-case probability distribution of the uncertain electricity demand, PV generation, hydrogen supply, and hydrogen demands, including BEVs and HFCVs. The numerical results show that the total expected operation costs of the distribution network with hydrogen refueling stations are increased by 3.29% compared to the deterministic solution once the worst-case probability distributions of the uncertain parameters are considered. Furthermore, the solution to the DRO problem provides more robust operation decisions compared with the SP counterpart. It is shown that as the DRO solution is more conservative than the solution to the SP problem, the total expected operation cost obtained by solving the DRO problem is 0.61% higher than that obtained by solving the SP problem.

Chapter 6

Summary

With the restructured power system, different system operators and private stakeholders coexist to operate and maintain the electricity networks. Moreover, the modern distribution network is shifting toward renewable energy sources due to environmental concerns associated with conventional resources. However, the increased penetration of renewable generation poses operational challenges in the distribution network. Networked microgrids can efficiently utilize renewable energy sources and improve the availability and reliability of the energy supply. The distribution system operator and microgrid operators are independent entities, and their privacy and security concerns limit the information shared between these entities. Therefore, a decentralized energy management framework is necessary to coordinate the power dispatch of the distribution network with networked microgrids. In this thesis, the first research work proposes a decentralized energy management system for unbalanced networked microgrids. The uncertainties in electricity demand and PV power generation, as well as the probabilistic operation modes of microgrids, are considered using Monte Carlo simulation and backward scenario reduction. The solution framework ensures the autonomous operation of the distribution network and microgrids using the Benders decomposition algorithm.

The second research work develops a stochastic expansion planning approach to determine the installation time, location, and capacity of battery energy storage systems in distribution networks with data centers. The significant increase in data center energy consumption affects the long-term security and reliability of the energy supply in the distribution network. The objective of the proposed expansion planning is to minimize the capital cost of the battery energy storage and the expected operation cost of the distribution network while ensuring the security of energy supply for the data centers and the reliability requirements of the distribution network. The interactions among the independent operators are captured

using the Benders decomposition algorithm. Monte Carlo simulation is used to address the uncertainties in the electricity demand, data center workload, solar PV generation, and the availability of the distribution branches. Then, a dissimilarity-based sparse subset selection algorithm is used to cluster these scenarios.

The third research work in this thesis addresses the coordinated planning of gas-fired distributed generators in the interconnected distribution and natural gas networks. The increasing reliance on natural gas for power generation in the distribution network may cause a shortage in the natural gas supply. Optimal coordination among the operators of the distribution and natural gas networks is crucial to obtain a feasible generation expansion plan in the distribution network. Therefore, the third research work presents a distributionally robust expansion planning framework for the gas-fired distributed generation in the interconnected distribution and natural gas networks with demand response. The proposed formulation considers the uncertainties in the electricity demands, natural gas demands, PV generation outputs, and demand bidding price. The Wasserstein distance is used to construct the ambiguity sets for the uncertain variables. The expansion planning decisions for installing gas-fired distributed generators in the distribution network are obtained under the worst probability distributions of the uncertain parameters. The Benders decomposition algorithm is used to solve the expansion planning problem in multi-stages to preserve the autonomous operation of the independent networks.

The fourth research work presents a coordinated operation of the distribution network and hydrogen refueling stations. The operation problem is formulated as a distributionally robust optimization. The ambiguity set is constructed based on Wasserstein distance to address the uncertainties in the electric demands, PV generation, hydrogen supply, and hydrogen demands. The proposed formulation coordinates the optimal dispatch of the generation assets in the distribution network and hydrogen refueling stations under the worst probability distribution of uncertain parameters. The Benders decomposition is leveraged to solve the operation problem and ensure the autonomous operation of the independent network by limiting the information shared between these independent operators.

BIBLIOGRAPHY

[1] M. Shahidehpour, Z. Li, S. Bahramirad, Z. Li, and W. Tian, "Networked microgrids: Exploring the possibilities of the iit-bronzeville grid," *IEEE Power and Energy Magazine*, vol. 15, no. 4, pp. 63–71, 2017. 1

[2] A. R. Malekpour and A. Pahwa, "Stochastic networked microgrid energy management with correlated wind generators," *IEEE Transactions on Power Systems*, vol. 32, no. 5, pp. 3681–3693, 2017. 1

[3] W.-J. Ma, J. Wang, V. Gupta, and C. Chen, "Distributed energy management for networked microgrids using online admm with regret," *IEEE Transactions on Smart Grid*, vol. 9, no. 2, pp. 847–856, 2016. 1

[4] W. Zhang and Y. Xu, "Distributed optimal control for multiple microgrids in a distribution network," *IEEE Transactions on Smart Grid*, vol. 10, no. 4, pp. 3765–3779, 2018. 1

[5] J. Zhou, Y. Xu, H. Sun, Y. Li, and M.-Y. Chow, "Distributed power management for networked ac–dc microgrids with unbalanced microgrids," *IEEE Transactions on Industrial Informatics*, vol. 16, no. 3, pp. 1655–1667, 2019. 1

[6] J. Lai and X. Lu, "Nonlinear mean-square power sharing control for ac microgrids under distributed event detection," *IEEE Transactions on Industrial Informatics*, vol. 17, no. 1, pp. 219–229, 2020. 1, 2

[7] J. Lai, X. Lu, A. Monti, and R. W. De Doncker, "Event-driven distributed active and reactive power dispatch for ccvsi-based distributed generators in ac microgrids," *IEEE Transactions on Industry Applications*, vol. 56, no. 3, pp. 3125–3136, 2020. 1, 2

[8] S. Ghaemi, J. Salehi, and F. Hamzeh Aghdam, "Risk aversion energy management in the networked microgrids with presence of renewable generation using decentralised optimisation approach," *IET Renewable Power Generation*, vol. 13, no. 7, pp. 1050–1061, 2019. 1, 2

[9] X. Wu, Y. Xu, X. Wu, J. He, J. M. Guerrero, C.-C. Liu, K. P. Schneider, and D. T. Ton, "A two-layer distributed cooperative control method for islanded networked microgrid systems," *IEEE Transactions on Smart Grid*, vol. 11, no. 2, pp. 942–957, 2019. 1, 2

[10] Q. Xu, T. Zhao, Y. Xu, Z. Xu, P. Wang, and F. Blaabjerg, "A distributed and robust energy management system for networked hybrid ac/dc microgrids," *IEEE Transactions on Smart Grid*, vol. 11, no. 4, pp. 3496–3508, 2019. 1, 2

[11] J. Wu and X. Guan, "Coordinated multi-microgrids optimal control algorithm for smart distribution management system," *IEEE Transactions on Smart Grid*, vol. 4, no. 4, pp. 2174–2181, 2013. 1, 2

[12] H. Gao, J. Liu, L. Wang, and Z. Wei, "Decentralized energy management for networked microgrids in future distribution systems," *IEEE Transactions on Power Systems*, vol. 33, no. 4, pp. 3599–3610, 2017. 1, 2

[13] Z. Wang, B. Chen, J. Wang *et al.*, "Decentralized energy management system for networked microgrids in grid-connected and islanded modes," *IEEE Transactions on Smart Grid*, vol. 7, no. 2, pp. 1097–1105, 2015. 1, 2

[14] Z. Liu, L. Wang, and L. Ma, "A transactive energy framework for coordinated energy management of networked microgrids with distributionally robust optimization," *IEEE Transactions on Power Systems*, vol. 35, no. 1, pp. 395–404, 2019. 1, 2, 3

[15] A. K. Marvasti, Y. Fu, S. DorMohammadi, and M. Rais-Rohani, "Optimal operation of active distribution grids: A system of systems framework," *IEEE Transactions on Smart Grid*, vol. 5, no. 3, pp. 1228–1237, 2014. 1, 2, 3

[16] H. K. Nunna and S. Doolla, "Demand response in smart distribution system with multiple microgrids," *IEEE transactions on smart grid*, vol. 3, no. 4, pp. 1641–1649, 2012. 1, 3

[17] M. Fathi and H. Bevrani, "Statistical cooperative power dispatching in interconnected microgrids," *IEEE Transactions on Sustainable Energy*, vol. 4, no. 3, pp. 586–593, 2013. 1, 3

[18] H. K. Nunna and S. Doolla, "Multiagent-based distributed-energy-resource management for intelligent microgrids," *IEEE Transactions on Industrial Electronics*, vol. 60, no. 4, pp. 1678–1687, 2012. 1, 3

[19] M. Fathi and H. Bevrani, "Adaptive energy consumption scheduling for connected microgrids under demand uncertainty," *IEEE Transactions on Power Delivery*, vol. 28, no. 3, pp. 1576–1583, 2013. 1, 3

[20] Z. Wang, B. Chen, J. Wang, M. M. Begovic, and C. Chen, "Coordinated energy management of networked microgrids in distribution systems," *IEEE Transactions on Smart Grid*, vol. 6, no. 1, pp. 45–53, 2014. 1, 3

[21] G. E. Asimakopoulou, A. L. Dimeas, and N. D. Hatziargyriou, "Leader-follower strategies for energy management of multi-microgrids," *IEEE transactions on smart grid*, vol. 4, no. 4, pp. 1909–1916, 2013. 1, 3

[22] The Power of Efficiency to Cut Data Center Energy Waste. Online. [Online]. Available: https://www.nrdc.org/experts/pierre-delforge/power-efficiency-cut-data-center-energy-waste 4

[23] Online. [Online]. Available: https://www.grandviewresearch.com/industry-analysis/data-center-construction-market 4

[24] M. Sedghi, A. Ahmadian, and M. Aliakbar-Golkar, "Optimal storage planning in active distribution network considering uncertainty of wind power distributed generation," *IEEE Transactions on Power Systems*, vol. 31, no. 1, pp. 304–316, 2016. 5

[25] P. Lazzeroni and M. Repetto, "Optimal planning of battery systems for power losses reduction in distribution grids," *Electric Power Systems Research*, vol. 167, pp. 94–112, 2019. 5

[26] M. Nick, R. Cherkaoui, and M. Paolone, "Optimal planning of distributed energy storage systems in active distribution networks embedding grid reconfiguration," *IEEE Transactions on Power Systems*, vol. 33, no. 2, pp. 1577–1590, 2018. 5

[27] M. Khalid, U. Akram, and S. Shafiq, "Optimal planning of multiple distributed generating units and storage in active distribution networks," *IEEE Access*, vol. 6, pp. 55 234–55 244, 2018. 5

[28] A. S. Awad, T. H. El-Fouly, and M. M. Salama, "Optimal ess allocation and load shedding for improving distribution system reliability," *IEEE Transactions on Smart Grid*, vol. 5, no. 5, pp. 2339–2349, 2014. 5

[29] M. Nick, M. Hohmann, R. Cherkaoui, and M. Paolone, "Optimal location and sizing of distributed storage systems in active distribution networks," in *2013 IEEE Grenoble Conference*. IEEE, 2013, pp. 1–6. 5

[30] X. Shen, M. Shahidehpour, Y. Han, S. Zhu, and J. Zheng, "Expansion planning of active distribution networks with centralized and distributed energy storage systems," *IEEE Transactions on Sustainable Energy*, vol. 8, no. 1, pp. 126–134, 2017. 5, 6

[31] H. Akhavan-Hejazi and H. Mohsenian-Rad, "Energy storage planning in active distribution grids: A chance-constrained optimization with non-parametric probability functions," *IEEE Transactions on Smart Grid*, vol. 9, no. 3, pp. 1972–1985, 2018. 5, 6

[32] P. M. de Quevedo, G. Munoz-Delgado, and J. Contreras, "Impact of electric vehicles on the expansion planning of distribution systems considering renewable energy, storage, and charging stations," *IEEE Transactions on Smart Grid*, vol. 10, no. 1, pp. 794–804, 2019. 5, 6

[33] H. Saboori and R. Hemmati, "Maximizing disco profit in active distribution networks by optimal planning of energy storage systems and distributed generators," *Renewable and Sustainable Energy Reviews*, vol. 71, pp. 365–372, 2017. 5, 6

[34] Y. Zhang, Z. Y. Dong, F. Luo, Y. Zheng, K. Meng, and K. P. Wong, "Optimal allocation of battery energy storage systems in distribution networks with high wind power penetration," *IET Renewable Power Generation*, vol. 10, no. 8, pp. 1105–1113, 2016. 5, 6

[35] A. Giannitrapani, S. Paoletti, A. Vicino, and D. Zarrilli, "Optimal allocation of energy storage systems for voltage control in lv distribution networks," *IEEE Transactions on Smart Grid*, vol. 8, no. 6, pp. 2859–2870, 2017. 5, 6

[36] Y. Zhang, S. Ren, Z. Y. Dong, Y. Xu, K. Meng, and Y. Zheng, "Optimal placement of battery energy storage in distribution networks considering conservation voltage reduction and stochastic load composition," *IET Generation, Transmission & Distribution*, vol. 11, no. 15, pp. 3862–3870, 2017. 5, 7

[37] X. Qian, S. Zhang, J. Liu, Y. Zheng, and W. Liu, "Hierarchical optimal planning of battery energy storage systems in radial distribution networks," in *2019 IEEE 3rd Conference on Energy Internet and Energy System Integration (EI2)*. IEEE, 2019, pp. 84–89. 5, 7

[38] M. Asensio, P. M. de Quevedo, G. Muñoz-Delgado, and J. Contreras, "Joint distribution network and renewable energy expansion planning considering demand response and energy storage—part i: Stochastic programming model," *IEEE Transactions on Smart Grid*, vol. 9, no. 2, pp. 655–666, 2018. 5, 7

[39] P. Wang, L. Xie, Y. Lu, and Z. Ding, "Day-ahead emission-aware resource planning for data center considering energy storage and batch workloads," in *2017 IEEE Conference on Energy Internet and Energy System Integration (EI2)*. IEEE, 2017, pp. 1–6. 7

[40] Y. Guo and Y. Fang, "Electricity cost saving strategy in data centers by using energy storage," *IEEE Transactions on Parallel and Distributed Systems*, vol. 24, no. 6, pp. 1149–1160, 2013. 7

[41] C. Ren, D. Wang, B. Urgaonkar, and A. Sivasubramaniam, "Carbon-aware energy capacity planning for datacenters," in *2012 IEEE 20th International Symposium on Modeling, Analysis and Simulation of Computer and Telecommunication Systems*. IEEE, 2012, pp. 391–400. 7

[42] D. Gmach, J. Rolia, C. Bash, Y. Chen, T. Christian, A. Shah, R. Sharma, and Z. Wang, "Capacity planning and power management to exploit sustainable energy," in *2010 International Conference on Network and Service Management*. IEEE, 2010, pp. 96–103. 7

[43] F. Kong and X. Liu, "Greenplanning: Optimal energy source selection and capacity planning for green datacenters," in *2016 ACM/IEEE 7th International Conference on Cyber-Physical Systems (ICCPS)*. IEEE, 2016, pp. 1–10. 7, 53

[44] L. Zhou, L. N. Bhuyan, and K. Ramakrishnan, "Dream: Distributed energy-aware traffic management for data center networks," in *Proceedings of the Tenth ACM International Conference on Future Energy Systems*, 2019, pp. 273–284. 8

[45] Y. Guo and M. Pan, "Coordinated energy management for colocation data centers in smart grids," in *2015 IEEE International Conference on Smart Grid Communications (SmartGridComm)*. IEEE, 2015, pp. 840–845. 8, 53

[46] L. Yu, T. Jiang, and Y. Zou, "Distributed real-time energy management in data center microgrids," *IEEE Transactions on Smart Grid*, vol. 9, no. 4, pp. 3748–3762, 2018. 8

[47] A. Vafamehr, M. E. Khodayar, S. D. Manshadi, I. Ahmad, and J. Lin, "A framework for expansion planning of data centers in electricity and data networks under uncertainty," *IEEE Transactions on Smart Grid*, vol. 10, no. 1, pp. 305–316, 2019. 8, 53

[48] A. Vafamehr, "Operation and planning of data centers in electricity networks," Ph.D. dissertation, 2019. 8, 73

[49] X. Zhang, M. Shahidehpour, A. S. Alabdulwahab, and A. Abusorrah, "Security-constrained co-optimization planning of electricity and natural gas transportation infrastructures," *IEEE Transactions on Power Systems*, vol. 30, no. 6, pp. 2984–2993, 2015. 8, 9, 12, 13, 95

[50] X. Zhang, M. Shahidehpour, A. Alabdulwahab, and A. Abusorrah, "Optimal expansion planning of energy hub with multiple energy infrastructures," *IEEE Transactions on Smart Grid*, vol. 6, no. 5, pp. 2302–2311, 2015. 8, 9, 95

[51] C. A. Saldarriaga, R. A. Hincapié, and H. Salazar, "A holistic approach for planning natural gas and electricity distribution networks," *IEEE transactions on power systems*, vol. 28, no. 4, pp. 4052–4063, 2013. 8, 9, 104, 112

[52] C. Unsihuay-Vila, J. W. Marangon-Lima, A. Z. De Souza, I. J. Perez-Arriaga, and P. P. Balestrassi, "A model to long-term, multiarea, multistage, and integrated expansion planning of electricity and natural gas systems," *IEEE Transactions on Power Systems*, vol. 25, no. 2, pp. 1154–1168, 2010. 8, 9

[53] F. Barati, H. Seifi, M. S. Sepasian, A. Nateghi, M. Shafie-khah, and J. P. Catalão, "Multi-period integrated framework of generation, transmission, and natural gas grid expansion planning for large-scale systems," *IEEE Transactions on Power Systems*, vol. 30, no. 5, pp. 2527–2537, 2015. 9, 95

[54] H. Fan, J. Lu, Z. Li, M. Shahidehpour, and S. Zhang, "Optimal planning of integrated electricity-gas system with demand side management," *IEEE Access*, vol. 7, pp. 176 790–176 798, 2019. 9

[55] S. Mansouri, A. Ahmarinejad, M. Ansarian, M. Javadi, and J. Catalao, "Stochastic planning and operation of energy hubs considering demand response programs using benders decomposition approach," *International Journal of Electrical Power & Energy Systems*, vol. 120, p. 106030, 2020. 10

[56] A. Dolatabadi, B. Mohammadi-Ivatloo, M. Abapour, and S. Tohidi, "Optimal stochastic design of wind integrated energy hub," *IEEE Transactions on Industrial Informatics*, vol. 13, no. 5, pp. 2379–2388, 2017. 10

[57] J. Qiu, Z. Y. Dong, J. H. Zhao, Y. Xu, Y. Zheng, C. Li, and K. P. Wong, "Multi-stage flexible expansion co-planning under uncertainties in a combined electricity and gas

market," *IEEE Transactions on Power Systems*, vol. 30, no. 4, pp. 2119–2129, 2015. 10

[58] S. Hemmati, S. Ghaderi, and M. Ghazizadeh, "Sustainable energy hub design under uncertainty using benders decomposition method," *Energy*, vol. 143, pp. 1029–1047, 2018. 10

[59] B. Zhao, A. J. Conejo, and R. Sioshansi, "Coordinated expansion planning of natural gas and electric power systems," *IEEE Transactions on Power Systems*, vol. 33, no. 3, pp. 3064–3075, 2018. 10

[60] C. He, L. Wu, T. Liu, and Z. Bie, "Robust co-optimization planning of interdependent electricity and natural gas systems with a joint n-1 and probabilistic reliability criterion," *IEEE Transactions on Power Systems*, vol. 33, no. 2, pp. 2140–2154, 2018. 10

[61] Y. Liu and T. Liu, "Research on system planning of gas-power integrated system based on improved two-stage robust optimization and noncooperative game method," *IEEE Access*, 2021. 10, 12, 13

[62] W. Hou, R. Zhu, H. Wei, and H. TranHoang, "Data-driven affinely adjustable distributionally robust framework for unit commitment based on wasserstein metric," *IET Generation, Transmission & Distribution*, vol. 13, no. 6, pp. 890–895, 2019. 11, 96, 110

[63] R. Zhu, H. Wei, and X. Bai, "Wasserstein metric based distributionally robust approximate framework for unit commitment," *IEEE Transactions on Power Systems*, vol. 34, no. 4, pp. 2991–3001, 2019. 11, 96, 126, 132

[64] C. Zhao and Y. Guan, "Data-driven stochastic unit commitment for integrating wind generation," *IEEE Transactions on Power Systems*, vol. 31, no. 4, pp. 2587–2596, 2015. 11, 97

[65] C. Duan, W. Fang, L. Jiang, L. Yao, and J. Liu, "Distributionally robust chance-constrained approximate ac-opf with wasserstein metric," *IEEE Transactions on Power Systems*, vol. 33, no. 5, pp. 4924–4936, 2018. 11, 96, 126, 132

[66] C. Wang, R. Gao, F. Qiu, J. Wang, and L. Xin, "Risk-based distributionally robust optimal power flow with dynamic line rating," *IEEE Transactions on Power Systems*, vol. 33, no. 6, pp. 6074–6086, 2018. 11, 96, 126

[67] C. He, X. Zhang, T. Liu, and L. Wu, "Distributionally robust scheduling of integrated gas-electricity systems with demand response," *IEEE Transactions on Power Systems*, vol. 34, no. 5, pp. 3791–3803, 2019. 11

[68] C. Wang, R. Gao, W. Wei, M. Shafie-khah, T. Bi, and J. P. Catalao, "Risk-based distributionally robust optimal gas-power flow with wasserstein distance," *IEEE Transactions on Power Systems*, vol. 34, no. 3, pp. 2190–2204, 2018. 11

[69] P. Zhao, C. Gu, D. Huo, Y. Shen, and I. Hernando-Gil, "Two-stage distributionally robust optimization for energy hub systems," *IEEE Transactions on Industrial Informatics*, vol. 16, no. 5, pp. 3460–3469, 2020. 11

[70] Y. Zhou, M. Shahidehpour, Z. Wei, Z. Li, G. Sun, and S. Chen, "Distributionally robust unit commitment in coordinated electricity and district heating networks," *IEEE Transactions on Power Systems*, vol. 35, no. 3, pp. 2155–2166, 2019. 11

[71] Y. Wang, Y. Yang, L. Tang, W. Sun, and B. Li, "A wasserstein based two-stage distributionally robust optimization model for optimal operation of cchp micro-grid under uncertainties," *International Journal of Electrical Power & Energy Systems*, vol. 119, p. 105941, 2020. 11

[72] Y. Zhou, M. Shahidehpour, Z. Wei, Z. Li, G. Sun, and S. Chen, "Distributionally robust co-optimization of energy and reserve for combined distribution networks of power and district heating," *IEEE Transactions on Power Systems*, vol. 35, no. 3, pp. 2388–2398, 2019. 11

[73] A. Zare, C. Chung, J. Zhan, and S. O. Faried, "A distributionally robust chance-constrained milp model for multistage distribution system planning with uncertain renewables and loads," *IEEE Transactions on Power Systems*, vol. 33, no. 5, pp. 5248–5262, 2018. 11

[74] A. Bagheri, J. Wang, and C. Zhao, "Data-driven stochastic transmission expansion planning," *IEEE Transactions on Power Systems*, vol. 32, no. 5, pp. 3461–3470, 2016. 11, 106, 130

[75] M. S. Mokhtari, M. Gitizadeh, and M. Lehtonen, "Optimal coordination of thyristor controlled series compensation and transmission expansion planning: Distributionally robust optimization approach," *Electric Power Systems Research*, vol. 196, p. 107189, 2021. 11, 106, 130

[76] Z. Lu, X. Xu, and Z. Yan, "Data-driven stochastic programming for energy storage system planning in high pv-penetrated distribution network," *International Journal of Electrical Power & Energy Systems*, vol. 123, p. 106326, 2020. 11, 12

[77] H. Gao, R. Wang, Y. Liu, L. Wang, Y. Xiang, and J. Liu, "Data-driven distributionally robust joint planning of distributed energy resources in active distribution network," *IET Generation, Transmission & Distribution*, vol. 14, no. 9, pp. 1653–1662, 2020. 11, 12

[78] Y. Cao, W. Wei, J. Wang, S. Mei, M. Shafie-khah, and J. P. Catalao, "Capacity planning of energy hub in multi-carrier energy networks: A data-driven robust stochastic programming approach," *IEEE Transactions on Sustainable Energy*, vol. 11, no. 1, pp. 3–14, 2020. 11, 12, 106

[79] S. He, H. Gao, L. Wang, Y. Xiang, and J. Liu, "Distributionally robust planning for integrated energy systems incorporating electric-thermal demand response," *Energy*, vol. 213, p. 118783, 2020. 11, 12, 106

[80] C. He, L. Wu, T. Liu, and M. Shahidehpour, "Robust co-optimization scheduling of electricity and natural gas systems via admm," *IEEE Transactions on Sustainable Energy*, vol. 8, no. 2, pp. 658–670, 2017. 12

[81] M. Umar, X. Ji, D. Kirikkaleli, and A. A. Alola, "The imperativeness of environmental quality in the united states transportation sector amidst biomass-fossil energy consumption and growth," *Journal of Cleaner Production*, vol. 285, p. 124863, 2021. 13

[82] C. Shao, C. Feng, M. Shahidehpour, Q. Zhou, X. Wang, and X. Wang, "Optimal stochastic operation of integrated electric power and renewable energy with vehicle-based hydrogen energy system," *IEEE Transactions on Power Systems*, vol. 36, no. 5, pp. 4310–4321, 2021. 13, 14, 16, 124

[83] C. Feng, C. Shao, Y. Xiao, Z. Dong, and X. Wang, "Day-ahead strategic operation of hydrogen energy service providers," *IEEE Transactions on Smart Grid*, 2022. 13, 14, 15, 16, 124, 130

[84] N. A. El-Taweel, H. Khani, and H. E. Farag, "Hydrogen storage optimal scheduling for fuel supply and capacity-based demand response program under dynamic hydrogen pricing," *IEEE Transactions on Smart Grid*, vol. 10, no. 4, pp. 4531–4542, 2019. 13, 14, 16, 130

[85] M. Hermesmann and T. Müller, "Green, turquoise, blue, or grey? environmentally friendly hydrogen production in transforming energy systems," *Progress in Energy and Combustion Science*, vol. 90, p. 100996, 2022. 13

[86] A. Zhou and J. Wang, "Behind-the-meter renewable hydrogen: Challenges and solutions," *The Electricity Journal*, vol. 35, no. 5, p. 107134, 2022. 13

[87] T. Wu, J. Wang, and M. Yue, "On the integration of hydrogen into integrated energy systems: Modeling, optimal operation and reliability assessment," *IEEE Open Access Journal of Power and Energy*, 2022. 13, 14, 15, 16

[88] A. Elgowainy, M. Mintz, U. Lee, T. Stephens, P. Sun, K. Reddi, Y. Zhou, G. Zang, M. Ruth, P. Jadun *et al.*, "Assessment of potential future demands for hydrogen in the united states," Argonne National Lab.(ANL), Argonne, IL (United States), Tech. Rep., 2020. 13

[89] C. F. Guerra, L. Reyes-Bozo, E. Vyhmeister, J. L. Salazar, M. J. Caparrós, and C. Clemente-Jul, "Sustainability of hydrogen refuelling stations for trains using electrolysers," *International Journal of Hydrogen Energy*, vol. 46, no. 26, pp. 13 748–13 759, 2021. 13

[90] R. Minjares, F. Rodríguez, A. Sen, and C. Braun, "Infrastructure to support a 100% zero-emission tractor-trailer fleet in the united states by 2040," *International Council on Clean Transportation*, 2021. 13

[91] H. Khani, N. A. El-Taweel, and H. E. Z. Farag, "Supervisory scheduling of storage-based hydrogen fueling stations for transportation sector and distributed operating reserve in electricity markets," *IEEE Transactions on Industrial Informatics*, vol. 16, no. 3, pp. 1529–1538, 2020. 14, 16

[92] J. Li, J. Lin, Y. Song, X. Xing, and C. Fu, "Operation optimization of power to hydrogen and heat (p2hh) in adn coordinated with the district heating network," *IEEE Transactions on Sustainable Energy*, vol. 10, no. 4, pp. 1672–1683, 2019. 14, 15, 16

[93] A. Mansour-Saatloo, Y. Pezhmani, M. A. Mirzaei, B. Mohammadi-Ivatloo, K. Zare, M. Marzband, and A. Anvari-Moghaddam, "Robust decentralized optimization of multi-microgrids integrated with power-to-x technologies," *Applied Energy*, vol. 304, p. 117635, 2021. 14, 15, 16, 17

[94] P. Zhao, C. Gu, Z. Hu, D. Xie, I. Hernando-Gil, and Y. Shen, "Distributionally robust hydrogen optimization with ensured security and multi-energy couplings," *IEEE Transactions on Power Systems*, vol. 36, no. 1, pp. 504–513, 2021. 14, 15, 16

[95] P. Zhao, X. Lu, Z. Cao, C. Gu, Q. Ai, H. Liu, Y. Bian, and S. Li, "Volt-var-pressure optimization of integrated energy systems with hydrogen injection," *IEEE Transactions on Power Systems*, vol. 36, no. 3, pp. 2403–2415, 2021. 14, 15, 16

[96] F. Qi, M. Shahidehpour, F. Wen, Z. Li, Y. He, and M. Yan, "Decentralized privacy-preserving operation of multi-area integrated electricity and natural gas systems with renewable energy resources," *IEEE Transactions on Sustainable Energy*, vol. 11, no. 3, pp. 1785–1796, 2020. 14, 15

[97] A. M. Abomazid, N. A. El-Taweel, and H. E. Farag, "Optimal energy management of hydrogen energy facility using integrated battery energy storage and solar photovoltaic systems," *IEEE Transactions on Sustainable Energy*, vol. 13, no. 3, pp. 1457–1468, 2022. 14, 16

[98] A. J. Conejo, E. Castillo, R. Minguez, and R. Garcia-Bertrand, *Decomposition techniques in mathematical programming: engineering and science applications*. Springer Science & Business Media, 2006. 23, 50

[99] A. Kargarian, G. Hug, and J. Mohammadi, "A multi-time scale co-optimization method for sizing of energy storage and fast-ramping generation," *IEEE Transactions on Sustainable Energy*, vol. 7, no. 4, pp. 1351–1361, 2016. 25, 26

[100] B. Chen, C. Chen, J. Wang, and K. L. Butler-Purry, "Sequential service restoration for unbalanced distribution systems and microgrids," *IEEE Transactions on Power Systems*, vol. 33, no. 2, pp. 1507–1520, 2017. 26, 27

[101] H. Ahmadi and J. R. Martı, "Linear current flow equations with application to distribution systems reconfiguration," *IEEE Transactions on Power Systems*, vol. 30, no. 4, pp. 2073–2080, 2014. 26

[102] S. Gill, I. Kockar, and G. W. Ault, "Dynamic optimal power flow for active distribution networks," *IEEE Transactions on Power Systems*, vol. 29, no. 1, pp. 121–131, 2013. 26

[103] K. Mongird, V. V. Viswanathan, P. J. Balducci, M. J. E. Alam, V. Fotedar, V. S. Koritarov, and B. Hadjerioua, "Energy storage technology and cost characterization report," Pacific Northwest National Lab.(PNNL), Richland, WA (United States), Tech. Rep., 2019. 36

[104] T. A. Nguyen, *Optimization in microgrid design and energy management*. Missouri University of Science and Technology, 2014. 36

[105] T. Erseghe, "Distributed optimal power flow using admm," *IEEE transactions on power systems*, vol. 29, no. 5, pp. 2370–2380, 2014. 42

[106] T. N. Santos, A. L. Diniz, and C. L. T. Borges, "A new nested benders decomposition strategy for parallel processing applied to the hydrothermal scheduling problem," *IEEE Transactions on Smart Grid*, vol. 8, no. 3, pp. 1504–1512, 2016. 50

[107] Z. K. Pecenak, V. R. Disfani, M. J. Reno, and J. Kleissl, "Multiphase distribution feeder reduction," *IEEE Transactions on Power Systems*, vol. 33, no. 2, pp. 1320–1328, 2017. 50

[108] A. Kargarian, G. Hug, and J. Mohammadi, "A multi-time scale co-optimization method for sizing of energy storage and fast-ramping generation," *IEEE Transactions on Sustainable Energy*, vol. 7, no. 4, pp. 1351–1361, 2016. 62

[109] M. E. Baran and F. F. Wu, "Network reconfiguration in distribution systems for loss reduction and load balancing," *IEEE Power Engineering Review*, vol. 9, no. 4, pp. 101–102, 1989. 63

[110] H. Ahmadi and J. R. Martı, "Linear current flow equations with application to distribution systems reconfiguration," *IEEE Transactions on Power Systems*, vol. 30, no. 4, pp. 2073–2080, 2014. 63, 64, 122

[111] X. Zhang, M. Shahidehpour, A. S. Alabdulwahab, and A. Abusorrah, "Security-constrained co-optimization planning of electricity and natural gas transportation infrastructures," *IEEE Transactions on Power Systems*, vol. 30, no. 6, pp. 2984–2993, 2015. 66

[112] A. Khodaei and M. Shahidehpour, "Microgrid-based co-optimization of generation and transmission planning in power systems," *IEEE transactions on power systems*, vol. 28, no. 2, pp. 1582–1590, 2012. 66

[113] V. S. Shekhawat, A. Gautam, and A. Thakrar, "Datacenter workload classification and characterization: An empirical approach," in *2018 IEEE 13th International Conference on Industrial and Information Systems (ICIIS)*. IEEE, 2018, pp. 1–7. 67

[114] E. Elhamifar, G. Sapiro, and S. S. Sastry, "Dissimilarity-based sparse subset selection," *IEEE transactions on pattern analysis and machine intelligence*, vol. 38, no. 11, pp. 2182–2197, 2015. 70, 81

[115] K. Mongird, V. V. Viswanathan, P. J. Balducci, M. J. E. Alam, V. Fotedar, V. S. Koritarov, and B. Hadjerioua, "Energy storage technology and cost characterization report," Pacific Northwest National Lab.(PNNL), Richland, WA (United States), Tech. Rep., 2019. 73

[116] T. A. Nguyen, "Optimization in microgrid design and energy management," Ph.D. dissertation, 2014. 73

[117] H. Ahmadi and J. R. Martı, "Linear current flow equations with application to distribution systems reconfiguration," *IEEE Transactions on Power Systems*, vol. 30, no. 4, pp. 2073–2080, 2015. 92

[118] A. Kargarian, G. Hug, and J. Mohammadi, "A multi-time scale co-optimization method for sizing of energy storage and fast-ramping generation," *IEEE Transactions on Sustainable Energy*, vol. 7, no. 4, pp. 1351–1361, 2016. 94

[119] O. Ciftci, M. Mehrtash, and A. Kargarian, "Data-driven nonparametric chance-constrained optimization for microgrid energy management," *IEEE Transactions on Industrial Informatics*, vol. 16, no. 4, pp. 2447–2457, 2020. 94

[120] J. Li, M. E. Khodayar, J. Wang, and B. Zhou, "Data-driven distributionally robust co-optimization of p2p energy trading and network operation for interconnected microgrids," *IEEE Transactions on Smart Grid*, vol. 12, no. 6, pp. 5172–5184, 2021. 94

[121] Q. Qdr, "Benefits of demand response in electricity markets and recommendations for achieving them," *US Dept. Energy, Washington, DC, USA, Tech. Rep*, vol. 2006, 2006. 95

[122] A. Satchwell and R. Hledik, "Analytical frameworks to incorporate demand response in long-term resource planning," *Utilities Policy*, vol. 28, pp. 73–81, 2014. 95

[123] C.-L. Su and D. Kirschen, "Quantifying the effect of demand response on electricity markets," *IEEE Transactions on Power Systems*, vol. 24, no. 3, pp. 1199–1207, 2009. 95

[124] P. M. Esfahani and D. Kuhn, "Data-driven distributionally robust optimization using the wasserstein metric: Performance guarantees and tractable reformulations," *Mathematical Programming*, vol. 171, no. 1, pp. 115–166, 2018. 96, 97, 111, 126, 134

[125] D. Ray, "Lazard's levelized cost of energy analysis—version 13.0," *Lazard: New York, NY, USA*, p. 20, 2019. 104

[126] K. Mongird, V. V. Viswanathan, P. J. Balducci, M. J. E. Alam, V. Fotedar, V. S. Koritarov, and B. Hadjerioua, "Energy storage technology and cost characterization report," Pacific Northwest National Lab.(PNNL), Richland, WA (United States), Tech. Rep., 2019. 104

[127] T. A. Nguyen, "Optimization in microgrid design and energy management," Ph.D. dissertation, 2014. 104

[128] U.S Energy Information Administration. [Online]. Available: https://www.eia.gov/dnav/ng/hist/n3010tx2m.htm 104

[129] U.S Energy Information Administration. [Online]. Available: https://www.eia.gov/dnav/ng/hist/rngwhhdm.htm 104

[130] Pjm data miner. [Online]. Available: https://dataminer2.pjm.com 106

[131] NREL. Nsrdb data viewer. [Online]. Available: https://maps.nrel.gov/nsrdb-viewer/ 106

[132] J. Li, J. Lin, H. Zhang, Y. Song, G. Chen, L. Ding, and D. Liang, "Optimal investment of electrolyzers and seasonal storages in hydrogen supply chains incorporated with renewable electric networks," *IEEE Transactions on Sustainable Energy*, vol. 11, no. 3, pp. 1773–1784, 2019. 130

[133] O. Utomo, M. Abeysekera, and C. E. Ugalde-Loo, "Optimal operation of a hydrogen storage and fuel cell coupled integrated energy system," *Sustainability*, vol. 13, no. 6, p. 3525, 2021. 130